Photometric Studies of Dwarf Elliptical Galaxies in the Virgo Cluster

Inauguraldissertation

zur
Erlangung der Würde eines Doktors der Philosophie
vorgelegt der
Philosophisch-Naturwissenschaftlichen Fakultät
der Universität Basel

von

Fabio Daniel Barazza

aus Basel

Basel, 2003

Genehmigt von der Philosophisch-Naturwissenschaftlichen Fakult¨at auf Antrag der

Herren Prof. Dr. R. Buser, Prof. Dr. O. Gerhard, PD Dr. B. Binggeli und Dr. R. Saglia

Basel, den 8. April 2003

Prof. Dr. Marcel Tanner

Dekan der Philosophisch-

Naturwissenschaftlichen Fakult¨at

Zusammenfassung

In der vorliegenden Arbeit werden die Resultate photometrischer Untersuchungen an Zwergelliptischen Galaxien im Virgo Haufen präsentiert. Als Datenbasis dienten in erster Linie Beobachtungen, die am Very Large Telescope (VLT) in B- bzw. R-Filtern durchgeführt wurden. Um eine genauere Untersuchung der Farbeigenschaften zu ermöglichen, wurden diese Daten mit Beobachtungen im U-Filter, durchgeführt am Dänischen 1.5m-Teleskop, ergänzt. Die Arbeit besteht im Wesentlichen aus der Bestimmung der grundlegenden photometrischen Eigenschaften, einer genauen Isophotenanalyse und der Untersuchung der Farben der Zwerggalaxien.

Die Oberflächenphotometrie, durchgeführt in allen drei Farbbändern, diente der Messung photometrischer Parameter wie effektiver Radius, effektive Oberflächenhelligkeit, totale scheinbare Helligkeit usw. und zur Bestimmung der Oberflächenhelligkeits-Profile. Diese Profile wurden anschliessend durch Sérsic-Modelle (Sérsic 1968) gefittet. Ein Vergleich der gefundenen Modellparameter (zentrale Oberflächenhelligkeit, Skalenlänge, “shape”-Parameter) mit denjenigen von grossen Elliptischen Galaxien ergibt einen fliessenden Übergang zwischen Zwergen und Riesen, wenn die Daten gegen die absolute Helligkeit aufgetragen werden. Einzig die meist schwachen Zwergellipsen der Lokalen Gruppe zeigen oft Abweichungen von dieser Beziehung. In dieser Darstellung erscheinen die Zwerge somit als Gegenstücke der grossen Ellipsen bei kleineren Helligkeiten. Andererseits zeigt sich, dass die hellsten Zwerge in unserer Stichprobe die grössten Abweichungen zwischen Profil und Modell zeigen und dass diese Abweichungen vor allem in den zentralen Bereichen auftreten. Diese Tatsache deutet darauf hin, dass zumindest die hellen Zwergellipsen eine komplexere Sternverteilung aufweisen als bisher angenommen.

Als Teil der Isophotenanalyse wurden insbesondere die Abweichungen der Isophoten von der Ellipsenform untersucht. Dabei konnten in vier Objekten Hinweise auf das Vorhandensein einer Scheibenkomponente gefunden werden. Zusammen mit einem bereits früher entdeckten Spiralmuster in einer der Galaxien (Jerjen et al. 2000), gibt es damit bereits fünf Zwergellipsen, die Anzeichen einer Scheibenkomponente zeigen. Sollte der Anteil dieser Objekte in unserer Stichprobe repräsentativ sein für die ganze Population von Zwergellipsen in Haufen, wäre das Vorhandensein einer Scheibenstruktur ein häufiges Merkmal dieses Galaxientyps. Diese spezifische Art von Haufenzwergen könnte ihren Ursprung in Prozessen haben, bei denen Scheibengalaxien durch die Wechselwirkung mit dem Haufen als ganzem, aber auch mit den einzelnen Galaxien, transformiert würden (Moore et al. 1998). Solche Transformationsprozesse könnnen ablaufen, wenn eine Scheibengalaxie in einen Haufen stürzt. Die beobachteten Objekte wären somit transformierte Spiralgalaxien, bei denen ein Teil der Scheibe intakt blieb.

Da die meisten Zwergellipsen in unserer Stichprobe Kerne in ihren Zentren aufweisen, wurde untersucht *wie* zentral diese Kerne sind, d.h. ob sie tatsächlich genau im Zentrum der Lichtverteilung liegen. Das Resultat bestätigt das Ergebnis einer früheren Studie (Binggeli et al. 2000), wonach ein grosser Teil der Kerne nicht im Zentrum der Lichtverteilung liegt, und dass die Grösse des Abstandes mit abnehmender Oberflächenhelligkeit zunimmt. Desweiteren wurde die Ausrichtung der Isophoten anhand des Posi-

tionswinkels ihrer Hauptachse untersucht. Dabei wurde festgestellt, dass Isophoten vor allem bei runden Objekten stark verdreht sein können. Da dies immer von beträchtlichen Veränderungen der Abflachung begleitet wird, ist diese Beobachtung höchstwahrscheinlich auf Projektionseffekte zurückzuführen, was wiederum darauf hindeutet, dass diese Zwergellipsen triaxiale Systeme sind.

Im Rahmen der Untersuchung der Farbeigenschaften der Galaxien konnte überraschend eine Beziehung zwischen der Abflachung und der Farbe der Objekte nachgewiesen werden: ründere Zwergellipsen sind im Mittel röter als flachere. Unter Einbezug von Daten aus der Literatur stellte sich dann heraus, dass die gefundene Beziehung tatsächlich die Metallizität und die Abflachung verknüpft: ründere Zwergellipsen sind metallreicher als flachere. Diese Eigenschaft kann im Zusammenhang mit galaktischen Winden verstanden werden. Durchläuft das Zentrum einer Zwerggalaxie eine Periode starker Sternentstehung, bildet sich aufgrund der stellaren Winde massereicher Sterne und der folgenden Supernova-Explosionen ein galaktischer Wind, der angereichertes Material nach aussen befördert. Frühere Simulationen zeigen, dass dies vorzugsweise in Richtung des stärksten Dichtegradienten, d.h. entlang der kleinen Halbachse, geschieht (De Young & Heckman 1994). Verliert eine Zwerggalaxie angereichertes Material aufgrund galaktischer Winde, wird dies also vor allem entlang der kleinen Halbachse geschehen und die Menge des ausströmenden Materials hängt von der Länge dieser Achse ab. In der gefundenen Beziehung zwischen Metallizität und Abflachung widerspiegeln sich daher die Auswirkungen früherer Sternentstehungs Episoden.

Im Weiteren wurde eine Beziehung zwischen dem Farbindex und dem Farbgradienten gefunden: blauere Galaxien haben ein eher rotes Zentrum und werden blauer gegen Aussen; bei den röteren Objekten ist es genau umgekehrt. Der Effekt zeigt sich sowohl in $U-B$, als auch in $B-R$ und bestätigt damit das Ergebnis einer früheren Untersuchung in $B-H$ (Pierini 2002). Der Ursprung dieser Beziehung ist allerdings unklar, auch weil mit Farbinformationen alleine nicht festgestellt werden kann, ob das Alter der vorhandenen Sterne oder die Metallizität ausschlaggebend sind.

Die Ergebnisse der Untersuchungen machen deutlich, dass Zwergellipsen in Haufen unterschiedliche Strukturen aufweisen können und im Allgemeinen komplexer sind als bisher angenommen. Höchstwahrscheinlich weist ein beträchtlicher Teil der Population eine Scheibenkomponente auf, was darauf hindeutet, dass diese Zwergellipsen transformierte Scheibengalaxien sind. Somit kann die Klasse der Zwergellipsen in Haufen zumindest in zwei Untergruppen aufgeteilt werden: in die “klassischen” Zwergellipsen, die leuchtschwächer sind und auch in kleineren Galaxiengruppen zu finden sind, und in die ehemaligen Scheibengalaxien, die ihr jetztiges Aussehen einer Transformation verdanken und im Mittel heller sind. Wichtig im Zusammenhang mit möglichen Entwicklungsmodellen von Zwergellipsen im Allgemeinen ist die Berücksichtigung der gefundenen Metallizitäts-Abflachungs Beziehung, die beispielsweise eher gegen die Möglichkeit spricht, dass Zwergellipsen aus Zwergirregulären entstehen.

Inhaltsverzeichnis

1
Introduction

Dwarf galaxies, as the name suggests, are rather small in size and have low masses and luminosities. However, they provide a rich diversity of stellar populations, star formation histories, morphologies, inner structures, and they populate the most different environments in the universe. Moreover, assuming that dwarfs are the building blocks of giant galaxies, they have to be considered as the basic units of galaxy formation in general. Therefore, dwarfs, being physically small and faint, are giant and bright in providing insights into galaxy evolution.

However, there does not exist a common definition for dwarf galaxies. In general, a criterion based on brightness is used. For instance, galaxies with $M_B > -18$ mag, or overall low surface brightness are called dwarfs, the former being the most popular definition. Yet, there is also a definition with a possible physical meaning: *a dwarf galaxy is neither a classical elliptical galaxy (E) nor does it contain an E-like bulge* (Binggeli 1993). In any case, since there are only very few galaxies which fulfill just one of the above conditions, the classification of dwarfs usually does not pose any problem. This also holds for the galaxies considered in this thesis; they are all dwarfs in either sense.

The first dwarf galaxies discovered are the two Magellanic Clouds, mentioned in a logbook written by Ferdinand Magellan during the first navy around the world. He did not know what exactly the two clouds were, which resembled broken off pieces of the Milky Way. In 1909, when the third dwarf galaxy was discovered, there was the debate whether there exist stellar systems outside the Milky Way and therefore, the true nature of the Magellanic Clouds and the new object was still unclear. The new dwarf was found by Wolf (1909) on a plate taken by Lorentz and rediscovered by Melotte (1926), hence its name WLM. In the 1920's it was realized that some observed nebulae are extragalactic objects. In the following more and more dwarfs, attributed today to the Local Group, were found (Hubble 1925, Baade 1963, Shapley 1938, 1939)

The first dwarfs outside of the Local Group were discovered by Holmberg (1950) around M81 and M101 in 1950. This study constitutes as well the definition of the fist nearby galaxy groups, since the mere existence of such systems was not well established at that time. The search for dwarf galaxies was then extended to the nearest galaxy cluster in Virgo. The work of Reaves (1956), in the framework of the sky survey of Shane & Wirtanen (1967), provided a large number of probable and possible dwarf members of the Virgo cluster. Hereafter, a systematic search and cataloging of dwarfs started: first again Reaves (1983) published a catalogue of 864 dwarfs in Virgo, followed by the Virgo Cluster Catalogue (VCC) by Binggeli et al. (1985). A similar compilation followed for the Fornax cluster by Ferguson (1989, the Fornax Cluster Catalogue, FCC).

Meanwhile, the number of Local Group dwarfs increased as well. For instance, van den Bergh (1972) discovered three new companions of M31 (And I, II, III) and the up to now last dwarf of the Local Group was found by Whiting et al. (1999) in Cetus.

1.1 Classification of dwarf galaxies

Like giant (or classical) galaxies, dwarfs can be subdivided into early and late types. Both groups on there part consist of two classes, which are already determining the properties of the galaxies. Using the classification system of Sandage & Binggeli (1984) the early-type dwarfs are composed of dwarf ellipticals (dE, dE,N) and dwarf S0s (dS0), whereas dwarf irregulars (Im, Sm) and blue compact dwarfs (BCD) constitute the late types. In Figure 1.1 an example for each class is shown.

Dwarf ellipticals

Obviously, the designation *dwarf* elliptical galaxy has to be understood with respect to giant ellipticals (E), with which they might share more than just the general appearance. Whether there is a continuity

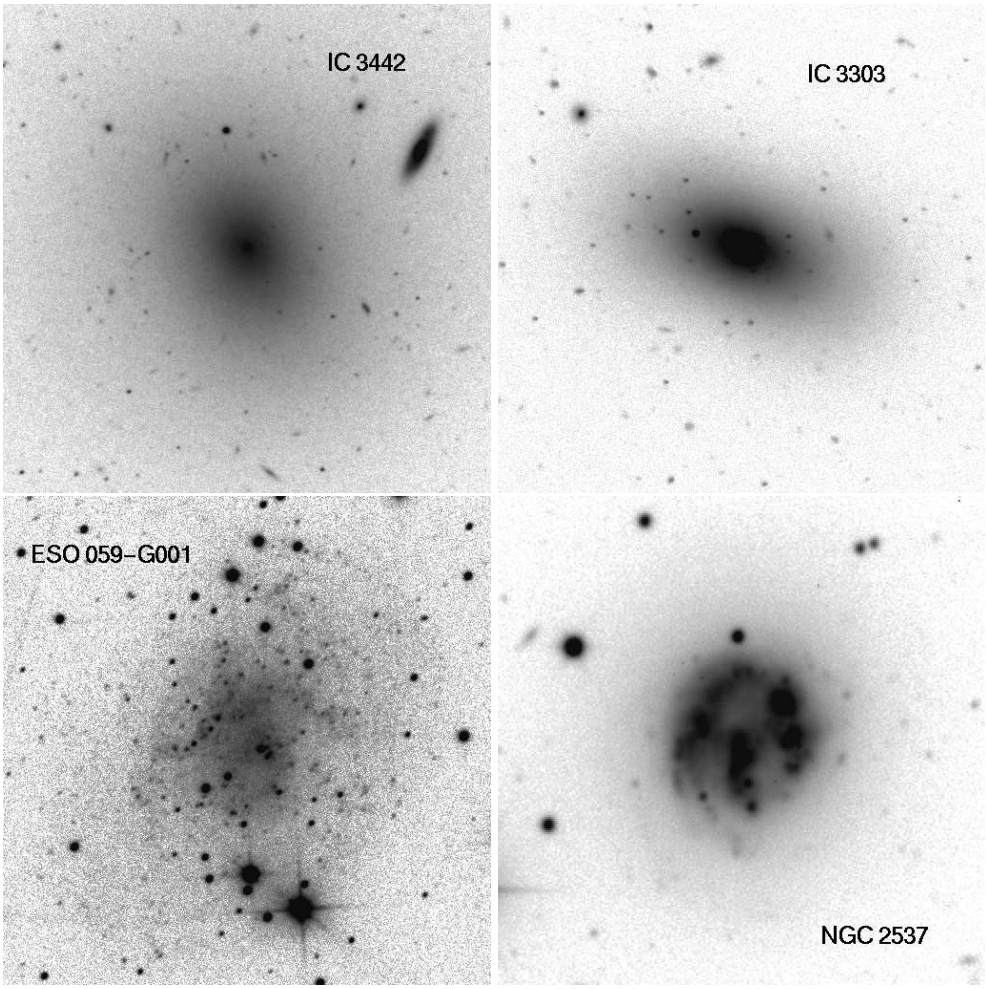

Abbildung 1.1: Examples for the different morphological classes of dwarf galaxies. (*top left*) R-band image of a dE,N, image size: $1\farcm7 \times 1\farcm7$. (*top right*) R-band image of a dS0,N, image size: $1\farcm7 \times 1\farcm7$. (*bottom left*) B-band image of a Im, image size: $6\farcm6 \times 6\farcm6$. (*bottom right*) B-band image of a BCD, image size: $3' \times 3'$.

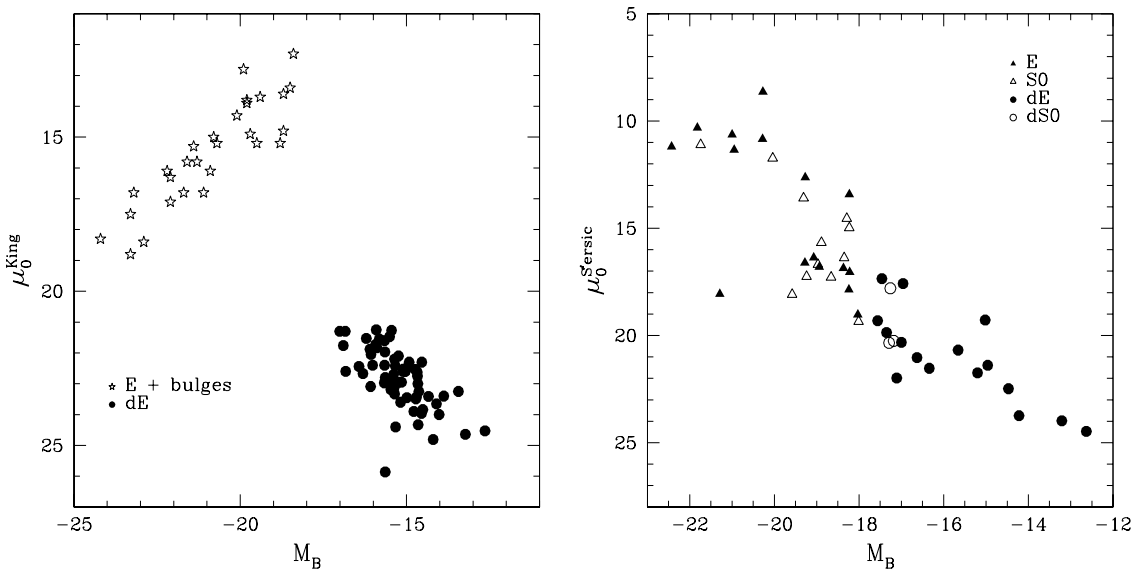

Abbildung 1.2: (*left*) Absolute magnitude in B versus central surface brightness derived with a King-model. Data are from Kormendy (1985) for Es and bulges and from Binggeli & Cameron (1991, 1993) for dEs. (*right*) Absolute magnitude in B versus central surface brightness derived with a Sérsic-model. Data are from Caon et al. (1993) for Es and S0s and from this thesis for dEs and dS0s.

between Es and dEs or whether these two classes of galaxies are completely different, depends somehow on the viewpoint. This is shown in Figure 1.2, where the absolute magnitude in B versus central surface brightness is plotted for early-type giants and dwarfs. In the left panel the central surface brightness was derived using a King model (King 1966). Es and dEs exhibit a totally different relation: in giant galaxies the central surface brightness decreases with increasing luminosity, whereas the opposite trend is evident for dwarf galaxies. The two classes seem to be completely distinct in this picture, since the two sequences can hardly be linked. This result clearly suggests different origins and formation scenarios for Es and dEs. On the other hand, the continuous sequence in the right panel, where giants and dwarfs share the same relation, indicates a physical continuity between the two classes. In this case the central surface brightnesses were determined using a Sérsic law (Sérsic 1968), which is believed to be the more appropriate model at least for bright early-type dwarfs. Hence, only being aware of the relation shown in the right panel, a common origin of giants and dwarfs would be assumed, regarding dwarf ellipticals as the smaller and fainter “relatives” of giant ellipticals.

Apparently, it cannot be decided on photometrical grounds alone which picture is correct, only optical properties can be described and differences to other morphological classes can be pointed out, without assessing the physical context. However, there are enough optical and morphological characteristics which are different for Es and dEs so that the establishment of two classes is justified. For instance the surface brightness of dEs is rather low, indicating a low intrinsic luminosity, and they exhibit a shallow intensity distribution, in contrast to Es, which have a steep surface brightness profile. In addition, a large number of dEs have a central nucleus (denoted dE,N in this case). Such a compact stellar system, which is distinct from the galaxy is not known in Es. There are different suggestions concerning the nature of these nuclei. They might be the remnants of the last central star formation event or even the result of the merger of several globular clusters, which sunk to the center of the galaxy through dynamical friction. Despite a

small overlap, these characteristics are also in good agreement with the usually adopted luminosity limit of $M_B > -18$ for dwarfs.

Dwarf S0s

The galaxies classified as dS0s are very similar to dEs and hardly differ from them in a purely optical manner. Yet, it is possible to apply the same distinction criterion like in the case of giant Es and S0s, which is a change of slope in the gradient of the radial light distribution. This feature indicates the transition from bulge to disk in a S0. Indeed, among dwarfs such objects can be found, even though only in small numbers. Therefore, a class for its own can be established without supposing the presence of a bulge in these dwarfs. However, dS0s might be two-component systems as well, consisting of a central lens-like structure surrounded by a more extended stellar envelope, with lower surface brightness. In the Virgo cluster only a small number (~ 20) of such objects have been found, most of them hosting a nucleus.

Dwarf irregulars

Continuing the sequence of late-type spiral galaxies, where the regular spiral structure has more and more vanished, we enter the domain of the dwarf irregulars. The Sm type still shows some rudiments of a spiral structure, whereas the Im galaxies appear totally chaotic. This implies of course that these galaxies are gas rich and currently form stars, what makes them completely different from early-type dwarfs. Since there is a continuous transition from Sd to Sm, it is somewhat arbitrary, where the distinction between giants and dwarfs is made. Using the above mentioned definition that a dwarf does not have a E-like bulge, leaves considerable space for interpretations, probably leading to strongly differing classifications. Therefore, the non-physical limit of $M_B = -18$ mag is the only objective option.

Blue compact dwarfs

Among the dwarf irregular galaxies there are objects with particular bright star forming regions, which are very compact and usually clustered around the center. These dwarf galaxies, often erroneously regarded as giant background ellipticals, have been assigned to a separate class, the blue compact dwarfs (BCD). The most extreme BCDs are almost stellar in appearance with no obvious underlying galaxy (Thuan & Martin 1981). Otherwise, the bright and blue HII knots (30 Doradus type) are embedded in a faint stellar envelope. The BCDs are commonly believed to be low surface brightness dwarfs, which we happen to be observed during a strong starburst event. The picture is that a dwarf irregular galaxy may alternate between the quiescent, low surface brightness state, with star formation on a low level, and the high surface brightness state, where several star bursts take place.

1.2 Possible connections and transitions

Figure 1.3 (which is adopted from Sandage & Binggeli 1984) shows the possible transitions between the discussed dwarf types (dashed lines) and their relation to the Hubble sequence, which is shown on top. The late-type giants become fainter, finally entering the domain of the dwarfs with the Sm/Im types. On the other hand, neither the placement of the BCDs on the right of the dwarf irregulars nor their possible connections to the Sm and Im types are evident. In contrast to the sequence of the giants, there is a large gap between the early and late types among the dwarfs. Commonly, this gap has been considered to

be real, since no dwarf spirals were known. In addition, it has been argued that dwarf irregulars might transform into dwarf ellipticals (indicated by the dashed lines) after having used up all their gas (Gerola et al. 1980, Davis & Phillipps 1988). However, this picture has been more and more doubted, since the properties of early and late-type dwarfs are so different that a transformation seems to be very unlikely. Moreover, there is more evidence arising that a rather large fraction of early-type dwarfs might have disk components and even spiral or bar features. Such galaxies would bridge the large gap between early and late-type dwarfs. Yet, the question mark in Figure 3 cannot be removed and the determination of the correct connections in that part of the diagram remains one of the major goals in dwarf galaxy research.

1.3 Evolutionary models for dwarf galaxies

While the dwarf irregulars seem to be strongly related to giant disk galaxies, extending their sequence toward lower luminosities and probably having the same evolutionary origin, a similar relationship between giant and dwarf ellipticals is not so evident. However, the standard picture commonly assigned to dwarf galaxies is that they formed from the gravitational collapse of primordial density fluctuations. The same is believed to hold for giant galaxies as well, yet they could also be the result of the merger of several dwarf galaxies. In a radically different model dwarf galaxies are the debris from the explosion during the initial burst of star formation or from the collision or merger of giant galaxies. The latter process seems to be a matter of fact, since such events have been observed in increasing numbers. The dwarfs usually developing in the tidal arms/streams of such encounters are collected in a subgroup of irregulars: the Tidal Dwarf Galaxies (Duc & Mirabel 1994, Duc et al. 1997). Therefore, the origin of dwarf irregulars in general either as the result of the gravitational collapse of a gas cloud or as debris from

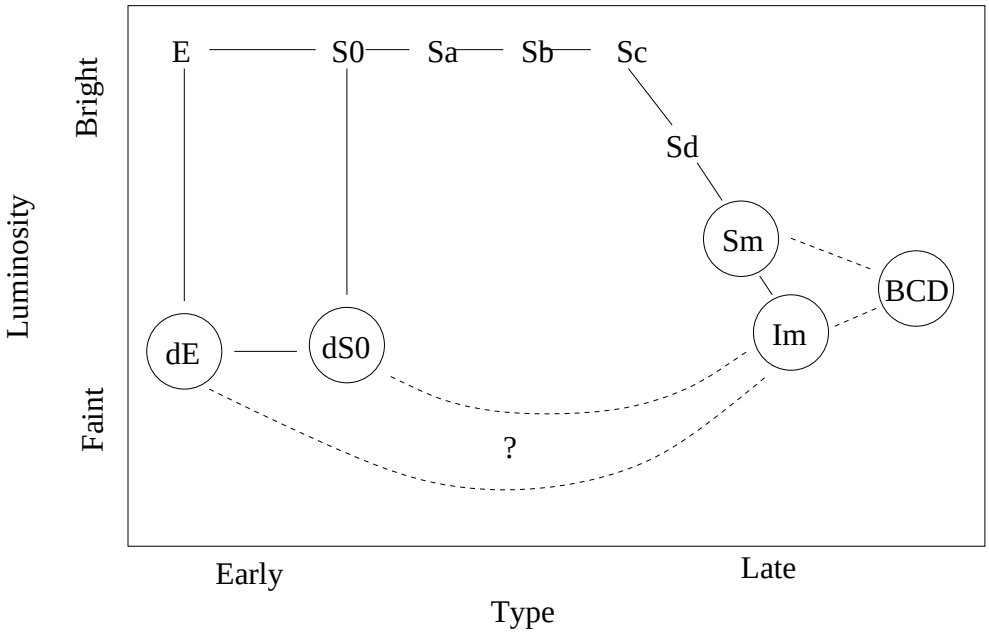

Abbildung 1.3: Classification scheme, showing possible transitions among the dwarf types and the relations to the giant galaxies. The Hubble sequence is shown on top. The dashed lines indicate possible transformation paths. Adopted from Sandage & Binggeli (1984).

galaxy collisions seems to be understood quite well. However, for early-type dwarfs the picture is not so evident. In addition, every evolutionary scenario for any dwarf galaxy type has to take into account the morphology-density relation (Binggeli et al. 1987, Ferguson & Sandage 1988, Binggeli et al. 1990): as for giants (Dressler 1980), early-type dwarfs are preferentially found in regions of higher galaxy density than late-type dwarfs. A model describing the origin of dwarf ellipticals in the centers of galaxy clusters and therefore also accounting for the morphology-density relation is presented by Moore et al. (1998). In this study the infall of small disk galaxies into a cluster is simulated. The mere gravitational interaction between the infalling galaxy and the individual cluster members leads to an entire transformation of the disk and a considerable loss of gas. Thereby, the stars and gas forming the disk are rearranged into a spheroidal structure. After this transformation from so called galaxy harassment, the remaining gas is believed to be used up in a final starburst leaving behind the gas free dwarf ellipticals we observe today. However, some of the transformed disk galaxies might be able to maintain at least parts of their disk structure, which is suggested by the disk components found in a couple of early-type dwarfs (see below).

Once a dwarf has formed, star formation will be the most important intrinsic process influencing its development. Subsequent stellar winds from massive stars and in particular supernovae explosions form a galactic wind, which strongly affects the early evolution of dwarfs (Larson 1974, Dekel & Silk 1986). These winds can carry away a significant fraction of the interstellar material and therefore leading to an earlier termination of star formation. As a consequence, dwarf galaxies are not able to enrich their interstellar medium as extensively as giant galaxies. Moreover, the material carried away by galactic winds is suggested to be particularly metal-rich (Vader 1986, 1987). These circumstances are responsible for the mass-metallicity relation (Faber 1973, Mould 1984): more massive galaxies are more metal-rich. However, since dwarf galaxies are believed to be dark matter dominated the material flown out could be captured by the dark halo and be reaccreted later on (Ferrara & Tolstoy 2000). Similarly, the outflow of a dwarf residing in the central parts of a cluster could be halted by the thermal pressure of the inter cluster medium (Murakami & Babul 1999). On the other hand, if the velocity with which the galaxy is moving through the cluster is high enough, the outflow material could be swept away by ram pressure stripping. In addition, the strength of the outflow seems also to depend on the shape, i.e. the flattening of the galaxy (see Appendix D). It is therefore evident that the mass is only one among several properties being responsible for the evolution of dwarf galaxies.

1.4 Specific properties of dwarf ellipticals

1.4.1 Flattening distribution

Besides their elliptical shape, the most apparent property of dwarf ellipticals is probably their flattness, which is usually defined as ellipticity ϵ, i.e. $\epsilon = 1 - b/a$, where a and b are the major- and minor-axis, respectively. There are different possibilities of measuring ϵ. Commonly, the ellipticity of a specific isophote is determined rather in the outer parts, e.g. the isophote with 25 mag per arcsec^2, and taken as reference for the whole galaxy. A more accurate procedure is to derive the mean ellipticity over a large radius range weighted by the luminosity. On the other hand, since the ellipticity is not varying strongly with increasing radius, both methods lead to similar results. However, in flattened dwarf ellipticals with a bright nucleus the ellipticity profile exhibits a sharp rise in the central parts. This feature is not due to the nucleus itself, which is round indeed, but caused by its gravitational influence on the motion of the nearby stars, forcing them on circular orbits. The inner parts of the galaxies have therefore to be excluded from the averaging. Strong ellipticity variations are always indicative of inner structures, like spirals or bars.

It is important to note that only apparent ellipticities can be measured. The values obtained are therefore always lower limits of the true (intrinsic) ellipticities. Hence, the higher probability of measuring lower ellipticities might be manifest in the flattness distributions shown in Figure 1.4 (left panel), where a slight tendency of lower ellipticities is evident. This is obviously valid for Es (empty histogram) and dEs (shaded histogram). On the other hand, the fraction of flatter objects seems to be slightly higher for dwarfs than for giants. This becomes clear in the right panel of Figure 1.4, where the cumulative distribution function is shown. The fact that dwarf ellipticals tend to be flatter than giants was already revealed in studies by Ryden & Terndrup (1994) and Binggeli & Popescu (1995), who also compared the distributions of different dwarf types. Moreover, it is shown in both studies that, even though the difference between Es and dEs is rather small, it is statistically significant. However, the result could be slightly biased, since among the flat dEs several might be disk-like objects, i.e. dS0, which is much harder to determine in the case of dwarfs. Otherwise, the different formation scenarios suggested for Es and dEs could lead to the different flattness distributions. If giants are mostly the result of mergers, their roundness would be plausible. On the other hand, early-type dwarfs are suggested to be the remnants of interactions between giant disk galaxies and their environment, leading to a flatter population.

1.4.2 Rotational support

In the context of the fact that dwarfs tend to be flatter than giants the question of rotational support arises. Because, if dwarf ellipticals are flattened by rotation, a reason for their larger rotation velocities would have to be found rather than a explanation for their flattness. Yet, the determination of the dynamics of dwarf ellipticals and their comparison to the one of giants reveals another dichotomy. Most of the giants are indeed flattened by rotation, but the sparse data for dwarfs indicate that they do almost not rotate, i.e. they must by flattened by velocity anisotropy. This is shown in Figure 1.5, where the ellipticity is plotted

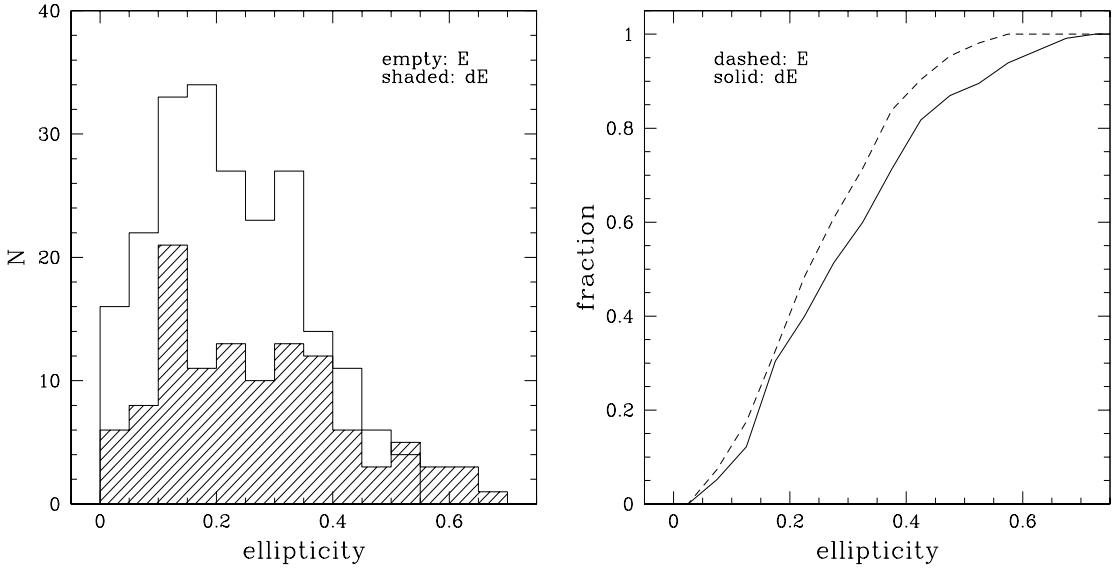

Abbildung 1.4: (*left*) Histogram of the ellipticity distribution for Es and dEs. (*right*) Cumulative distribution function for Es and dEs. Samples are: 217 Es from Franx et al. (1991) and 115 dEs from Binggeli & Jerjen (1998).

versus V_{rot}/σ, with V_{rot} being the rotation velocity and σ the velocity dispersion. The line indicates the theoretical value of V_{rot}/σ, assuming a rotational supported spheroid of corresponding ellipticity. It is evident that the dwarf ellipticals tend to be slow rotators, in contrast to the giants, whereas it is not surprising that dS0s have larger rotation velocities.[1] There are two dEs, which have to be regarded as flattened by rotation, constituting the counter-examples (labeled in the plot). However, IC3328 has a disk, since a spiral structure has been discovered in this galaxy (Jerjen et al. 2000). There remains therefore only FS76 as a normal dE, which is flattened by rotation. Hence, the available data suggest that there is a considerable difference concerning the kinematical status between giant and dwarf ellipticals. On the other hand, a final conclusion cannot be drawn, due to the scarcity of the kinematical data on-hand for dwarf galaxies. In the context of the possible formation processes discussed above the presence of rotating and non-rotating giant ellipticals could be indicative of two different origins. The rotating systems could originate from a gravitational collapse, taking over the angular momentum of the gas cloud and the non-rotating systems might be the result of a merger event, where possible angular momenta of the merging galaxies are destroyed (the merging scenario can, however, not account for dwarfs). Similarly, a disk galaxy could loose the angular momentum during its transformation to a dwarf galaxy in the harassment scenario (Moore et al. 1998).

1.4.3 Surface brightness profiles and isophote shapes

In general, the surface brightness profiles of dwarf galaxies are fitted with an exponential model ($I(r) = I_0 \exp(-r/r_0)$, where I_0 is the central intensity and r_0 is the scale length), which is a straight line in a magnitude representation ($\mu(r) = \mu_0 + 1.086(r/r_0)$, where μ_0 is the central surface brightness). The profiles of bright early-type dwarfs however deviate considerably from such a model, above all in the central parts. They are more similar to the profiles of giant ellipticals, which are usually fitted

[1] Simien & Prugniel (2002) find a similar distribution of dEs and dS0s in their $V_{rot}/\sigma - \epsilon$ plot, using however a luminosity criterion for the dwarfs, whereas I use the morphological classification.

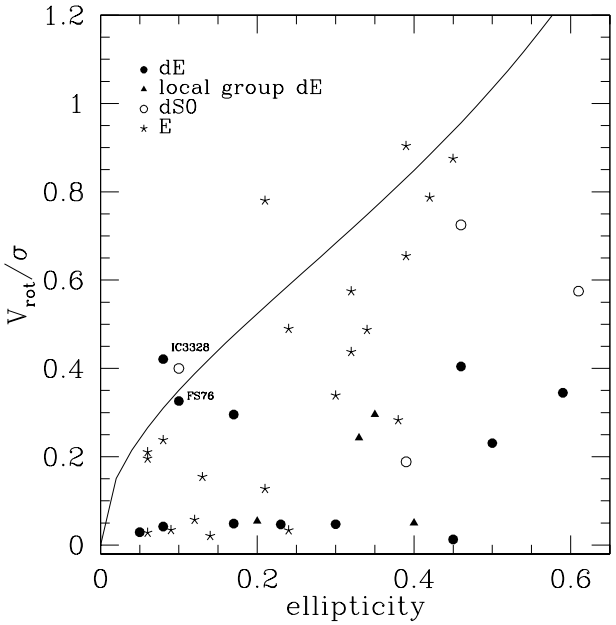

Abbildung 1.5: Plot of the ellipticity versus V_{rot}/σ, where V_{rot} is the rotation velocity and σ the velocity dispersion. The line represents the theoretical prediction of a spheroid flattened by rotation. The data are from: Simien & Prugniel (2002): 8 dE, Geha et al. (2002): 6 dE, Bender et al. (1991): 5 dE, De Rijcke et al. (2001): FS76, de Zeeuw et al. (2002): 21 E

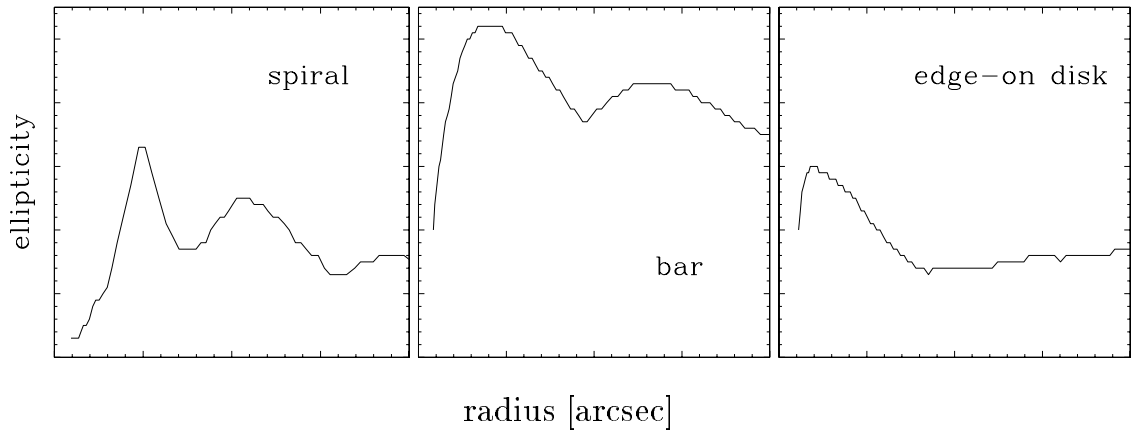

Abbildung 1.6: Three observed ellipticity profiles, sampling the manner in which specific structures leave their traces in the shapes of the isophotes. *left:* IC 783, *middle:* NGC 4431, *right:* IC 3468

with de Vaucouleurs' $r^{1/4}$-law ($\mu(r) \propto (-r/r_0)^{1/4}$). Using a model with three free parameters clearly improves the fit. Therefore a generalized form of the exponential law is commonly applied, which was originally introduced by Sérsic (1968) and where the exponent, n, represents the third free parameter ($\mu(r) \propto (-r/r_0)^n$). This model can indeed be used for different galaxy types (see above), since the exponential- and $r^{1/4}$-law are included, taking $n = 1$ and $n = 0.25$, respectively. Most photometric as well as fit parameters are correlated with the luminosity (but with too large scatters in order to use them as distance indicators (Binggeli & Jerjen 1988)).

Valuable informations about inner structures and the presence of additional components can be obtained by a detailed analysis of the shapes of the isophotes. The basic procedure is the determination of the best-fitting ellipse for each isophote within an appropriate radial range. The parameters of these ellipses, e.g. ellipticity and position angle of the major-axis, and especially their alterations towards the outer parts indicate hidden substructures. This is qualitatively shown in Figure 1.6, by means of real ellipticity profiles of three early-type dwarfs extensively discussed below. The ellipticity variations shown in the left panel are indicative for the presence of a spiral structure. The different peaks coincide with the spiral arms. The pattern in the middle panel is similar, yet the peaks are broader and the whole structure is more flattened, which is evidence for a bar. Finally, in the right panel the short and sharp peak in the inner part of the galaxy might indicate the presence of a central disk, which we happen to observe edge-on. It is important to stress that all these structures are not visible on the optical images, but can be tracked down by this simple means. However, in order that the ellipticity profile is able to provide such insights, the accuracy of the determination of the parameters needed must be very high and likewise the resolution of the frames used. In addition, the search for hidden inner structures cannot be based on this method alone, but must be supplemented with a general analysis of the intensity distribution (e.g. a Fourier decomposition) or an appropriate deconvolution of the images, in order to enhance the features (e.g. unsharp masking). A detailed discussion of these methods and the obtained results can be found in chapter 3.

Another possibility to determine specific characteristics of the isophote shapes is to expand the differences between ellipses and isophotes in a Fourier series. The *sine* and *cosine* parameters obtained provide informations about the specific features of these deviations. In particular the fourth *cosine* para-

meter, commonly denoted as a_4, has turned out to be very significant. It allows to divide the galaxies in two groups according to their isophotal properties: disky, if $a_4 > 0$, or boxy, if $a_4 < 0$. The two different shapes are sketched in Figure 1.7. Galaxies with disky isophotes are usually believed to have a disk component, which is embedded in an elliptical stellar distribution (Rix & White 1990), whereas boxy isophotes might be caused by stars on box orbits. The presence of correlations between these isophotal properties and other parameters of the galaxies have mainly been investigated for giant ellipticals. It turned out that boxy galaxies tend to be more luminous and are more likely strong radio and X-ray sources than disky galaxies (Bender et al. 1989). Moreover, they more frequently show isophotal twists. The distribution of a_4 with respect to ellipticity indicates that strong diskyness/boxyness is only exhibited by more flattened objects, whereas the rounder shaped galaxies have nearly elliptical isophotes (Bender et al. 1989). A similar trend has also been found for early-type dwarfs (Ryden et al. 1999, see below). In addition, almost all disky galaxies are fast rotators, which might be due to the presence of the suspected disk component. Also, disky objects tend to have lower central velocity dispersions, which is furthermore amplified by the fact that they are less luminous, hence less massive. This relation is shown in Figure 1.8, where the shape parameter, expressed as $a_4/a * 100$, where a is the major-axis of the corresponding isophote, is plotted versus the logarithm of the central velocity dispersion for giant ellipticals. The data for eight dwarfs have been added, by arbitrarily shifting the vertical scale (the values for the dwarfs are indicated on the right axis of the panel). Despite the low number of dwarfs, for which data are available, a relation of similar strength like for the giants is evident. However, due to the scarcity of the available data for dwarfs, the significance of the shape parameter a_4 in terms of their structure is still unclear and final conclusions cannot be drawn.

1.4.4 Nuclei

The most apparent feature, present in most bright early-type dwarfs ($M_B < -16$), is a central luminosity excess, commonly identified as the central nucleus (usually a nucleated dE is denoted as dE,N). These nuclei have a stellar appearance and quite different luminosities, the brightest reaching up to 10% of the total light of the parent galaxy (Stiavelli et al. 2001, appendix C). The fraction of nucleated dwarfs decreases with decreasing luminosity. Moreover, considering the distribution of dwarf ellipticals in clusters it turns out that dE,Ns are more concentrated to the cluster centers, i.e. to regions of higher galaxy density, than dEs (Binggeli et al. 1987, Ferguson & Sandage 1989, Conselice et al. 2001). The decision whether a nucleus is present is usually based on a visual evaluation of the optical image and of the central parts

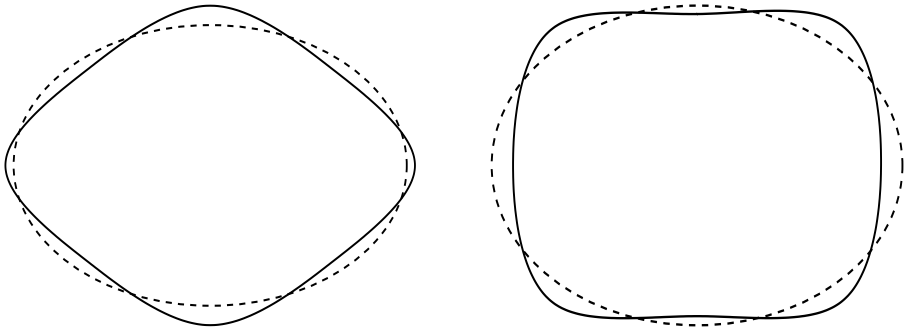

Abbildung 1.7: Qualitative examples of disky (left) and boxy (right) isophotes (solid lines).

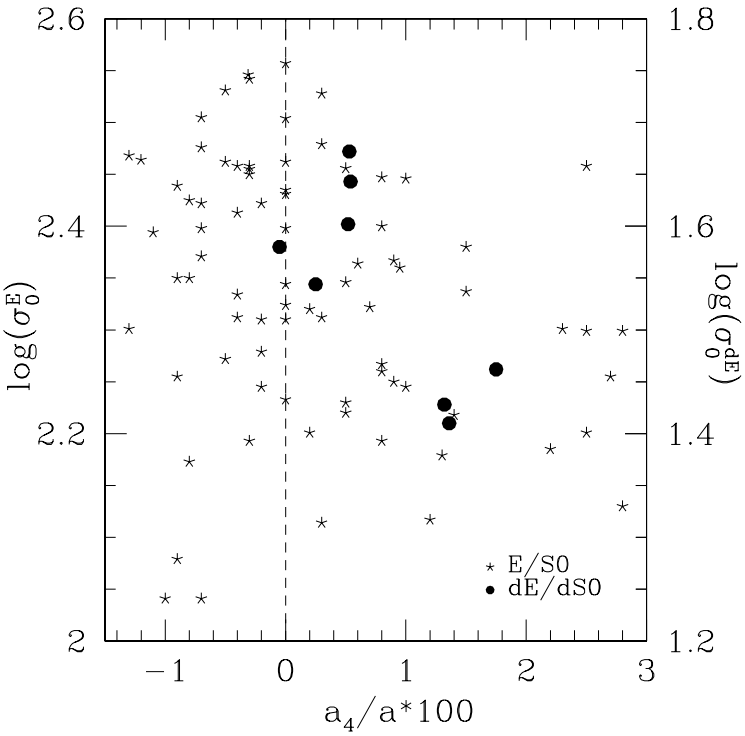

Abbildung 1.8: Shape parameter a_4 in the form $a_4/a{*}100$ (a is the major-axis of the corresponding isophote) versus the logarithm of the central velocity dispersion for giant and dwarf ellipticals. The data for the giants are from Bender et al. (1989). The shape parameters for the dwarfs are from Ryden et al. (1999) or from this thesis. See the caption of Figure 1.5 for the sources of σ_0^{dE}.

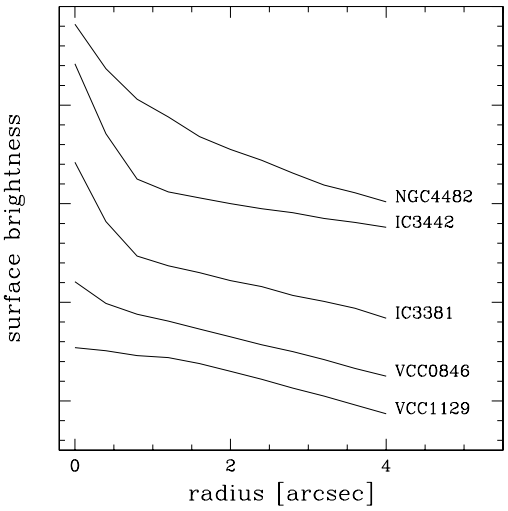

Abbildung 1.9: The central parts of the surface brightness profiles of five dwarf ellipticals. NGC4482, IC3442, and IC3381 are nucleated, VCC0846 is probably nucleated and VCC1129 is not nucleated. The vertical scales have been arbitrarily shifted to obtain a suitable presentation.

of the surface brightness profile. However, the determination is not obvious in all cases. In Figure 1.9 the central part of a selection of five surface brightness profiles is shown, four stem from nucleated dwarfs and one from a non-nucleated object. VCC1129 is clearly non-nucleated, whereas IC3442 and IC3381 have nuclei of different luminosities. The presence of a nucleus in VCC0846 is regarded as uncertain. In view of the quite shallow profile of NGC4482 the central region might be interpreted as bulge rather than as nucleus. However, the nucleus is part of this bright central region, but not as striking as in the fainter dwarfs.

The true nature of the nuclei is still largely unknown. They are commonly regarded as huge compact

star clusters, residing in or near the center of the parent galaxy and being dynamically decoupled from the underlying stellar population. Indeed, the fact that these nuclei can be offset from the center of the overall brightness distribution supports the assumption that they constitute an independent entity. An example of a displaced nucleus is shown in Figure 1.10. It is likely that the nuclei are not at rest in the center of the potential, but oscillate about or even orbit these centers (Miller & Smith 1992, Taga & Iye 1998). In fact, the strength of these movements seems to depend on the compactness of the galaxies and therefore on the depth of the potential well (see below). Regarding the origin of the nuclei there are currently two scenarios under discussion. In the first the nuclei are the result of the last star formation episode, which took place in the center of the galaxy and in which the remaining gas has been used up or blown away (Davies & Phillipps 1988). In the second they stem from the merging of several globular clusters, which sunk to the center of the galaxy through dynamical friction (Oh & Lin 2000, Lotz et al. 2001). However, both scenarios have their shortcomings. If the last starburst is the origin of the nuclei, we would expect a positive colour gradient, i.e. a reddening towards to outer parts, since the nucleus would consist of a younger stellar population, or at least a difference in the colours between the nucleus and the underlying stars. Yet, both does not seem to be the case. The nuclei have essentially the same colour like the host galaxies and the colour gradients are not always positive; in contrast, in our sample most of the galaxies have a negative colour gradient. Supposing the merger scenario, we would expect a lower specific globular cluster frequency for nucleated dEs than for the non-nucleated objects, in particular regarding galaxies with very bright nuclei. But again, this is not the case; on the contrary, the dE,N have a higher specific globular cluster frequency than the dEs (Miller et al. 1998). It is therefore not possible, with the data currently available, to definitely determine the origin of the nuclei in dwarf ellipticals.

1.4.5 Total colours and colour gradients

The colour properties of galaxies are principally a very strong tool in revealing past or ongoing star formation and the evolutionary processes in general. However, besides the mere difficulty in determining accurate colour indices or even colour gradients (in particular for dwarfs), the results obtained are in most cases ambiguous, making their interpretation difficult. Essentially, different stellar populations or different metallicities find their expression in different colours: redder indicates a higher metallicity or an older stellar population. In addition, the presence of dust strongly affects the colours, causing a signi-

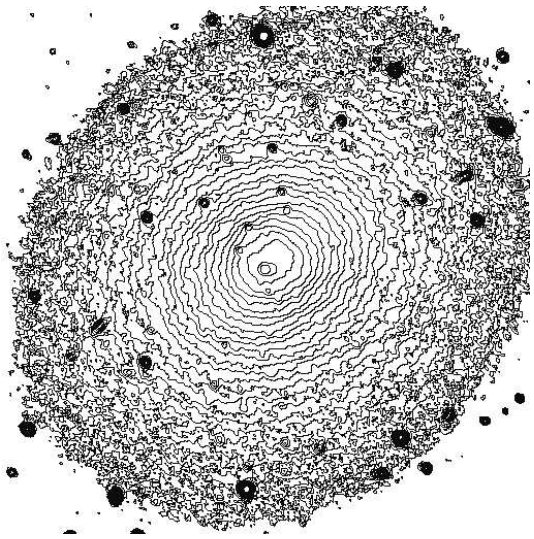

Abbildung 1.10: Isophotes of IC3019 starting at 21 mag with spacings of 0.1 mag.

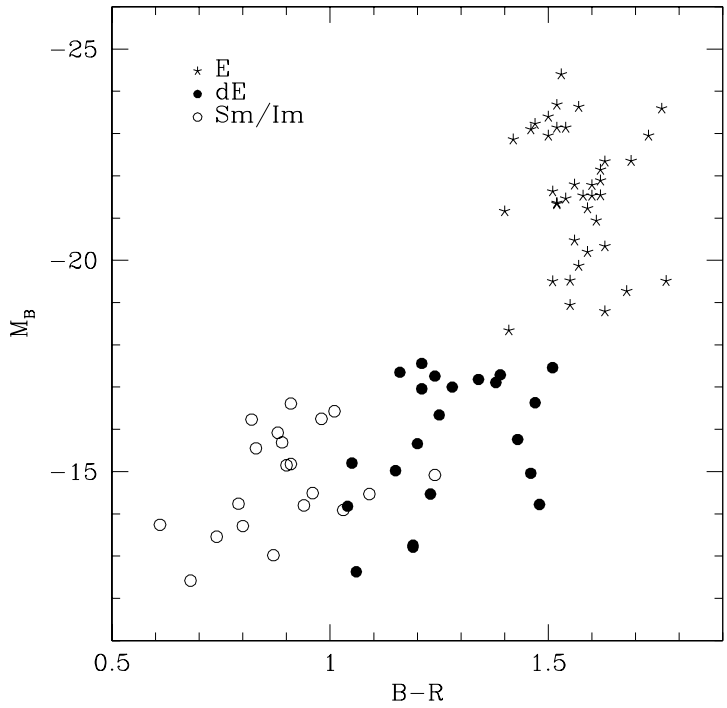

Abbildung 1.11: The colour-magnitude relation for different types of stellar systems. The sources are: E: Peletier et al. (1990), dE: this study, Sm/Im: Parodi et al. (2002).

ficant reddening. Despite these uncertainties, the colour properties are widely used to explore specific features of galaxies, also because their interpretation can be constrained by independent measures. The colour-magnitude relation, as an illustration, is a well known property shared by different types of stellar systems; an example is shown in Figure 1.11. Obviously, brighter galaxies tend to be redder, which can be due to age (i.e. an older stellar population), to a higher metallicity or even to the presence of dust. With the colour information alone it is not possible to discriminate between these different effects. Nevertheless, taking into account all relevant characteristics of the different galaxy types, the connections become more evident. Hence, the fact that Es are redder than dEs is interpreted as metallicity effect: the stronger gravitational potentials of giants protect them more effectively from considerable mass losses and they can therefore not only better prevent the outflow of metals, but they are also able to enrich their interstellar medium more strongly with heavy elements. On the other hand the colour difference between early and late-type dwarfs is believed to be due to different stellar populations. Indeed, in contrast to dwarf ellipticals, dwarf irregulars possess substantial amounts of gas, leading to ongoing star formation and to the presence of a young (i.e. blue) stellar population. These interpretations are eased by the fact that the amount of dust is assumed to be small in giant ellipticals and close to zero in dwarf ellipticals.

Total apparent colours can only provide the colour properties of the dwarfs in broad outlines. In order to obtain a more detailed view in this context, the determination of radial colour gradients has turned out to be a useful tool. In fact, the different galaxy classes exhibit in general different radial colour gradients, which can also be interpreted in terms of different evolutionary processes. Hence, spiral galaxies have a negative or blue colour gradient (i.e. they become bluer towards the outer parts), which is due to the old (red) stellar population in the bulge and the star forming activities in the spiral arms. On the other hand, in giant ellipticals having normally the same gradient, the change of colour is not caused by different stellar populations but reflects a metallicity gradient. The strong gravitational potential inherent in these

galaxies allows the re-processing of the available interstellar medium (ISM) for several times, leading to a considerable enrichment of the ISM with heavy elements particularly in the central parts (Saglia et al. 2000). Therefore the metallicity is much higher in the center than in the outer parts, which is expressed by the negative colour gradient. Dwarf ellipticals however are usually found to have positive colour gradients (Vader et al. 1988). Since these less massive systems will suffer from significant mass losses during their star formation phases, they will not be able to enrich their ISM as strong as the giants and therefore the different stellar populations will dominate their colour properties. In the center, where the gravitational potential is the strongest, the galaxy will be able to accumulate most of the gas and maintain star formation for a longer time than in the outer parts. This leads to a centrally concentrated young stellar population and thus to a positive colour gradient. We will see below, however, that the connections seem to be much more complex than this.

1.5 Aim and outline of this thesis

As exemplified above, there are some reasons to believe that, despite their morphological similarities, dEs constitute a different class of stellar systems than giant ellipticals. Hence, the properties applying for Es cannot be extrapolated to dEs. Moreover, the group of objects commonly classified as dEs does not seem to be as homogeneous as believed so far. There is evidence that besides the "normal" dEs, characterised by a rather uniform stellar distribution and just a possible nucleus as substructure, a more complex subgroup of dEs might exist. In fact, such objects could be found in clusters as results of transformation processes of infalling disk galaxies. Due to there specific origin this kind of dE might not be found in galaxy groups and their study might therefore be restricted to the dense regions of galaxy clusters. However, further knowledge of the evolution of galaxy clusters in general could be obtained by finding clear evidence that a large fraction of early-type dwarfs in clusters are former disk galaxies and have to be distinguished from most dEs in groups. This thesis is aimed at the search of such evidence and at the description of the specific properties of the corresponding objects.

With the observational data of exceptional quality, collected with the VLT in B- and R-filters, at hand, I performed an accurate photometric exploration and a detailed isophotal analysis of 25 early-type dwarf galaxies in the Virgo cluster. Main objective of the photometry was to determine, whether the surface brightness profiles of the mostly bright dEs in the sample can also be well fitted with a Sérsic model (Sérsic 1968) like the Es. It seems that in the Sérsic representation the dEs indeed continue the sequence of the Es towards smaller luminosities (Jerjen & Binggeli 1997). However, if the profiles of dEs exhibit significant deviations from the models, these dwarfs cannot be regarded as the scaled down versions of giants. I looked for such deviations and for possible relations to other properties of the dEs.

The isophotal analysis was performed in order to study the deviations of the isophotes from pure ellipses as well as the location of the nuclei, present in most of the dEs, with respect to the brightness distribution. In addition, I looked for isophotal twists and discuss their possible origins. The results obtained indicate that several dEs in the sample have a more complex structure. By means of a Fourier decomposition and a specific version of unsharp masking I could confirm the presence of disk features in four dEs.

The study of the colours was expected to yield indications of the stellar content of the dwarfs and, in particular, to clarify the differences to dEs in groups. The VLT data have therefore been supplemented with data taken at the Danish-1.5 m Telescope in the U-filter. In particular, I studied the colour gradients and found a relation to the total colour index, confirming an earlier result (Pierini 2002). Surprisingly, the colour analysis even provided informations about the influence of star formation events on the inter-

stellar material of dEs and, hence, its enrichment with heavy elements. The fact, that the impacts of star formation are still observable in galaxies, which are mainly composed of old stars, puts strong constrains on possible formation and transformation scenarios.

- **Chapter 2:** VLT surface photometry and isophotal analysis of early-type dwarf galaxies in the Virgo cluster (paper submitted to A&A)
  Describes the photometry and the isophotal analysis as well as parts of the observations and the reduction procedures of the VLT-sample. In addition, all relevant data and parameters of the galaxies are given.

- **Chapter 3:** More evidence for hidden spiral and bar features in bright early-type dwarf galaxies (Barazza, Binggeli & Jerjen 2002, A&A, 391, 823)
  Presents the discovery of disk structures in four objects and describes a Fourier decomposition of the galaxy light as well as a special version of unsharp masking as tools for the image processing. Simulations, performed in order to test the reliability of the Fourier decomposition are shown in appendix A.

- **Chapter 4:** Colour properties of early-type dwarf galaxies
  Describes the colour study and the observations of the La Silla-sample. The other photometric parameters of this sample are given in appendix B.

- **Chapter 5:** Concluding remarks
  The concluding remarks are presented, which also take into account the earlier study of off-center nuclei in dENs (appendix C) and the metallicity-flattening relation (appendix D).

- **Appendix A:** The bar in IC779 and simulations of Fourier transformations
  Shows evidence for a bar in a dE of the Canes Venatici cloud and presents the simulations performed to examine the reliability of the used Fourier decomposition in chapter 3.

- **Appendix B:** Basic data and photometric parameters of the La Silla sample

- **Appendix C:** Off-center nuclei in dwarf elliptical galaxies (Binggeli, Barazza & Jerjen 2000, A&A, 359, 447)
  An earlier study of the location of nuclei with respect to the brightness distribution in dEs.

- **Appendix D:** A metallicity-flattening relation for dwarf elliptical galaxies (Barazza & Binggeli 2002, A&A, 394, L15)
  Presents a surprising discovery in the course of the colour study.

2
VLT surface photometry and isophotal analysis of early-type dwarfs in the Virgo cluster

Abstract

We have carried out surface photometry and an isophotal analysis for a sample of 25 early-type dwarf (dE and dS0) galaxies in the Virgo cluster based on CCD images taken at the VLT with FORS1 and FORS2. For each galaxy we present B and R-band surface brightness profiles, as well as the radial colour ($B-R$) profile. We further give total apparent BR magnitudes, effective radii, effective surface brightnesses and total colour indices. The light profiles have been fitted with S´ersic models and the corresponding parameters are compared to the ones for other classes of objects. In general, dEs and dS0s bridge the gap in parameter space between the giant ellipticals and the low-luminosity dwarf spheroidals in the Local Group, in accordance with previous findings. However, the observed profiles of the brightest cluster dwarfs show significant deviations from a simple S´ersic model, indicating that there is more inner structure than just a nucleus. This picture is reinforced by our isophotal analysis where complex radial dependencies of ellipticity, position angle, and isophotal shape parameter a_4 are exhibited not only by objects like IC3328, for which the presence of a disk component has been confirmed, but by many apparently normal dEs as well. In addition, we find a relation between the effective surface brightness (or effective radius) and the strength of the offset of the galaxy's nucleus with respect to the center of the isophotes. Dwarfs with large nuclear offsets also tend to have stronger isophotal twists. However, such twists are preferentially found in apparently round ($\epsilon < 0.3$) galaxies and are always accompanied by significant radial changes of the ellipticity, which is clearly pointing to a projection effect. In sum, our findings suggest the presence of substructure in most, and preferentially in the less compact, bright early-type dwarfs. The physical (dynamical) meaning of this has yet to be explored.

2.1 Introduction

Dwarf elliptical galaxies (hereafter dEs, subsuming "dwarf spheroidals" and dwarf S0s) are by far the most numerous type of galaxies in the local universe (see Ferguson & Binggeli (1994) for a review).

As they prefer the high density environment of galaxy clusters, the most suitable places for their study are the two nearest clusters in Virgo and Fornax, where catalogues of dEs have been established as part of extensive surveys (Binggeli et al. 1985, hereafter VCC; Ferguson 1989). The numerical dominance of dEs in these two galaxy aggregates is evident in the studies of the corresponding galaxy luminosity functions (Sandage et al. 1985, Ferguson & Sandage 1988). A host of photographic and CCD studies of Virgo and Fornax dwarfs in the eighties and early nineties led the fundament to our knowledge of the basic photometric properties of dwarf ellipticals (Caldwell 1983, Binggeli et al. 1984, Bothun et al. 1986, Caldwell & Bothun 1987, Binggeli & Cameron 1991, 1993). Little dE photometry was added to this until recently. Ryden et al. (1999), still working with low-resolution CCD images, went a step further by analyzing the isophotal shapes of a large sample of dEs, finding many dwarfs to be "disky" and "boxy" just as the giants. Miller et al. (1998) observed 24 Virgo dwarfs with the HST to derive the specific Globular Cluster Frequency (S_N) for dEs. Based on the same high-resolution HST images, Stiavelli et al. (2001) analyzed the innermost regions (cusp slopes) of these galaxies. However, it proved difficult to connect the central properties with the *global* dwarf structures; the drawback of HST here is clearly the small field of view.

On the other hand, enormous progress has recently been achieved at the kinematic "frontline". After almost a decade of stagnation in kinematic measurements (see Ferguson & Binggeli 1994), several groups are now reporting their (partially conflicting) results on the (non-) rotational properties of early-type dwarfs. For instance, Geha et al. (2001) used Keck II to measure rotation profiles for six Virgo dwarfs. No evidence for significant rotation was found among the target objects. A similar programme is being run at the VLT (de Rijcke et al. 2002). The earlier conjecture that dwarf ellipticals in general are not rotation-supported is definitively confirmed by these studies (also Thomas et al. 2003). However, it has also become clear that among the brightest cluster early-type dwarfs, in particular the dS0s, there are many rotation-supported systems (Simien & Prugniel 2002).

There are also *photometric* hints at the existence of disk galaxies among the bright cluster early-type dwarfs. Jerjen, Kalnajs & Binggeli (2000, 2001) discovered weak spiral structures and a bar in two Virgo dEs and subsequently Barazza et al. (2002) found spiral and bar features in three additional objects. These findings are in fact based on the same VLT images for which surface photometry is presented in the present paper. Deep, high-resolution VLT imaging, providing a sufficiently large field of view, is certainly ideally suited for the study of the photometric properties of Virgo and Fornax dEs. With the present surface photometry and isophotal analysis of 25 early-type Virgo dwarfs based on high-quality B and R VLT images we aim at a more systematic exploration of the structural complexity of dwarf ellipticals. We especially address the question whether a Sérsic model is an appropriate representation of the empirical surface brightness profiles of dEs. The isophotal analysis is used to derive ellipticity, position angle and isophotal shape profiles. In addition, we map nuclear offsets and isophotal twists of the sample dEs. Overall, our findings show that these seemingly dull stellar systems are quite complex in structure. Dwarf elliptical galaxies are neither the scaled down version of giant ellipticals nor simply the final state of a star forming dwarf irregular galaxy that has converted all its gas into stars.

The plan of this paper is as follows. In Sect. 2.2 we introduce the dwarf galaxy sample and provide some global photometric parameters. The data reduction and photometric calibration are described in Sect. 2.3. Sect. 2.4 and 2.5 are dedicated to the surface photometry and the isophotal analysis. The discussion and summary is given in Sect. 2.6.

2.2 Sample and observations

The dE galaxies studied here were originally chosen from the Virgo Cluster Catalog (VCC; Binggeli et al. 1985) for the purpose of measuring their distances by means of the Surface Brightness Fluctuation method to explore the 3-dimensional structure of the Virgo cluster (Jerjen et al. 2003). As it is a main requirement for the successful application of this method, galaxies were primarily selected on their morphological appearance, i.e. type "dE" or "dS0", and on their apparent size, i.e. an isophotal radius $r_{B,25} > 30''$. Within these constraints, the sample was selected in a way to get a good coverage in velocity space ($-730\,\mathrm{km\,s^{-1}} < V_\odot < 1850\,\mathrm{km\,s^{-1}}$) and in the celestial distribution ($12^h09^m <$ R.A.(2000) $< 12^h32^m$; $+08^\circ26' <$ Decl.(2000) $< +15^\circ45'$). The core sample contained 16 bright early-type dwarfs which, however, could be increased by 9 more dwarfs, as these happened to lie in the field of view of the CCD. Among these are five rather faint dwarfs (VCC0850, VCC0962, VCC0998, VCC1093, VCC1129). The total sample considered here comprises therefore 25 objects, 22 of which were imaged in B and R filters (or R_s, which is the corresponding filter used on FORS2; in the following we only use R) and three (IC3303, IC3518, UGC7854) in R only.

The images were obtained using the first two units of the Very Large Telescope (VLT) at ESO Paranal Observatory in service mode over a period of two semesters: at UT1+FORS1 (Antu) during an observing run on July 10-14, 1999 and at UT2+FORS2 (Kueyen) during dark time periods in March-May 2000. The detectors of the FORS (FOcal Reducer/Low dispersion Spectrograph) instruments are thinned and anti-reflection-coated Tektronix (FORS1) and SiTE (FORS2) CCDs with 2048×2048 pixels. By default, service observations were taken in standard resolution mode, with a high gain and a pixel scale of $0\farcs2$ pixel^{-1} that yields a field of view of $6\farcm8 \times 6\farcm8$. The CCDs were read out in the four-port mode, i.e. four amplifiers read out one quarter of the CCD each. Three exposures of $400 - 600$ sec durations with slightly different pointings were secured in each filter for each galaxy. More details of the observations are to be reported elsewhere (Jerjen et al., in preparation). The basic properties of the sample galaxies are listed in Table 2.1. The columns are as follows:

columns (1) and (2): identifications of the galaxies; for the coordinates see VCC.

column (3): morphological type in the classification system of Sandage & Binggeli (1984), taken from the VCC;

column (4): absolute B-band magnitude, based on the apparent magnitude given in column 6 and a mean Virgo cluster distance of 17 Mpc;

column (5): heliocentric radial velocity in km s^{-1} (from the VCC and Binggeli et al. 1993, except for VCC0928, where the value of Conselice et al. 2001 is given).

The following entries are from the photometry presented below (Sect. 2.4). We give their meaning here as well. It should be noted that *all values in magnitudes are corrected for galactic extinction* using the maps of Schlegel et al. (1998). Values with a colon are uncertain.

columns (6) and (9): total apparent magnitude in B and R, respectively;

columns (7) and (10): effective radius in arcsec [$''$] in B and R, respectively;

columns (8) and (11): effective surface brightnesses in B [mag/$\Box''$] and R [mag/$\Box''$], respectively;

columns (12): total (mean) $B - R$ colour index.

The mean absolute magnitude in B for all dwarfs is $\langle M_{B_T} \rangle = -15.76$. Taking only the 16 dwarfs originally selected into account (without the five faint objects mentioned above) we get $\langle M_{B_T} \rangle = -16.42$, which is indeed rather bright for dwarf galaxies. The mean colour of the sample is $\langle B-R \rangle = 1.27$. This is quite blue for early-type dwarfs, but there are three very blue outliers whose colour might be affected by other objects: parts of VCC0962 ($B - R = 1.04$) are hidden by a bright foreground star, VCC0815 ($B-R = 1.05$) probably has a bright background object near its nucleus, and VCC0850 ($B-R = 1.06$)

Tabelle 2.1: Basic data and model-free parameters of the early-type dwarfs considered in this study (extinction-corrected)

VCC (1)	Name (2)	Type (3)	M_{B_T} (4)	$v_\odot$ (5)	B_T (6)	r^B_{eff} (7)	μ^B_{eff} (8)	R_T (9)	r^R_{eff} (10)	μ^R_{eff} (11)	$B-R$ (12)	Notes
0009	IC3019	dE1,N	−17.11	1804	14.04	30.81	23.48	12.66	34.48	22.35	1.38	a
0490	IC0783	dS0(3),N	−17.18	1293	13.97	27.31	23.15	12.63	28.35	21.89	1.34	b
0781	IC3303	dS0(5),N:		−254				13.56	10.30	20.62		
0810		dE0,N	−14.47	−340	16.68	9.92	23.66	15.45	9.94	22.44	1.23	
0815		dE2, N	−15.20:	−700	15.95:	13.54:	23.61:	14.90:	12.93:	22.46:	1.05:	
0846		dE1,N:	−14.96	−730	16.19	12.35	23.65	14.73	15.35	22.66	1.46	
0850		dE,N	−12.63:		18.52:	8.81:	25.24:	17.46:	8.27:	24.05:	1.06:	c
0856	IC3328	dE1,N	−16.96	972	14.19	20.66	22.76	12.98	18.07	21.26	1.21	d
0928		dE6,N	−15.02	−254	16.13	9.11	22.93	14.98	8.60	21.65	1.15	
0929	NGC4415	d:E1,N	−17.46	910	13.69	19.26	22.11	12.18	20.72	20.76	1.51	
0940	IC3349	dE1,N	−16.34	1563	14.81	19.42	23.25	13.56	18.35	21.88	1.25	b
0962		dE3	−14.18:		16.97:	22.00:	25.68:	15.93:	17.90:	24.19:	1.04:	
0998		dE4,N:	−13.21		17.94	11.37	25.22	16.75	11.11	23.98	1.19	
1010	NGC4431	dS0(5),N	−17.29	913	13.86	17.23	22.04	12.47	17.05	20.63	1.39	b
1036	NGC4436	dE6/dS0(6),N	−17.26	1163	13.89	16.37	21.96	12.65	14.90	20.51	1.24	
1087	IC3381	dE3,N	−17.00	645	14.15	19.35	22.58	12.87	18.06	21.15	1.28	
1093		dE0,N	−14.22		16.93	12.23	24.37	15.45	14.34	23.23	1.48	
1104	IC3388	dE5,N	−15.66	1704	15.49	11.76	22.84	14.29	11.30	21.56	1.20	e
1129		dE3	−13.26		17.89	7.56	24.28	16.70	7.43	23.05	1.19	
1254		dE0,N	−15.76	1350	15.39	15.11	23.29	13.96	14.74	21.80	1.43	f
1261	NGC4482	d:E5,N	−17.56	1850	13.59	19.18	22.00	12.38	18.91	20.76	1.21	
1355	IC3442	dE2,N	−16.63	1332	14.52	30.80	23.96	13.05	36.83	22.88	1.47	
1422	IC3468	E1,N:	−17.35	1372	13.80	20.34	22.34	12.64	18.95	21.03	1.16	b
1567	IC3518	dE5/dS0(5),N		1440				13.25	26.12	22.33		g
1895	UGC7854	d:E6		1032				13.80	11.51	21.11		

Values followed by a colon have to be considered as uncertain due to disturbing background or foreground objects.

[a] Whether this galaxy is really nucleated is not clear. The object considered as nucleus is very faint and largely off-centered. It could therefore also be a bright globular cluster which in projection happens to lie close to the center. In the VCC the galaxy is classified as dE,N, whereas Miller et al. (1998) regard it as non-nucleated. Stiavelli et al. (2001) present a HST observation of this galaxy and provide the results of different profile fits as well as the determination of the nuclear cusp slope.

[b] disk features discovered (Barazza et al. 2002)

[c] The VCC type of this galaxy, which heavily overlaps with VCC0846, is ImIV? We suggest a reclassification as dE,N. In support of this, the galaxy has not been detected in the HI survey of Hoffman et al. (1989).

[d] spiral structure discovered (Jerjen et al. 2000)

[e] As part of the Hubble Space Telescope (HST) key project the luminosity of the tip of the red-giant branch (TRGB) for this galaxy has been determined (Harris et al. 1998): $I_{TRGB} = 26.82 \pm 0.06$. The corresponding distance is $d = 15.7 \pm 1.5$ Mpc (using $M_I^{TRGB} = -4.2 \pm 01$).

[f] A velocity profile has recently been derived by Geha et al. (2001), showing that this galaxy is not rotating.

[g] This galaxy could not be fully integrated, since its shape is strongly non-elliptical. The values given are estimates, using $B_T = 14.52$ from Binggeli & Cameron (1993) and our $\langle B-R \rangle = 1.27$.

is partially overlapping with VCC0846. Excluding these three dwarfs we get $\langle B-R \rangle = 1.30$.

2.3 Photometric procedures

The image reduction and data analysis were performed with ESO's MIDAS package. Three exposures were available for each science field. Before combining them, the three frames were bias-subtracted and flat-fielded. Cosmic rays were removed by taking the median of the three pre-reduced exposures. As the quality of the twilight flats provided was not very satisfactory, we were forced to improve the flatness of some of the backgrounds. The problem became obvious when we tried to do the usual way of sky subtraction by fitting a tilted plane to sky regions on the frame outside the domain of the galaxies, and as unaffected as possible by foreground stars: strong intensity gradients remained in the background of many images, above all in the R (or R_s) frames, obviously being due to improper flat-fielding, i.e. improper flat fields in R (or R_s). To tackle the problem, we decided to fit polynomials up to the third order to the backgrounds, in order to get rid of the strongest gradients. This can of course be quite dangerous in cases where the galaxy covers a substantial part of the frame, leaving only small parts for the fitting procedure. If the fitting procedure is thus affected by the galaxy, there will be a maximum in the resulting background at the position of the galaxy. Such a polynomial would introduce a much larger uncertainty in the resulting image than a simple tilted plane solution. We therefore checked all fitted high-order backgrounds for possible contaminations with the galaxy (correlations with the galaxy position) and reduced the sky-regions used where necessary until we had convinced ourselves that the best possible solution was found. Any remaining gradient in the background was then finally removed by fitting, and subtracting, a second sky model, this time a tilted plane in all cases. The gradient of this plane together with the mean intensity of the background subtracted allowed us to quantify, up to which surface brightness the background is reliably determined. The corresponding values (in $\mathrm{mag}/\Box''$) for the sample galaxies are given in columns 3 and 4 of Table 2.2 for the B and R frames, respectively.

Next the frames were cleaned from disturbing foreground stars or background galaxies. The regions around the galaxies were automatically cleaned with an algorithm designed for this purpose, whereas objects on the galaxy itself were erased by hand.

For the zero-pointing we used standard stars from Landolt (1992). The fields with the standard stars had been imaged several times during the observing nights. We could therefore determine the zero point and extinction parameters for each night separately. The center, as well as the ellipticity and position angle of the major axis for each galaxy were determined at the isophotal level of $\sim 25\mathrm{mag}/\Box''$ by means of the ellipse fitting routine FIT/ELL3. These parameters were then used to obtain a growth curve (integrated light profile) by integrating the galaxy light in elliptical apertures of fixed center, ellipticity and position angle of the major axis. Some bright galaxies in our sample could not be integrated completely in this way because they had not been placed at the center of the frame, but slightly off in order to have enough regions for the background fitting. In these cases we integrated the *outer parts* of the galaxy only in one quadrant (obviously the one opposite to the quadrant containing the center) and extrapolated the results to the whole galaxy. In Table 2.2, columns 5 and 6 we give the equivalent (*maximum*) radii for the B and R frames, respectively, up to which a full integration was possible. A ∞-sign indicates that the whole galaxy is on the frame. In the case of VCC1254 only one quadrant was used for the whole galaxy, as it is located very close to the giant M49.

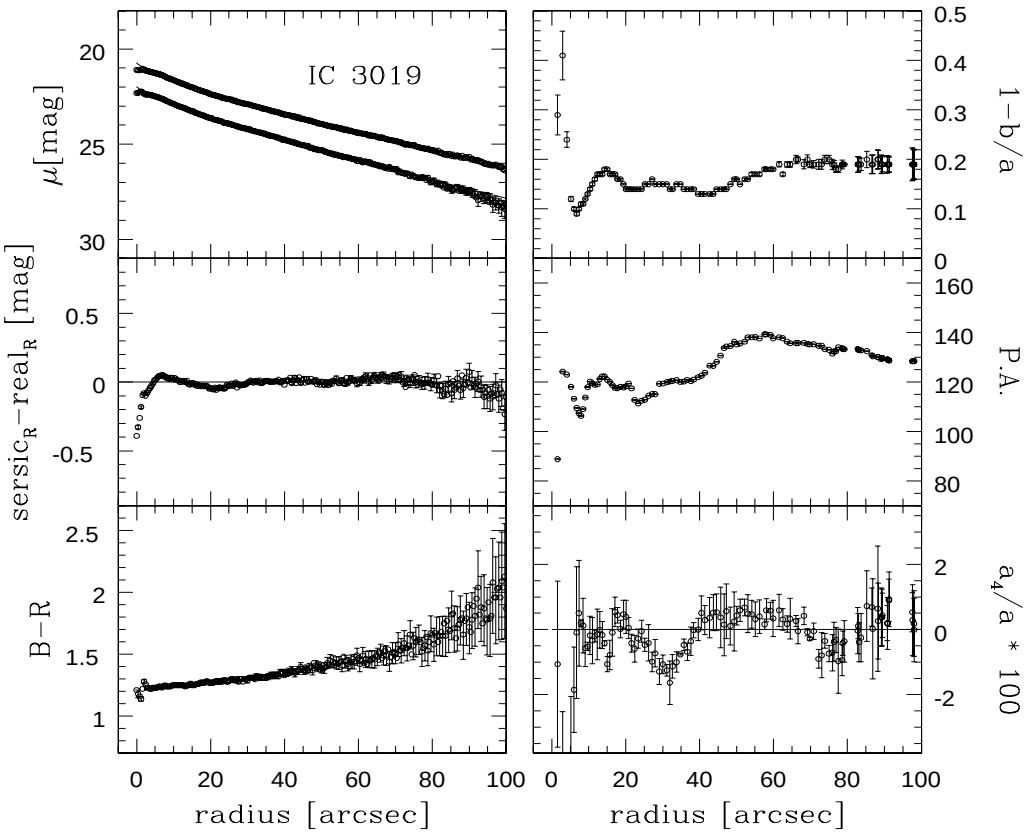

Abbildung 2.12: Plots of the basic parameters for the photometry and the isophotal analysis versus equivalent radius $\sqrt{ab}$, where a and b are the major- and minor-axis, respectively. For the errors of the photometric parameters (left column) the remaining gradient on the frames after the flat-fielding and the amount of the background subtracted have been taken into account. The fact that in some cases only a quarter of the galaxy light in the outer parts could be integrated is not considered in the error estimates. Error bars are only shown for every other data point. The errors of the isophotal parameters (right column) have been derived by means of a Fourier expansion (for details see Bender & Möllenhoff 1987). Ellipses have only been fitted to isophotes completely present on the frames. The error bars are mostly smaller than the plot symbols.

upper left: surface brightness profiles in B (lower curve, where available) and R (upper curve). Error bars are only shown for the profile in B (or in R, if B is not available). A tick mark indicates the confidence limit of our photometry in R (Table 2.2, column 3), if not present, it roughly corresponds to the right margin of the plot;

middle left: model profile (from a Sérsic fit) minus profile observed in R;

lower left: $B - R$ colour-profile;

upper right: ellipticity profile in R;

middle right: profile of the position angle of the major-axis in R, from top counterclockwise;

lower right: the profile of the isophotal shape parameter a_4 in R expressed as $a_4/a * 100$, where a is the length of the major-axis of the corresponding isophote.

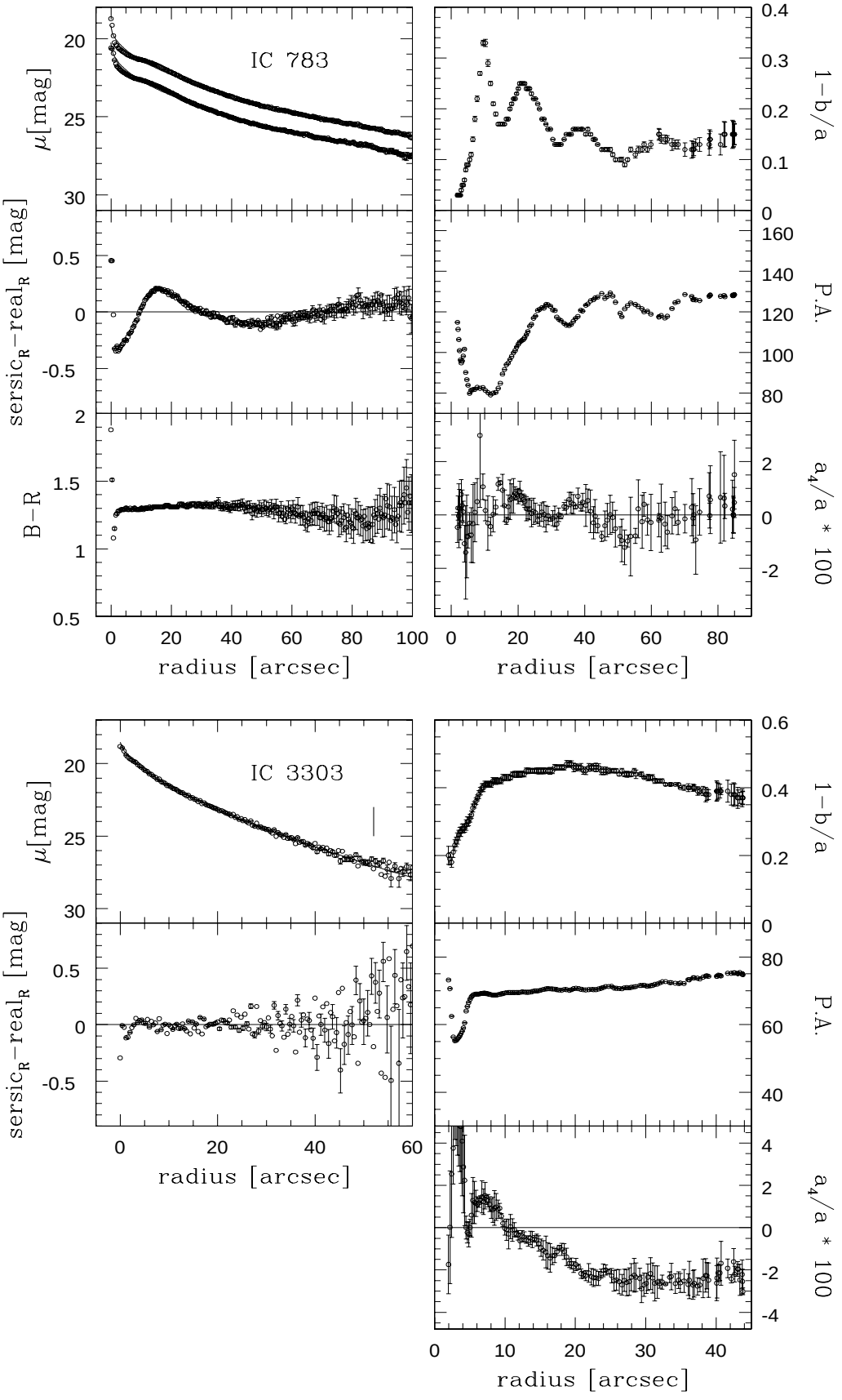

Figure 2.12 continued

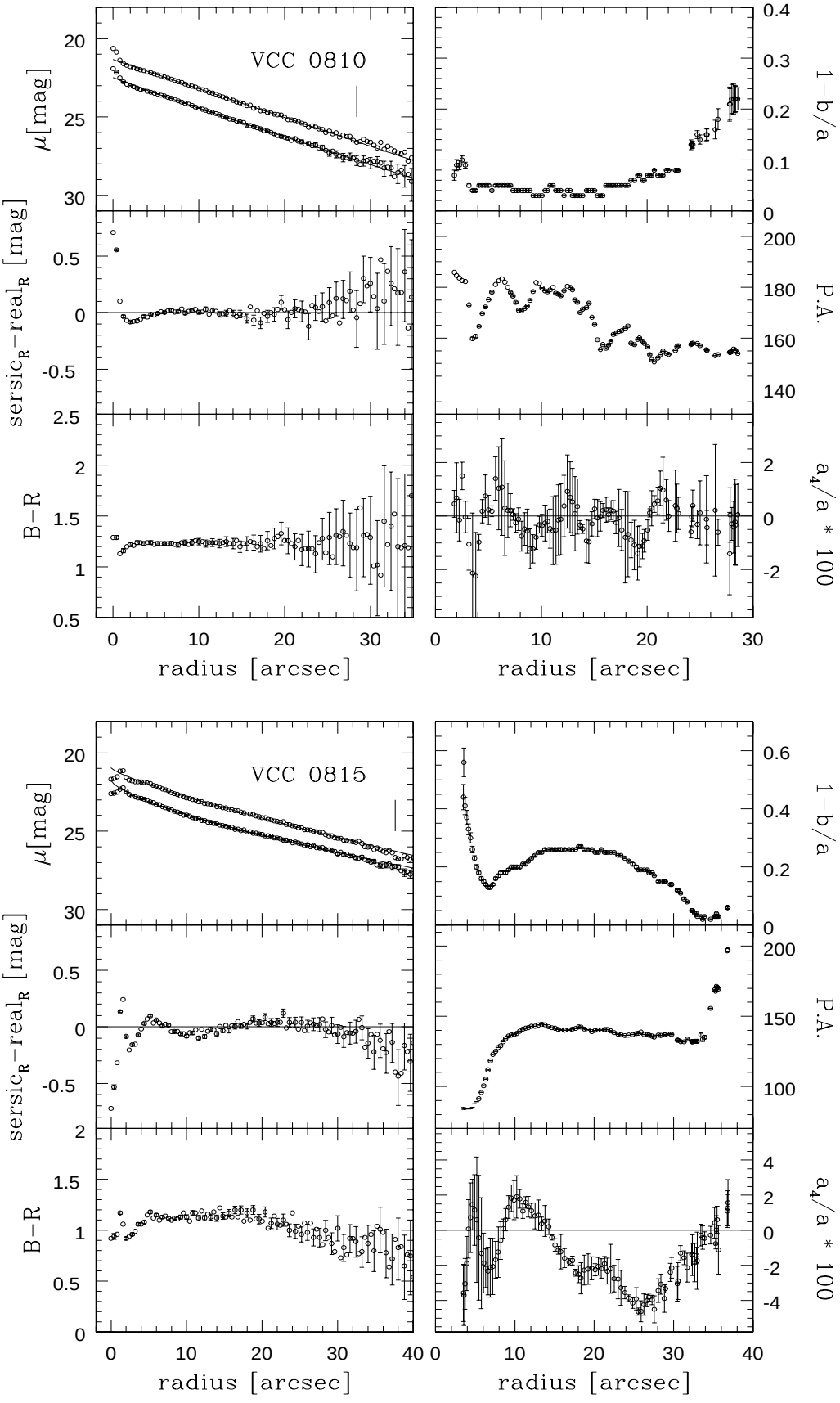

Figure 2.12 continued

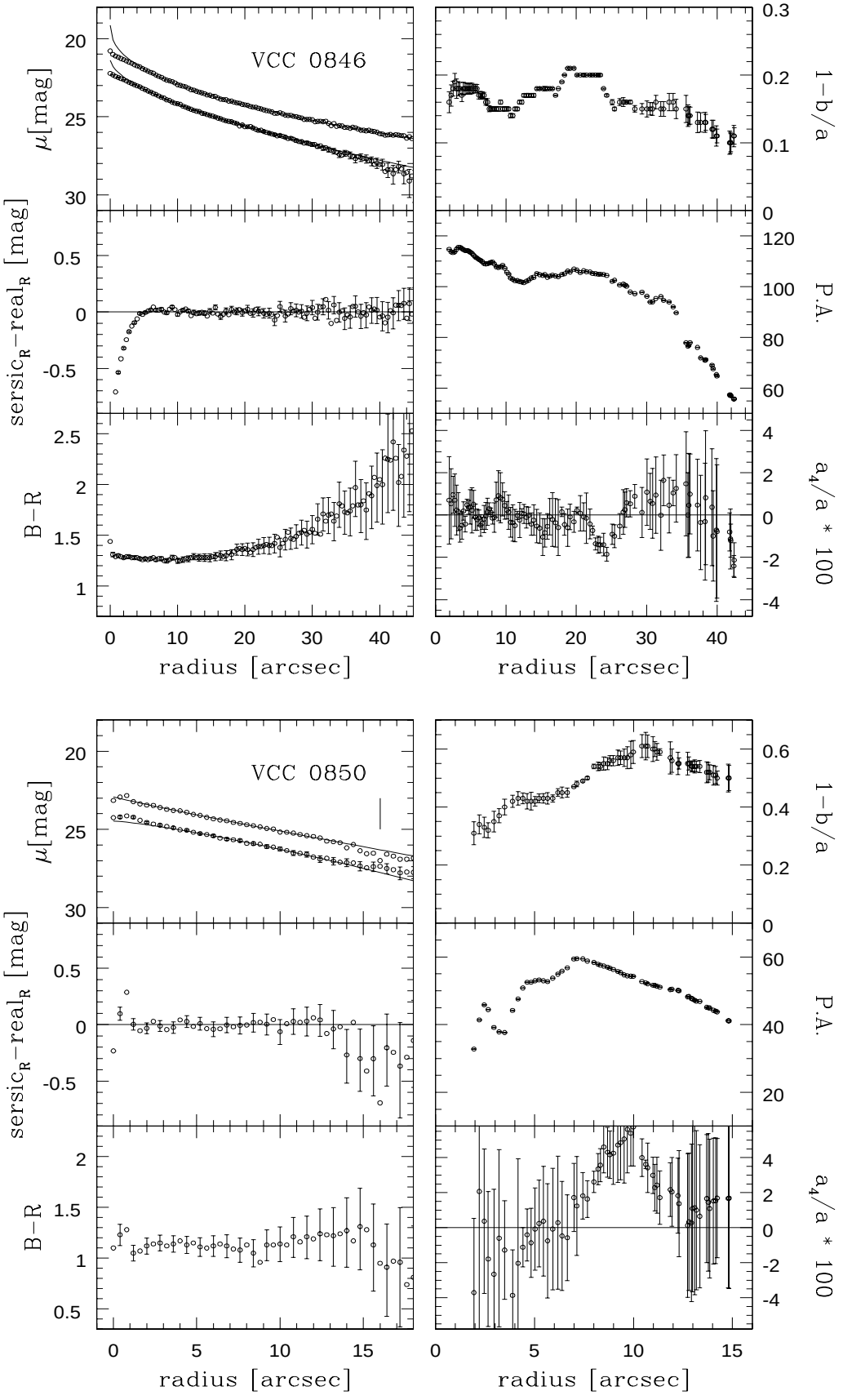

Figure 2.12 continued

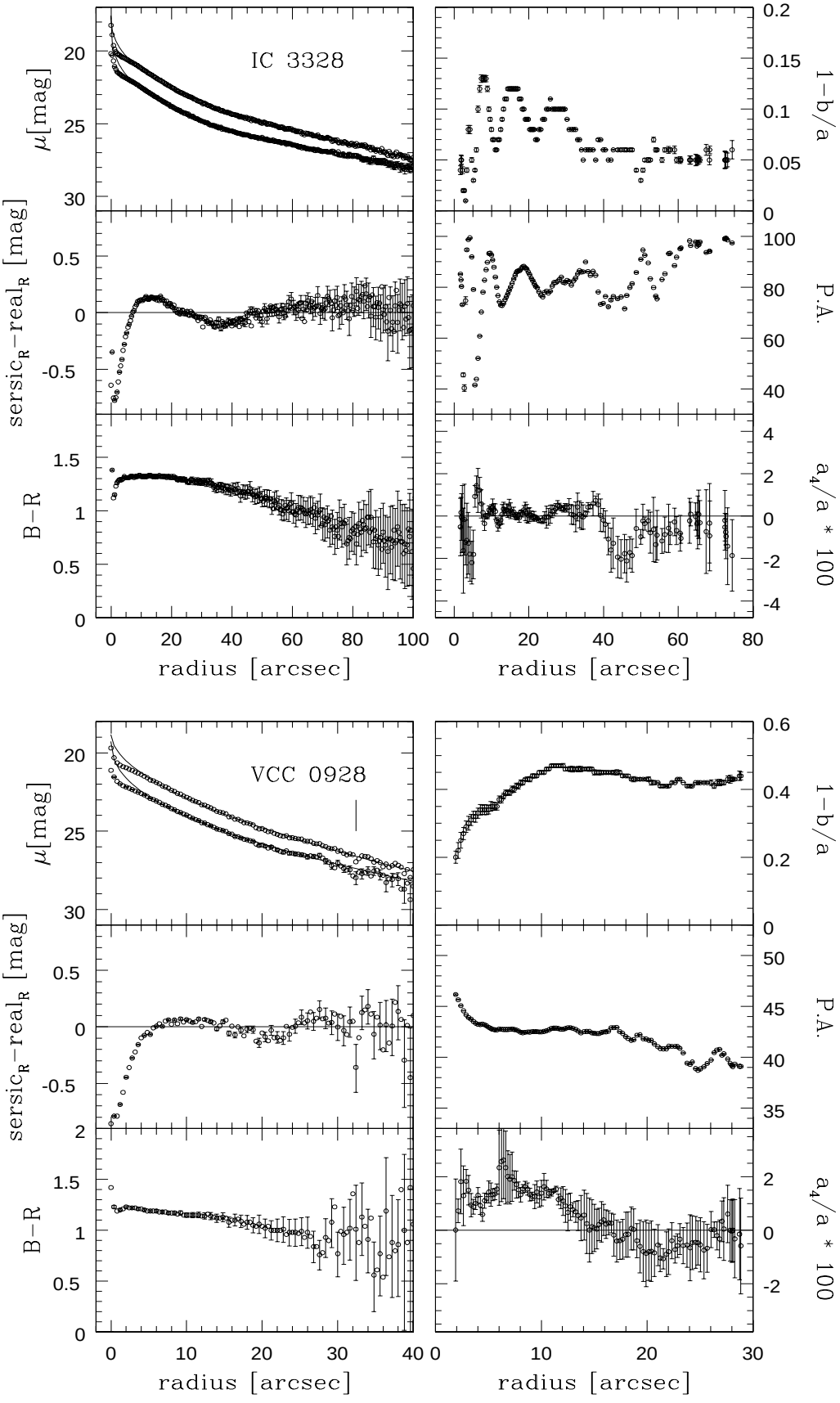

Figure 2.12 continued

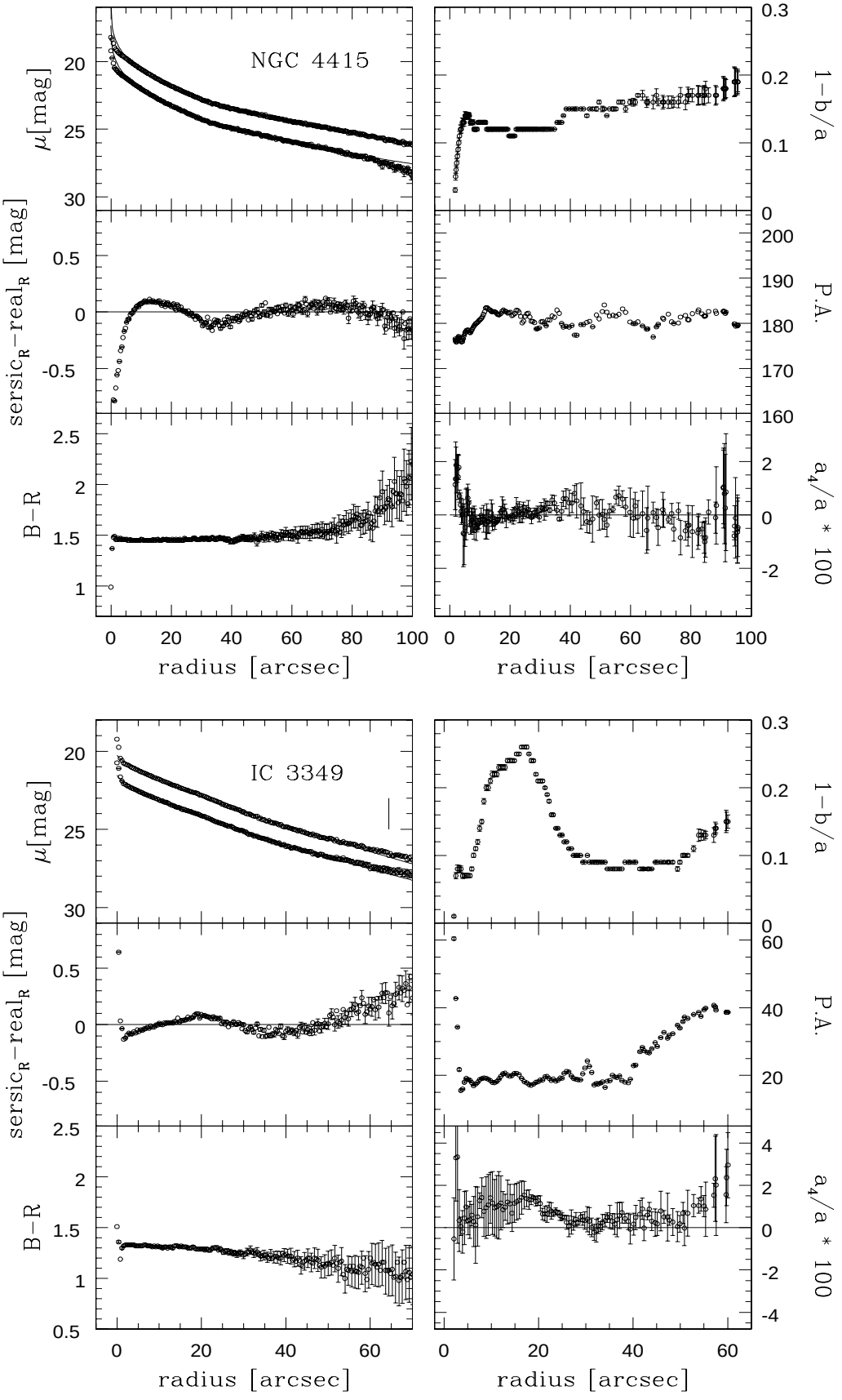

Figure 2.12 continued

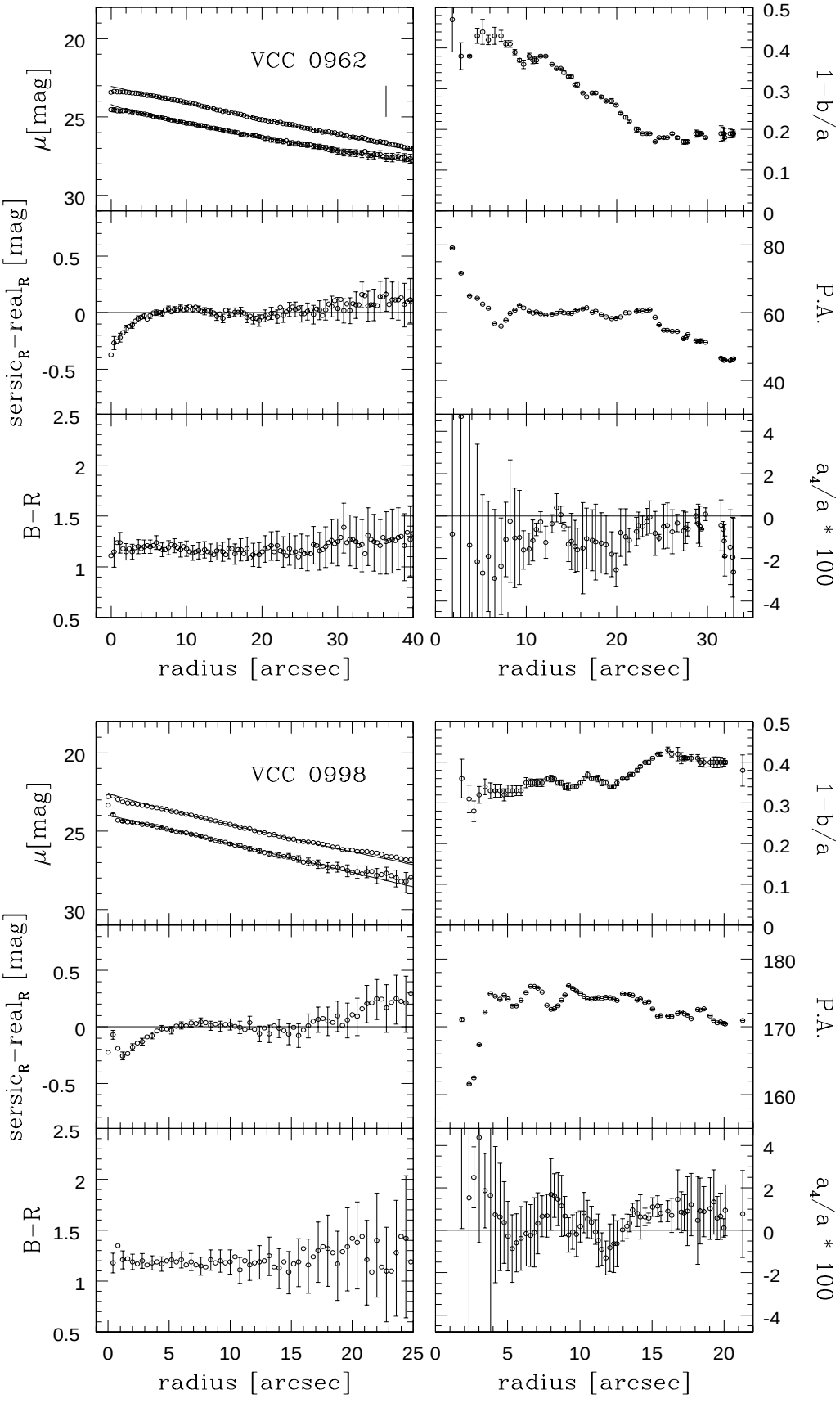

Figure 2.12 continued

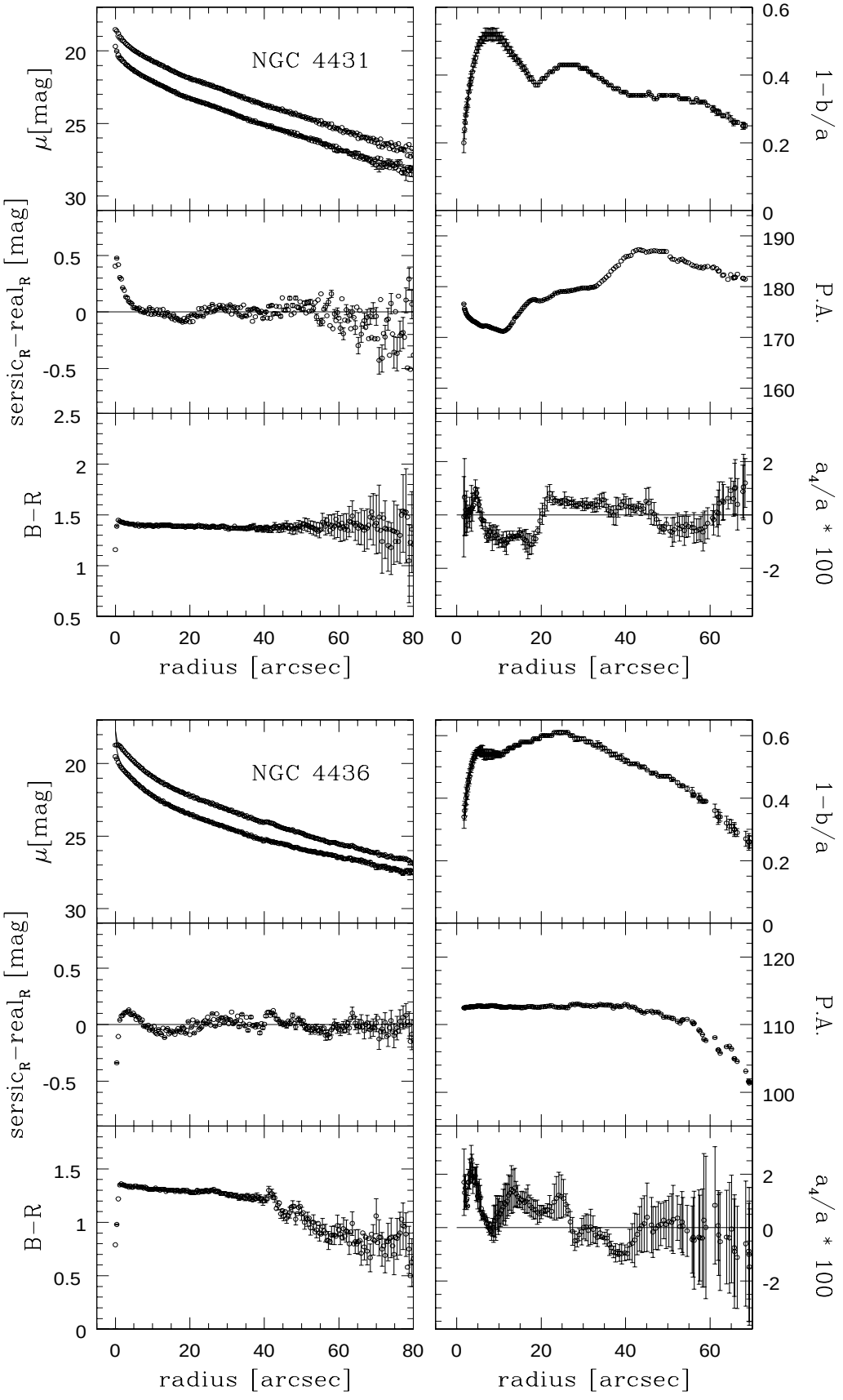

Figure 2.12 continued

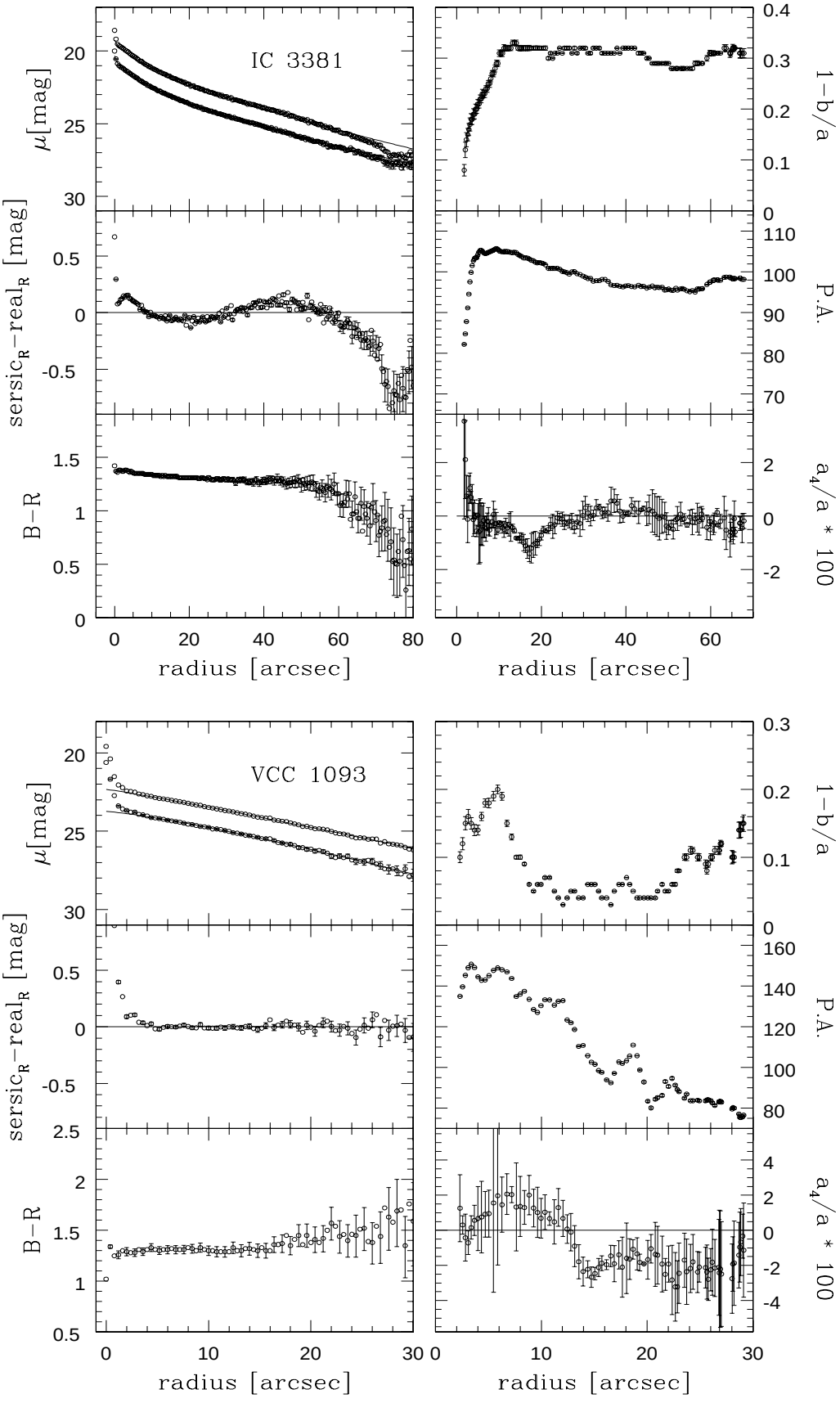

Figure 2.12 continued

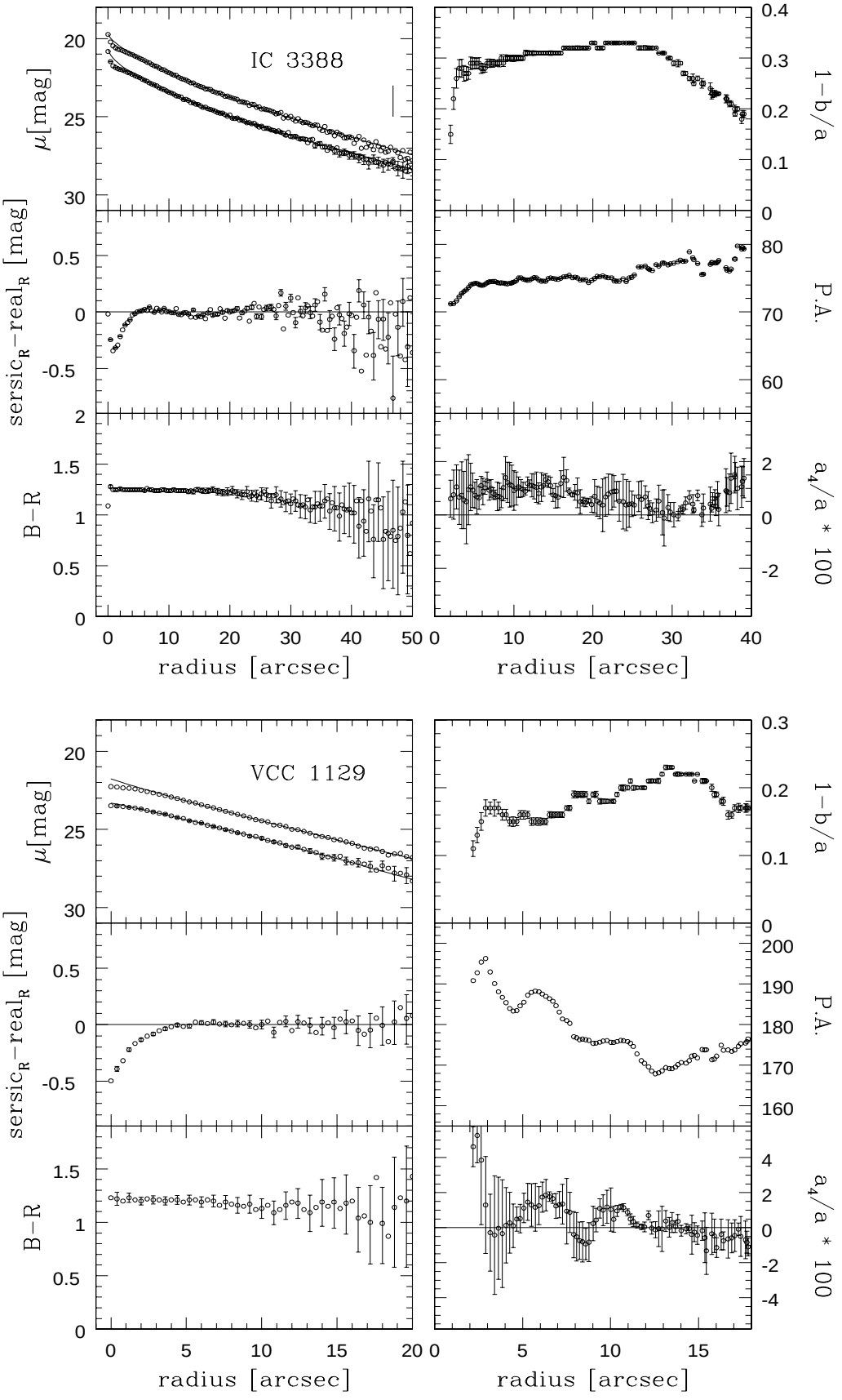

Figure 2.12 continued

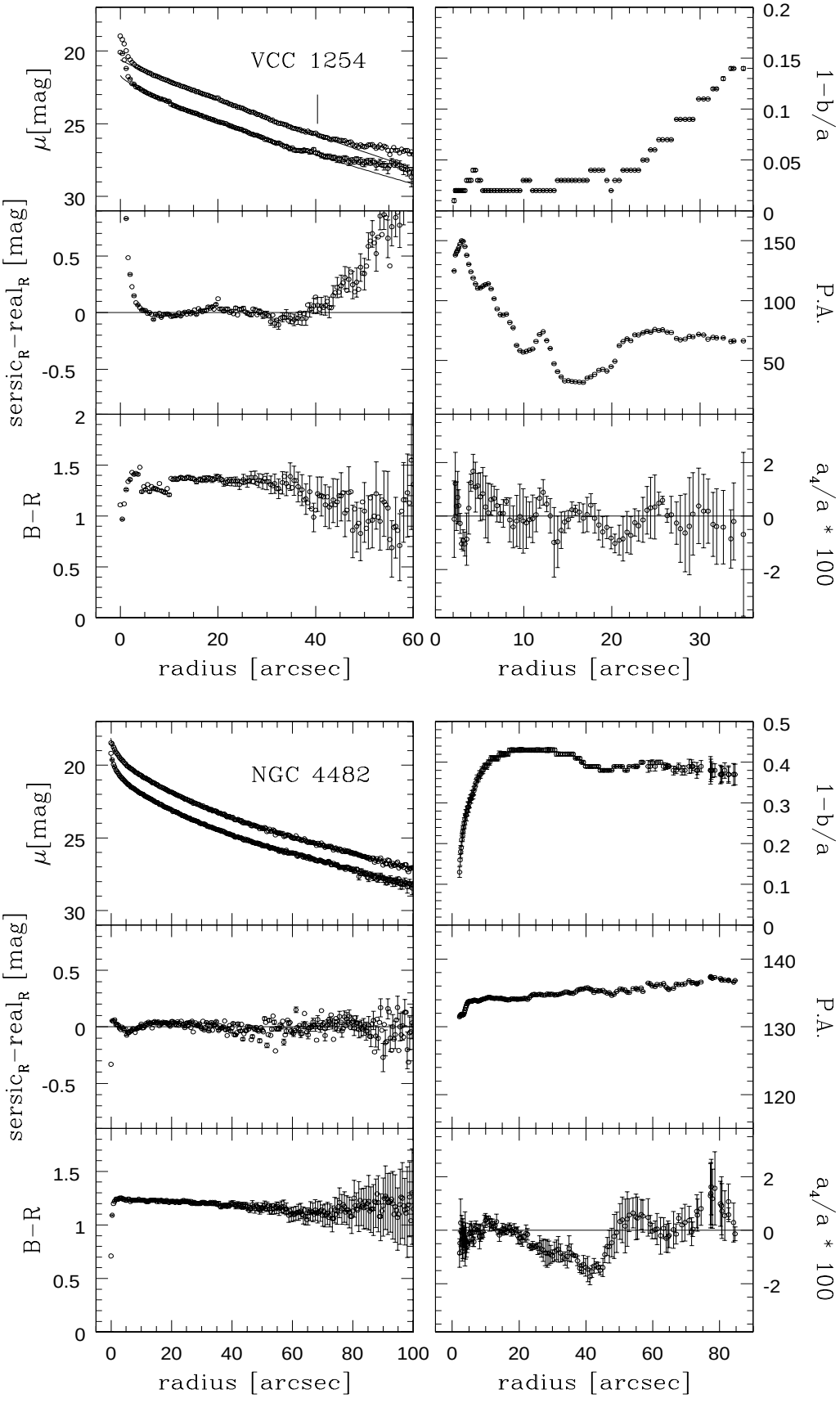

Figure 2.12 continued

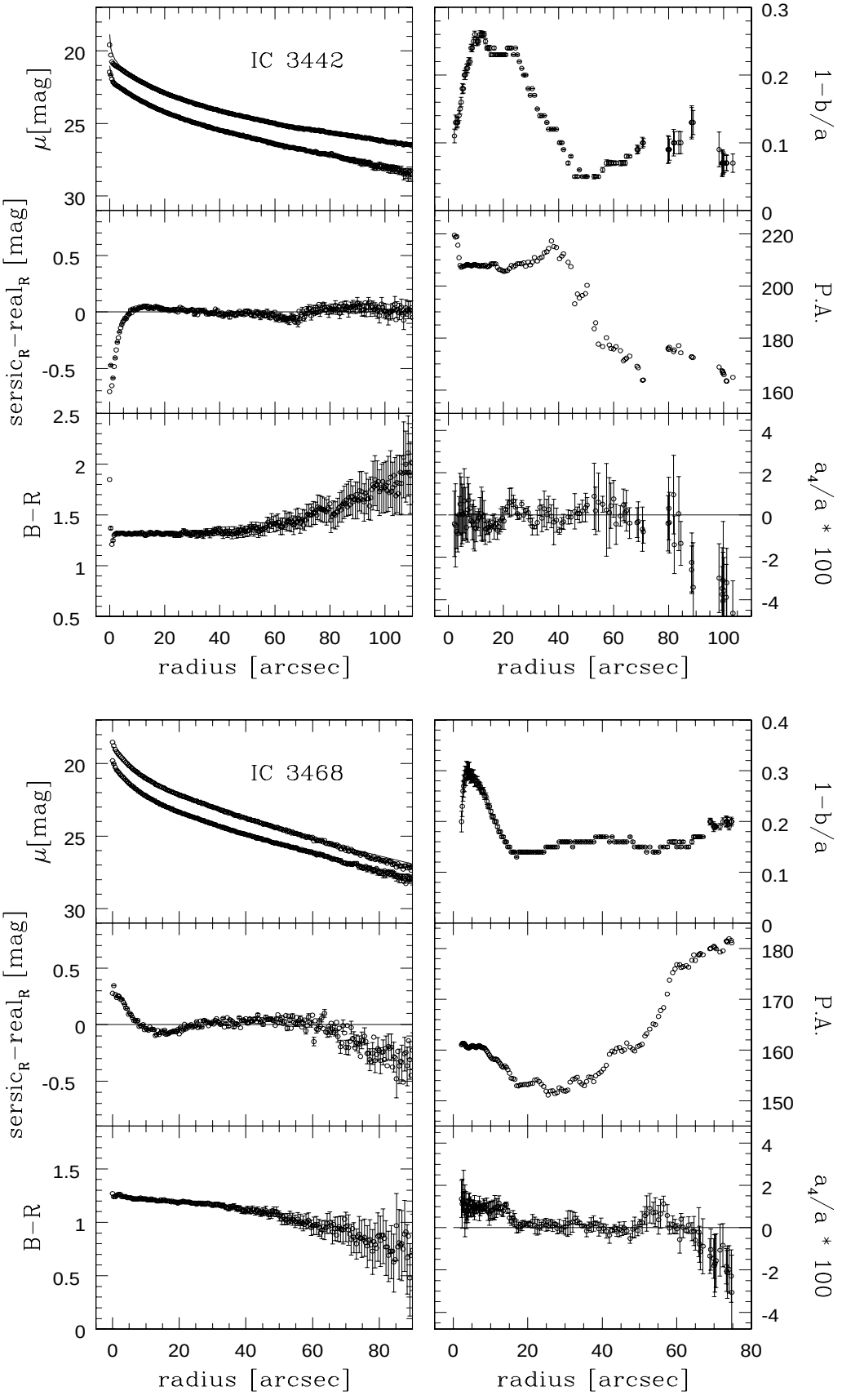

Figure 2.12 continued

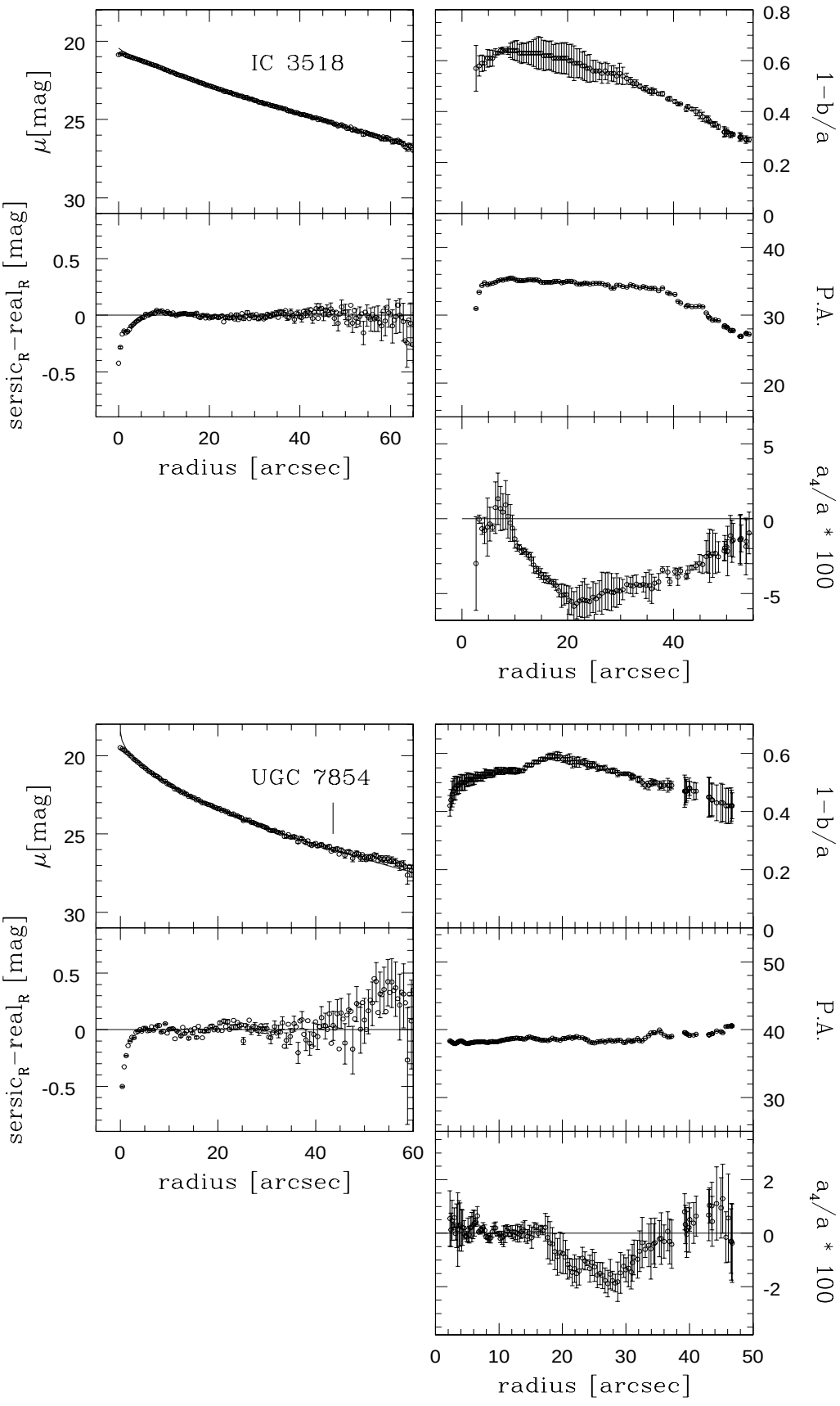

Figure 2.12 continued

Tabelle 2.2: Surface brightnesses up to which the background could be reasonably well determined and maximum radii for full elliptical integration. A ∞ sign indicates that the whole galaxy is on the frame.

VCC (1)	Name (2)	μ^B_{sky} (3)	μ^R_{sky} (4)	r^B_{max} (5)	r^R_{max} (6)	VCC (1)	Name (2)	μ^B_{sky} (3)	μ^R_{sky} (4)	r^B_{max} (5)	r^R_{max} (6)
0009	IC3019	28.09	27.65	∞	120	1010	NGC4431	27.77	27.20	88	100
0490	IC0783	28.52	26.66	100	100	1036	NGC4436	27.77	27.20	40	40
0781	IC3303		27.18		∞	1087	IC3381	28.14	27.93	60	60
0810		30.12	26.58	∞	∞	1093		27.14	27.93	16	16
0815		30.12	26.58	32	32	1104	IC3388	29.97	27.76	∞	∞
0846		30.12	26.58	∞	∞	1129		29.97	27.76	∞	∞
0850		30.12	26.58	∞	∞	1254		26.51	25.70	0	0
0856	IC3328	28.47	27.45	120	120	1261	NGC4482	28.89	27.45	120	120
0928		27.77	26.62	24	24	1355	IC3442	30.73	28.70	120	120
0929	NGC4415	27.99	27.65	∞	120	1422	IC3468	28.85	27.86	100	100
0940	IC3349	27.77	26.62	80	80	1567	IC3518		27.70		76
0962		27.77	26.62	64	∞	1895	UGC7854		26.10		∞
0998		27.77	27.20	∞	∞						

2.4 Surface photometry

2.4.1 Model-free photometric parameters and radial profiles

As described above, we determined the growth curve for each galaxy by integrating the galaxy light in elliptical apertures. The intensity at which this curve becomes asymptotically flat yields the total apparent magnitude. Only in a few cases, however, the first integration promptly led to a reasonably flat growth curve. Usually the outer shape of the growth curve shows a continuous increase or a maximum followed by a continuous decrease, indicating a slight, erroneous excess or deficiency in the sky level. The shape of the curve can therefore be used to do a fine-tuning of the sky level by simply adding or subtracting a constant to the whole frame. Once the growth curve is corrected to be asymptotically flat, the effective radius can then be read off where the growth curve reaches half of its asymptotic value. Using the equation

$$\langle\mu\rangle_{eff}\,[\mathrm{mag}/\Box''] = m + 5\,\log(r_{eff}['']) + 1.995\ , \tag{2.1}$$

where m is the total apparent magnitude and r_{eff} is the effective radius, we get the effective surface brightness, $\langle\mu\rangle_{eff}$. These model-free parameters are listed in Table 2.1. The meaning of the columns has already been given there (recall that all values are extinction-corrected).

Surface brightness profiles can be obtained by differentiating the growth curve with respect to equivalent radius $r = \sqrt{ab}$, where a and b are the major- and minor-axis, respectively. We used a resolution of $0\farcs4$, which corresponds to two pixel lengths. The *extinction-corrected profiles* are shown in Fig. 2.12

(left column on top). The upper curve is the R profile and the lower curve the B profile. Error bars are only shown for the B profile. They can be considered as upper limits for the profile in R. Only in the outer parts the error bars are larger than the plot symbols. The errors have been estimated using the remaining gradients on the frame after flat fielding and the intensity of the subtracted background. They therefore indicate the accuracy of the profile at the corresponding surface brightness level and do not take into account the fact that in some cases only one quarter of the galaxy light has been integrated.

In the bottom left panel of Fig. 2.12 we plot the $B-R$ colour profile. For dwarf galaxies in general one would expect rather flat profiles, i.e. no strong colour gradients. In the case of dwarf ellipticals a positive gradient, i.e. a reddening towards the outer parts, could be explained by the presence of a younger population of stars in the center, where the last star formation event took place (Vader et al. 1988). Surprisingly, almost half of the galaxies in our sample (10) exhibit a negative colour gradient, getting bluer towards the outer parts. This could mean that there is a metallicity gradient in these galaxies. Indeed, for five of these objects either a disk component has been discovered or at least indications of the presence of a disk have been found (Jerjen, Kalnajs & Binggeli 2000; Barazza et al. 2002). A separate, more elaborate investigation of the colour properties of dwarf ellipticals is in preparation (Barazza et al. 2003).

2.4.2 The Sérsic law: fits and parameters

The surface brightness profiles of dwarf galaxies, including dEs, can usually be fitted quite well by an exponential model (De Vaucouleurs 1959; Binggeli & Cameron 1991). However, the profiles of *bright* early-type dwarfs are known to deviate considerably from an exponential law (Caldwell & Bothum 1987; Binggeli & Cameron 1993). This deviation depends systematically on the luminosity of the dwarfs. Bright objects show a shallow luminosity excess in the inner parts, which cannot be caused by the presence of a nucleus. A better representation of the profiles of early-type dwarfs is provided by a Sérsic model (Sérsic 1968). This model, which is a simple generalization of De Vaucouleurs' $r^{1/4}$ and exponential laws, can be written as

$$\sigma(r) = \sigma_0 e^{-(r/r_0)^n}, \tag{2.2}$$

where σ is the surface brightness (intensity per area) at the equivalent radius r. There are three free parameters, which are determined by a fitting procedure: the central surface brightness σ_0, the scale length r_0, and the shape parameter n. It is this latter parameter that takes care of the systematic, inner deviations from an exponential described above. The Sérsic model has turned out to be very appropriate for dwarf ellipticals (e.g. Young & Currie 1994: Binggeli & Jerjen 1998; Ryden et al. 1999). We fitted our surface brightness profiles with this model in the magnitude representation, which is

$$\mu(r) = \mu_0 + 1.086(r/r_0)^n, \tag{2.3}$$

with $\mu_0 = -2.5\log\sigma_0 + const.$ A $\chi^2_{\rm min}$ fit to the profiles has been performed outside of $4''$ and above the level of $27\mathrm{mag}/\Box''$ in B and $26\mathrm{mag}/\Box''$ in R. This range has been chosen in order to exclude the nuclei and to avoid the outer parts of the galaxies which might be affected by flat-field uncertainties. The best-fitting parameters (again *extinction-corrected*) are given in Table 2.3:

column (1) and (2): identifications of the galaxies;

columns (3) and (5): central surface brightness in B $[\mathrm{mag}/\Box'']$ and R $[\mathrm{mag}/\Box'']$, respectively;

columns (4) and (7): scale length (in arcsec $['']$) in B and R, respectively;

columns (5) and (8): shape parameter in B and R, respectively.

In Fig. 2.13 we plot these parameters versus absolute magnitude in B. For comparison we have added a sample of giant ellipticals and S0s from Caon et al. (1993), the data for the dEs and dSphs of the Local

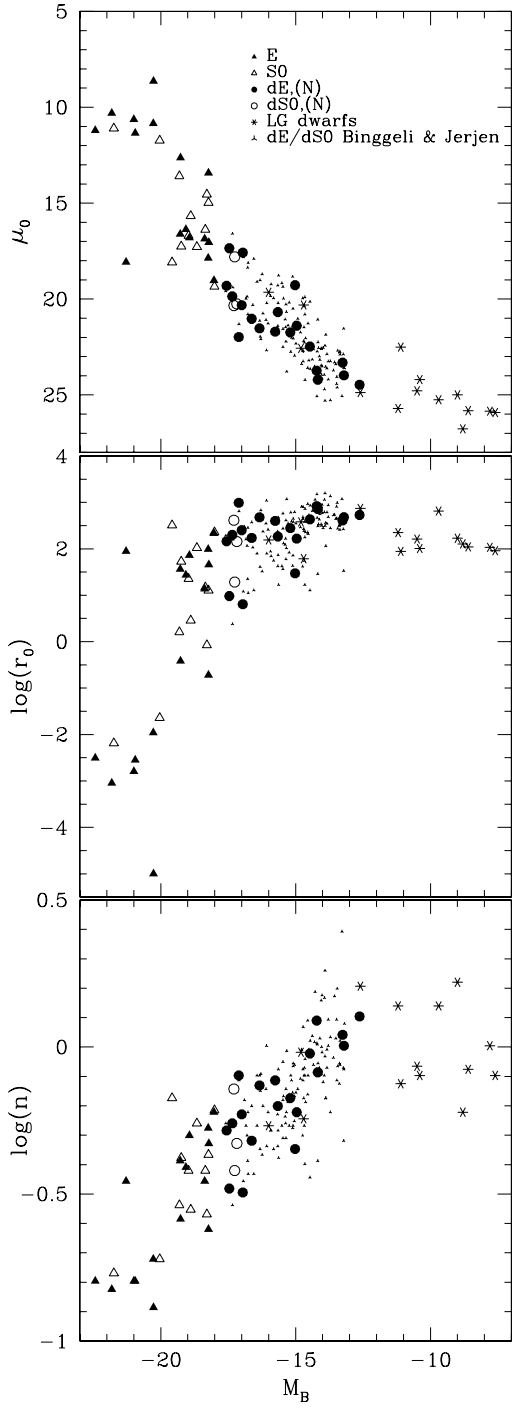

Abbildung 2.13: The parameters of the best-fitting Sérsic model, central surface brightness (μ_0), scale length (r_0), and shape indicator (n), plotted versus absolute magnitude for different galaxy types. All data are in the B-band. Es and S0s are from Caon et al. (1993), Local Group dSphs are from Jerjen, Binggeli & Freeman (2000) and dE,(N)s/dS0,(N)s are from this study. Added as well is the large photographic sample of Virgo early-type dwarfs from Binggeli & Jerjen (1998), shown as dots.

Group from Jerjen, Binggeli & Freeman (2000), and the large photographic sample of early-type dwarfs in Virgo (partly coinciding with ours) from Binggeli & Jerjen (1998). The $M_B - \mu_0$ diagram (top panel) shows a rather tight relation comprising all different types of spheroidal objects. As already found and commented upon by Jerjen & Binggeli (1997) and Jerjen, Binggeli & Freeman (2000), the early-type dwarfs perfectly bridge the gap between the faint dSphs of the local group and the giant ellipticals. The

Tabelle 2.3: Parameters of the Sérsic fit and of the isophotal analysis.

VCC (1)	Name (2)	μ_0^B (3)	r_0^B (4)	n^B (5)	μ_0^R (6)	r_0^R (7)	n^R (8)	$\langle\epsilon\rangle$ (9)	$\langle P.A.\rangle$ (10)	$\Delta P.A.$ (11)	$\langle\frac{a_4}{a}*100\rangle$ (12)	$\langle\delta r_N\rangle$ (13)
0009	IC3019	21.98	12.25	0.80	20.71	11.92	0.76	0.16	123.7	33.0	−0.29	2.45
0490	IC0783	20.25	1.80	0.47	19.17	2.49	0.51	0.18	106.8	50.2	0.20	0.78
0781	IC3303				18.52	2.02	0.63	0.42	69.4	15.6	−0.43	0.34
0810		22.48	5.38	0.95	21.33	5.80	0.99	0.05	139.0	4.9	−0.08	0.42
0815		21.74	3.50	0.67	20.96	5.18	0.80	0.21	131.7	60.5	−1.08	0.79
0846		21.39	2.07	0.60	19.14	0.55	0.43	0.17	103.7	43.2	−0.05	0.63
0850		24.47	6.69	1.27	22.92	4.70	0.93	0.51	54.2	12.3	1.66	0.45
0856	IC3328	17.58	0.08	0.32	17.59	0.54	0.42	0.09	80.7	29.0	−0.05	0.20
0928		19.28	0.37	0.45	18.83	0.92	0.55	0.42	42.5	4.5	0.99	0.19
0929	NGC4415	17.35	0.12	0.33	15.59	0.07	0.31	0.13	60.2	8.1	−0.01	0.26
0940	IC3349	21.53	5.95	0.74	20.25	6.30	0.77	0.16	20.2	22.3	0.79	0.37
0962		24.21	9.03	0.82	23.05	10.27	0.98	0.31	59.1	12.8	−1.10	0.78
0998		23.98	5.99	1.01	22.56	4.95	0.89	0.36	174.0	4.9	0.31	0.56
1010	NGC4431	20.34	5.17	0.72	18.94	5.15	0.72	0.43	140.5	16.1	−0.20	0.46
1036	NGC4436	17.80	0.24	0.38	17.76	1.29	0.51	0.55	112.5	7.3	0.52	0.91
1087	IC3381	20.32	3.15	0.59	19.25	4.31	0.66	0.30	101.4	10.7	−0.31	0.21
1093		23.74	10.40	1.23	22.33	9.61	1.09	0.08	117.1	67.7	−0.36	0.52
1104	IC3388	20.68	2.30	0.63	19.71	3.13	0.71	0.30	74.9	5.3	0.83	0.27
1129		23.32	5.11	1.10	21.76	3.76	0.93	0.18	90.1	20.4	0.59	0.21
1254		21.70	4.99	0.77	20.60	7.21	0.91					
1261	NGC4482	19.31	1.82	0.52	18.14	2.00	0.54	0.40	134.5	4.6	−0.27	0.40
1355	IC3442	21.03	2.14	0.48	18.87	0.58	0.37	0.16	56.7	44.5	−0.10	1.93
1422	IC3468	19.86	2.49	0.55	18.81	3.12	0.60	0.18	157.1	29.3	0.41	0.33
1567	IC3518				20.43	7.52	0.81	0.56	34.2	8.6	−3.16	1.37
1895	UGC7854				18.50	1.29	0.55	0.54	38.5	2.0	−0.25	0.37

known dichotomy between Es and dEs in a luminosity-central surface brightness plot (e.g. Binggeli & Cameron 1991) vanishes in the Sérsic representation. The relations in the remaining two plots are not as striking, although in both diagrams a certain continuity between the different galaxy classes is evident, above all among the ellipticals. In contrast, the faint local group dSphs stand slightly apart.

2.4.3 Accuracy of the fi t

The best-fitting Sérsic model profiles are plotted as solid lines through the data points in Fig. 2.12 (upper left panel). The general trend of the observed profiles is matched quite well by the models. However, in some cases the decrease of the observed profile is not as smooth as the model in the inner parts. This is shown in the second plot of the first column in Fig. 2.12, where the difference between the observed profiles and the models is plotted. Error bars are shown for every other data point (mostly smaller than the plot symbols). The large residuals caused by the nuclei are not very surprising, as the very central parts ($r < 4$") have been excluded for the fit, but a few of the bright objects show considerable deviations from the model in the regions just outside of the nucleus as well. A rather strong scatter is shown by the dwarfs where a spiral structure has been discovered (IC0783, IC3328). Hence, in these cases a bad fit might be expected. But also “normal” dEs, like VCC0928 or NGC4415, show a remarkable deviation.

In order to quantify the deviations and to find out whether they are related to other properties of the galaxies, we determined the mean, absolute residual between the observed profile and the fit (only for the R-band data):

$$\langle S_{res} \rangle = \sqrt{\frac{\sum_N (\mu_p - \mu_m)^2}{N}} \tag{2.4}$$

with N, the number of isophote data points between $4''$ and $26\mathrm{mag}/\Box''$ in R (the range used for the fit), μ_p, the surface brightness measured for the isophote, μ_m, the corresponding surface brightness of the model profile. This is of course simply the standard deviation (1σ scatter) of the points around the model fit. In Fig. 2.14 we plot $\langle S_{res} \rangle$ versus effective surface brightness, μ_{eff}. The error bars represent the mean error of the profile in the fitting range. Obviously, the more compact (or brighter) objects tend to have larger residuals. Most of the faint objects ($\mu_{eff} > 22$ mag) have residuals within the errors, i.e. their profiles are well represented by a Sérsic model. This is not the case for the brighter galaxies. It is important to note that the mean error bars shown here are much larger than the actual errors *in the central parts* where the largest deviations from the model occur, i.e. the deviations shown in Fig. 2.14 are clearly significant. For dS0s the rather large residuals might be explained by the fact that many of these galaxies are believed to have a two-component structure, showing a high surface brightness, lens-like feature within a more extended low surface brightness part. Hence, a two-component model suitable for disk systems might be more appropriate for these objects. However, the result remains that *not a single bright early-type dwarf in our sample is well represented by the Sérsic model*. Whether a second component might be present in many "pure" dEs as well cannot be answered with these data. As the deviations mainly occur in the central parts of the profiles, a Nuker law (Lauer et al. 1995, Byun et al. 1996) or even a King model (King 1966) which are commonly used to fit the central features of early-

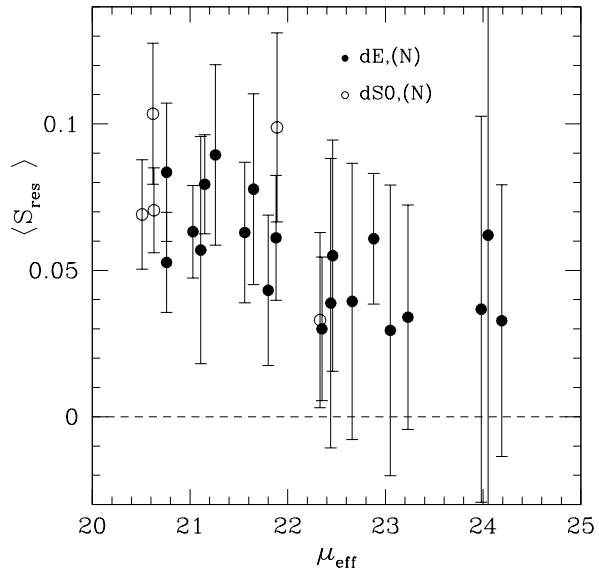

Abbildung 2.14: Effective surface brightness in R plotted versus the mean, absolute residual between profile observed and model-profile (see text for details). The error bars represent the mean error of the profile in the corresponding range.

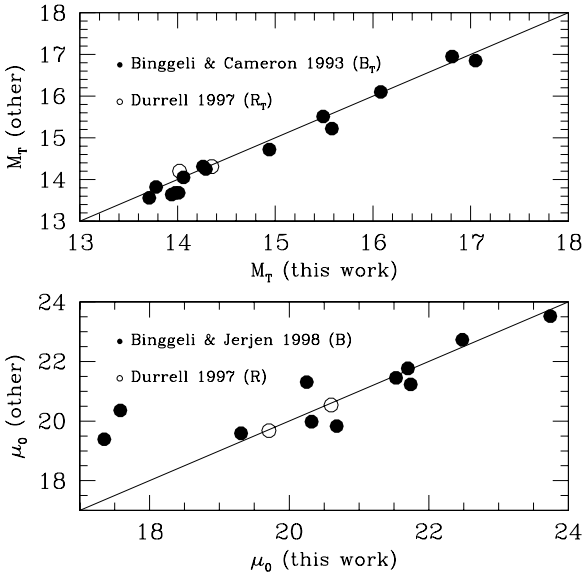

Abbildung 2.15: Comparison of our total apparent magnitude in B (filled circles) and R (open circles) (upper panel) and of the central surface brightness from the Sérsic fit in B (filled circles) and R (open circles) (lower panel) to data from the literature.

type galaxies might be more suitable. However, this would increase the number of fit-parameters and make the comparison with other objects more difficult. Therefore, the Sérsic model is still a useful fitting law for a general analysis of the photometric properties of different object classes.

2.4.4 Comparison with data from the literature

In the upper panel of Fig. 2.15 we compare our total magnitudes with available data from the literature. Binggeli and Cameron (1993) give total apparent magnitudes in B for a large sample of Virgo dEs. The 14 objects in common with our sample are shown as filled circles. In general, the data agree quite well. However, there are significant differences for some galaxies, which amount to 0.3 mag or more in four cases. Only two objects can be compared with the data from Durrell (1997) in the R-band (open circles). It is evident from Fig. 2.15 (upper panel) that our magnitudes tend to be slightly fainter than the ones from the literature. This could indicate that we have overestimated the background in some frames, due to the presence of several galaxies on the frame, leaving only a small region of the sky. Overall, we estimate the errors of the total apparent magnitudes to be 0.15 mag in both filters.

In the lower panel of Fig. 2.15 we compare our central surface brightnesses in B and R, derived by a Sérsic fit, to the data of Binggeli and Jerjen (1998) and Durrell (1997), respectively. Obviously, the two brightest objects strongly disagree. The fact that Binggeli and Jerjen used growth-curves for the fitting procedure cannot account for these differences (see their discussion of this point). However, since brighter objects usually have a steeper rise of the profile in the central parts, only slightly different Sérsic fits can have large deviations of the central surface brightness. Also, the brightest objects show generally the strongest deviations from the Sérsic law (see 4.3 above).

2.5 Isophotal analysis

Thanks to the high resolution of our observations we were able to perform an accurate analysis of the isophotal properties of the sample galaxies. To determine the corresponding parameters, we fitted ellipses to the isophotes, using a method described by Bender & Möllenhoff (1987), which is implemented in MIDAS as FIT/ELL3. In addition, we derived the deviations of the isophotes from pure ellipses and expanded them in a Fourier series. The fourth cosine parameter, a_4, indicates the shape of the corresponding isophote: an isophote with a negative a_4 is called "boxy", otherwise it is called "disky" (see Bender & Möllenhoff (1987) for details). In this way, we determined the ellipticities, the position angles of the major-axis and the shape parameters for all isophotes between $r \approx 2''$ and $\mu \approx 26.5$ mag in R with an interval of 0.05 mag for each galaxy. In Fig. 2.12, right column, we plot these three parameters versus equivalent radius. The error bars have been determined using the prescription of Bender & Möllenhoff (1987). The ellipticity is defined as $\epsilon = 1 - b/a$ where a and b are the major- and minor-axis respectively, and a_4 is given as $a_4/a * 100$.

Since the center of the ellipse searched for is a free parameter in the fitting procedure, we could simultaneously measure the distance, δ_N, between the nucleus (or the center of the innermost isophote for not-nucleated dwarfs) and the center of the overall brightness distribution. This allows to determine a possible off-center position of the nucleus or the concentricity of the successive isophotes. The isophotal contours of the sample galaxies are shown in Fig. 2.16.

In order to investigate whether there are correlations between the isophotal parameters and other properties of the galaxies, we determined their mean, global values. The range within which the averaging was performed was again the same as for the profile fitting: outside the central $4''$ and above an isophotal level of $26\mathrm{mag}/\Box''$. Following the procedures of Ryden et al. (1999), the parameters of the isophotes contributing to the mean have been weighted by the fraction of intensity corresponding to that isophote. In this way the faint outer regions, where the errors are large, are automatically given less weight. Hence, the intensity - or luminosity - weighted mean is:

$$\langle z \rangle = \frac{\sum z dI}{\sum dI} \tag{2.5}$$

where z represents ϵ, $P.A.$, a_4 or δr_N, and dI is the contribution of intensity of the isophote. In addition to these mean values, we determined the maximal isophotal twist of the galaxies within the considered radial range. The parameters are listed in Table 2.3, where the columns are:

column (9): ellipticity defined as $\epsilon = 1 - b/a$;

column (10): position angle of the major-axis, measured from top counterclockwise;

column (11): maximal isophotal twist;

column (12): isophotal shape parameter given as $\frac{a_4}{a} * 100$;

column (13): nuclear off-set in arcsec, if no nucleus is present, the innermost isophote is taken as reference.

We omit VCC1254 in this analysis, since its isophotal parameters can not be determined with the required accuracy, due to its proximity to M49.

2.5.1 The isophotal shape parameter a_4

Giant ellipticals as well as dwarf ellipticals owe their name to the fact that the shape of their isophotes is nearly elliptical. The shape parameter a_4 has been developed in order to quantify the deviations of the isophotes from an elliptical shape and to find correlations between these deviations and other properties

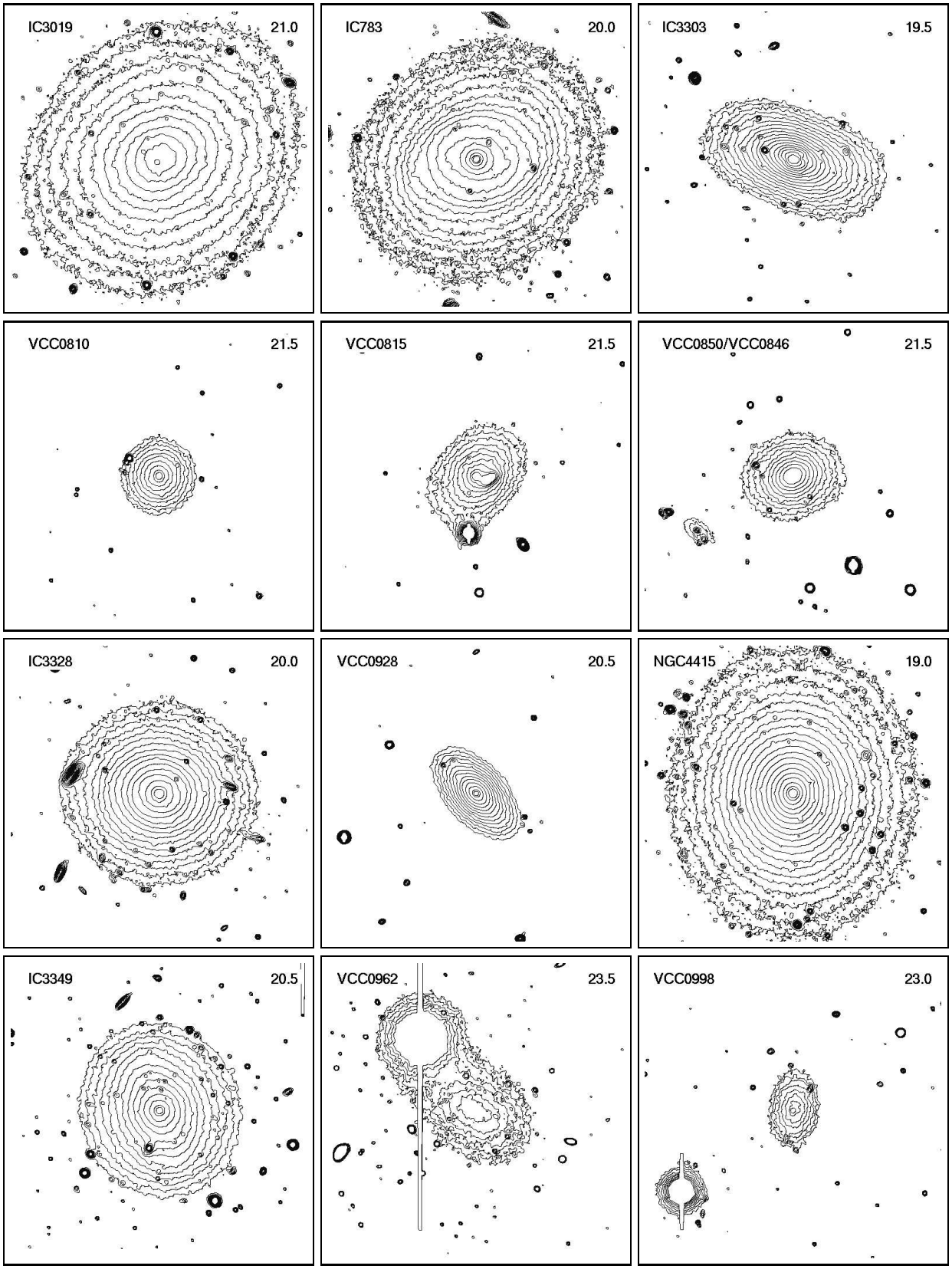

Abbildung 2.16: Isophotal contours of the R-band images. The galaxy name is given in the upper left corner. The surface brightness of the innermost isophote is indicated in the upper right corner, the interval is 0.25 mag. The images are $1\farcm7$ on a side, corresponding to ~ 8 kpc.

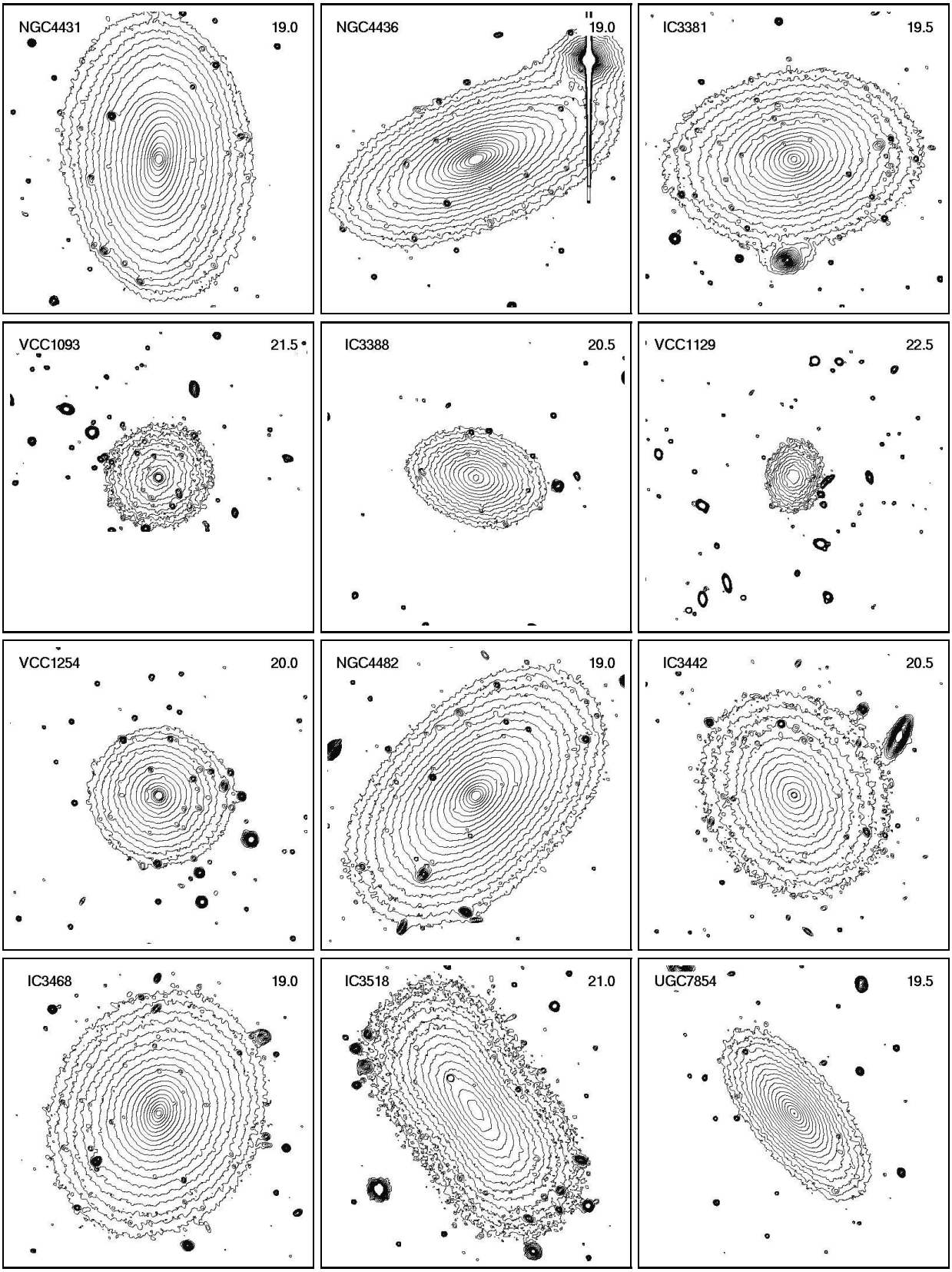

Figure 2.16 continued

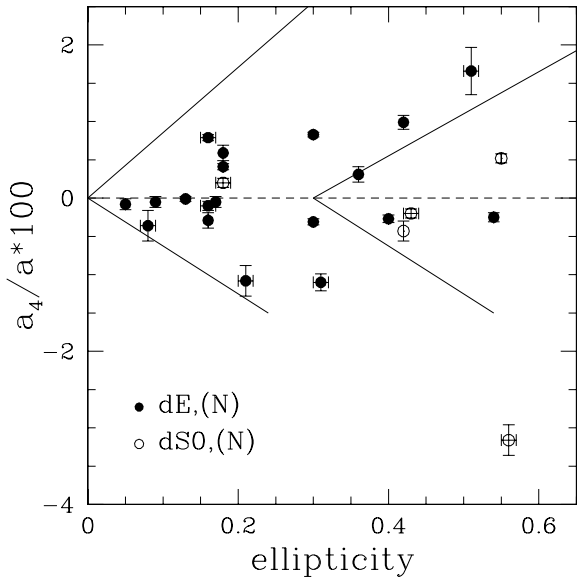

Abbildung 2.17: Ellipticity versus shape parameter represented as $a_4/a * 100$ for dE,(N)s (solid circles) and dS0,(N)s (open circles). The lines are the same like in Fig. 2.12 of Bender et al. (1989) and indicate the distribution of giant ellipticals. Shown are also the 1σ errors of the averaging.

of the galaxies. Isophotes whose a_4 is negative are called boxy, since their shape resembles a rectangle, and those with a positive a_4 are called disky, because they are more pointed, lemon-like, than the corresponding ellipse. It is generally believed that a galaxy with disky isophotes has a disk component; however, only disks seen nearly edge-on can be identified by a_4 (Carter 1987, Rix & White 1990). Moreover, there is a relation between a_4 and the radio and X-ray emission (at least for giant ellipticals), in the sense that boxy ellipticals tend to be the stronger sources. These correlations are shown in the study of Bender et al. (1989), who also find that apparently more flattened galaxies are either disky or boxy, whereas rounder objects tend to have $a_4 \sim 0$ (see their Fig. 1). A similar trend for *dwarf* ellipticals as well is shown by Ryden et al. (1999). Interestingly, however, these authors find about a dozen rather flattened galaxies which do not have boxy or disky isophotes, i.e. strongly flattened dwarfs do not show a gap in the distribution of a_4 between boxy and disky. We find the same behavior in our sample. In Fig. 2.17 we plot ellipticity versus $a_4/a * 100$. The lines are the same as in Bender et al. (1989) and bracket the distribution of giant ellipticals. The general trend that rounder galaxies have $a_4 \sim 0$ seems to be valid for giants as well as for dwarfs. On the other hand, we find flattened dwarfs ($\epsilon > 0.3$) with $a_4 \sim 0$ – in contrast to the findings for giants and in agreement with Ryden et al. (1999).

However, in view of the profiles for a_4 shown in Fig. 2.12, the significance of its weighted average is not so evident. Most of the profiles show large scattering and frequently change between the boxy and disky regime. Others have a boxy inner part and a disky outer part (or vice versa), rendering it difficult to asses a unique interpretation to the whole galaxy. For instance, VCC1093 is strongly disky in the central parts, but has nevertheless a negative global $\langle a_4 \rangle$. O. Lehmann (diploma thesis, Basel 2002, unpublished) has tried to reproduce the a_4 *profiles* of a number of individual cases with multi-component models. By evaluating a best set of component parameters a satisfactory solution could indeed be found for most dwarfs. However, these models are probably not unique, nor do they seem to be physically very

meaningful, as Stiavelli et al. (1991) have shown that the isophotal shape of being either boxy or disky might depend on the viewing angle. A more promising approach would involve 3D models along the lines of Ryden (1992).

Nevertheless, for some individual cases the (projected) shape parameter is quite straightforward to interpret. Consider for example the a_4-profile of IC3388 (Fig. 2.12): all isophotes in the radius range used are disky, hence, it is justified to classify the galaxy as a whole as disky, suggesting that it hosts a disk component. Or NGC4431, where a hidden bar has been discovered (Barazza et al. 2002): the boxyness of the a_4-profile in the central parts clearly reflects the bar and the radius, where the isophotes become disky indicates the extend of the bar.

2.5.2 Off-center nuclei

Even though the position of a nucleus with respect to the overall light distribution might not be considered as part of an isophotal analysis, we discuss this phenomenon in this context, since the measurement of the nuclear offset goes together with the determination of the isophotal parameters (see above). Moreover, offsets found not only represent off-centered nuclei but might also indicate that consecutive isophotes are not concentric.

In general, the nature of dE nuclei is still unknown; mostly they are regarded as massive compact star clusters which form separate dynamical entities, without being totally decoupled from the rest of the galaxy. They might have formed in the last burst of star formation in the evolutionary transition from dwarf irregulars to dEs (Davies & Phillipps 1988). Simulations suggest that such nuclei oscillate about the center of the galaxy (Miller & Smith 1992, Taga & Iye 1998). However, in these simulations the rotation of the main body is a crucial condition, which would not be complied by most of the dwarf ellipticals. On the other hand, Sweatman (1993) showed in his models that oscillations of central objects can also be explained by inherent motions due to statistical fluctuations, without going back to rotation.

More recently it was suggested that the nuclei could be the result of the merging of several globular clusters which sunk to the center of the galaxy through dynamical friction (Lotz et al. 2001). In the same study it was also shown that brighter nuclei tend to be in brighter host galaxies. However, a lower globular cluster specific frequency (S_N) suggested for dE,Ns cannot be found; on the contrary, dE,N have a higher S_N than dEs (Miller et al. 1998). Oh & Lin (2000) studied a similar scenario including extra galactic tidal perturbations accounting for the fact that nucleated dEs are more concentrated to the center of the cluster than non-nucleated dEs. In addition, they found that the nuclei may be slightly off-center within ~ 1 Gyr after each globular cluster merger event. Indeed, in their study of 78 nucleated dwarf ellipticals and dwarf S0s, Binggeli et al. 2000 (hereafter BBJ) found that $\sim 20\%$ of the objects have off-centered nuclei. They also found a weak correlation between the strength of the offset and the effective surface brightness: fainter objects tend to have larger offsets. However, since the resolution of their data was rather low, the significance of this effect is not clear.

We therefore did the same analysis with our data, i.e. for each galaxy we determined the distances between the centers of the isophotes and the position of the nucleus. In case of an object without nucleus, i.e. for a dE, the innermost isophote was taken as reference. Due to the photon noise a small offset is always measured, even in the case of an exactly centered nucleus. To assess the resulting systematic and random errors we followed BBJ and performed Monte Carlo simulations for the method described, using model galaxies with nuclei placed at the center or slighly offset. It turned out that the noise causes a minimum offset of $0\farcs2$, i.e. one pixel length, and that a real offset is always underestimated, i.e. offsets measured larger than $0\farcs2$ are real and are at the same time lower limits of the real displacements. (For details of the measurement and of the error estimation see BBJ). In Fig. 2.18 we plot the logarithm

of the nuclear offsets obtained versus effective surface brightness in R. Here we distinguish between dEs and dE,N. The dashed line indicates our lower detection limit of $0\farcs2$. The relation for the dE,Ns is evident: *objects with lower effective surface brightnesses tend to have larger nuclear offsets*, confirming the results of BBJ. This cannot be due to larger errors in determining the position of a nucleus of a fainter object, since these uncertainties always lead to an underestimation of the offsets (see above). We would therefore rather assume that, for example, the three dE,Ns with $\mu_{eff} > 23\,\mathrm{mag}$ have larger offsets than the ones measured. An even stronger relation is found when plotting $\log(\delta_N)$ versus the logarithm of the effective radius (Fig. 2.19). In this case, actually, the dEs and the dS0,(N)s follow the same relation like the dE,Ns, except six objects forming almost a distinct group within a narrow range of effective radii. This outcome seems to be significant, since the same partition is seen when using the larger sample of BBJ, which we reexamined for this purpose (not shown here).

In the context of the scenarios mentioned above, the relations found in Figs. 2.18 and 2.19 might be interpreted as follows: assuming that a central star cluster would oscillate around the center of the galaxy, we would expect that the oscillations are the stronger the shallower the potential well is, which in turn is reflected by larger effective radii and fainter effective surface brightnesses. On the other hand, if the nucleus is the result of the merging of several globular clusters, a correlation between offset and r_{eff} or μ_{eff} is not a natural outcome, e.g. Oh & Lin (2000) do not find a magnification of the effective radius after a merger event in their models. The case of simple oscillations is therefore more likely.

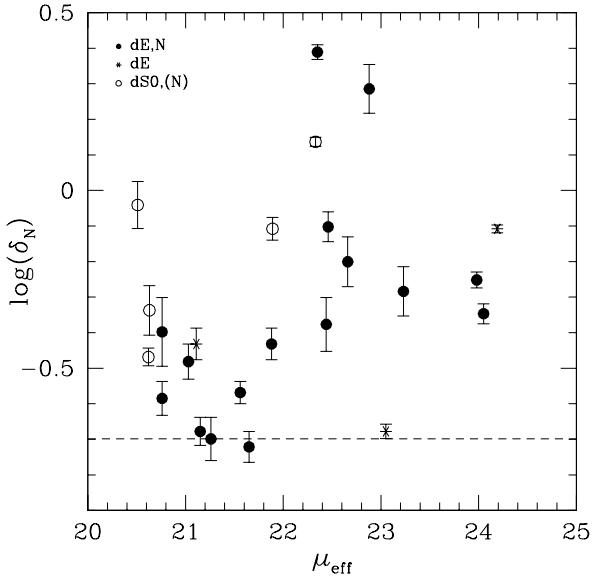

Abbildung 2.18: The logarithm of the nuclear offset versus the effective surface brightness in R. The dashed line indicates our lower detection limit of $0.2''$, i.e. offsets above this line are real and, in fact, lower limits of the true displacements. The error bars are the 1σ errors of the averaging. The meaning of the symbols is indicated.

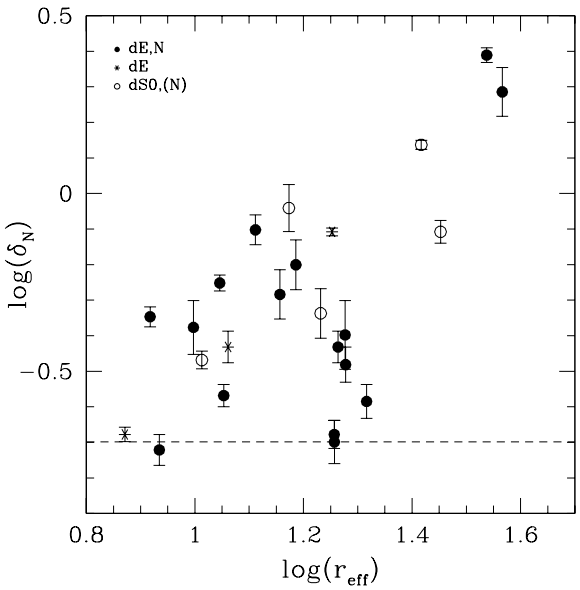

Abbildung 2.19: As Fig. 2.18 but plotting the logarithm of the nuclear offset versus the logarithm of the effective radius in R.

2.5.3 Isophotal twists

In giant elliptical galaxies isophotal twists are a quite common phenomenon (Jedrzejewski 1987, Kormendy & Djorgovski 1989), usually divided into outer and inner twists. The latter are believed to be mainly caused by tidal effects (Kormendy 1982) or even by errors in the flat-fielding and background subtraction process (Fasano & Bonoli 1990), while inner twists are attributed to the two-component nature of many ellipticals (Nieto et al. 1992). Indeed, there are similar features in the profiles of isophotal parameters of Es and SB0s galaxies. Moreover, there is a correlation between isophotal twists and flattening in ellipticals (Galletta 1980). Finally, Ryden et al. (1999) determined isophotal twists in their sample of dwarf ellipticals, finding however only a weak relation with luminosity: brighter galaxies tend to have smaller values of isophotal twists.

Using the usual range ($4'' < r, \mu \leq 26\mathrm{mag}/\Box''$) we determined the largest isophotal twist, $\Delta P.A.$, of the galaxies in our sample (column 10 of Table 2.3). In Fig. 2.20 we plot the twists derived versus ellipticity. It is striking that *strong isophotal twists are only exhibited by galaxies with* $\epsilon < 0.3$; more flattened objects show only weak twists. The relation found is very similar to the one presented by Galletta (1980) for giant ellipticals (see his Fig. 1). However, it could be argued that ellipticities and, above all, position angles of round galaxies have in general larger errors. Since for a round isophote already a small change of its shape, probably caused by noise, can lead to a large change of the position angle, we might expect a strong scatter in the radial profile of the galaxy and thus a larger twist. Nevertheless, we believe that the relation found is real for the following reasons: (1) We measure inner twists, as the typical position where the twists occur is at ~ 1.31 effective radii (average for galaxies with $\Delta P.A. > 20$). Measurement errors in these bright regions of the galaxies are negligible. Moreover, the outer limit considered is at a surface brightness level of 26 mag, which is well within the confidence level (see Table 2.2). The errors of position angle measurements in this range are indeed very small (see error bars of the $P.A.$ profiles

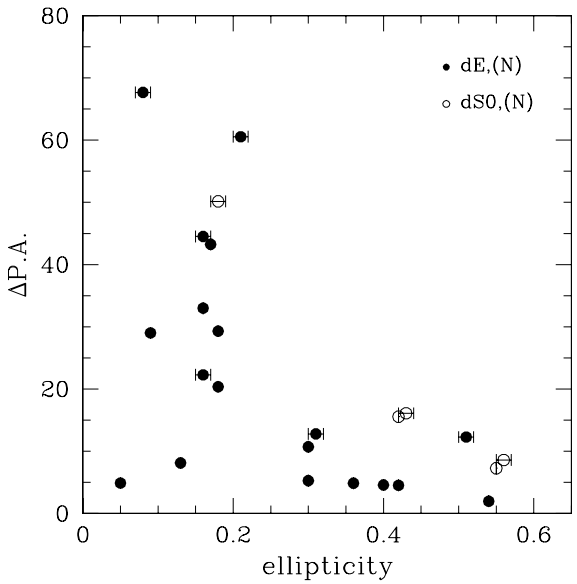

Abbildung 2.20: Isophotal twist, $\Delta P.A.$, versus ellipticity. The meaning of the symbols is indicated.

in Fig. 2.12), hence large scatter caused by noise are very unlikely. (2) The border line between galaxies with and without strong twists occurs at an ellipticity of ~ 0.3, which is still fairly round, i.e. there is no reason why there should not also be strongly twisted dwarfs with ϵ slightly larger than 0.3. (3) Even

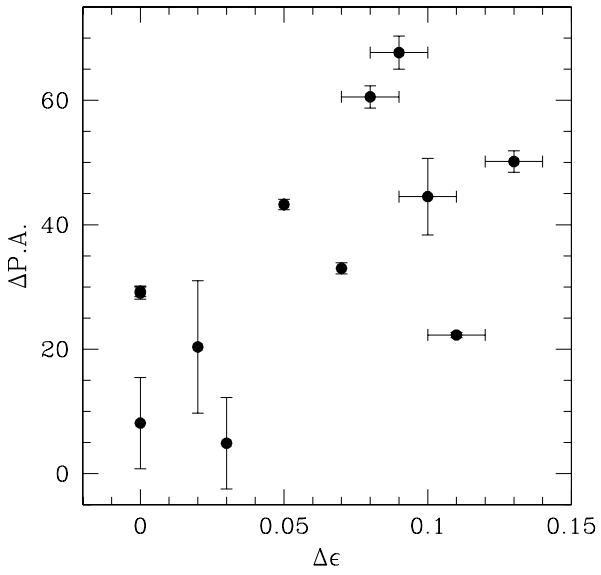

Abbildung 2.21: Isophotal twist, $\Delta P.A.$, versus the corresponding change of ellipticity, $\Delta\epsilon$, for galaxies with $\epsilon < 0.3$. (Two plot symbols strongly overlap at $\Delta\epsilon \approx 0$, $\Delta P.A. \approx 29$.)

if we would assume that the determination of twists for round galaxies is due to photometric inaccuracy, the spread of values exhibited by these objects must be real, as it does not depend on luminosity (no correlation was found between twist and total magnitude). (4) Considering the $P.A.$ profiles in Fig. 2.12, it is evident that the variations of the position angles are systematic and not irregular, as would be expected, if they were caused by measurement errors. Strong oscillations are only found in galaxies for which the presence of a spiral structure has been shown (IC0783, IC3328) and, hence, the strong scatter is explicable.

In order to asses the meaning of the twists observed it is important to consider the fact that we can only measure apparent ellipticities. As the distribution of intrinsic ellipticities for dwarf ellipticals has a maximum at ~ 0.3 with a sharp decline for rounder shapes (Binggeli & Popescu 1995), most of the objects with $\epsilon < 0.3$ in our sample might suffer from projection effects, i.e. they appear rounder than they really are. On the other hand, assuming that these objects are triaxial ellipsoids, we would expect to observe an apparent isophotal twist, if the intrinsic axial ratios would change with radius (Binney 1978). Indeed, large twists are only exhibited by galaxies with $\epsilon < 0.3$ and might therefore be due to *projection* and not to intrinsic changes of the position angles. In Fig. 2.21 the isophotal twists are plotted versus the change of ellipticity, measured in the same radial range in which the twist is observed. Only galaxies with $\epsilon < 0.3$ are shown. A rather striking correlation is in fact evident: *strong twists seem to occur only when a considerable change of the ellipticity takes place as well*. This strongly supports the conjecture that the twist effect (Fig. 2.20) is due to the *projection of intrinsically triaxial ellipsoids*.

Besides the twist-ellipticity relation, we also found a weaker correlation between twist and effective surface brightness. Thus, a connection between isophotal twist and nuclear offset might be expected and is indeed present, at least for the dE,Ns. Fig. 2.22 shows that *galaxies with stronger twists have larger nuclear offsets*. As the measurement of the offsets should not be affected by projection effects, the origin of the relation in Fig. 2.22 is difficult to understand. However, assuming that the isophotal twists are real, the connections between effective surface brightness/radius, offset, and twist might indicate that less compact objects also tend to have stronger anomalies in their isophotal properties.

2.5.4 Ellipticity profiles

Most of the galaxies show a rather steep central rise in the ellipticity profile, particularly obvious in the brightest nucleated objects (see Fig. 2.12). This is not the nucleus itself, which is much smaller in size, but it might be due to the gravitational influence of the nucleus on the orbits of the nearby stars. Indeed, simulations indicate that already a rather low massive object in the center can scatter stars off the central density cusp and therefore disrupt box orbits and forcing the stars on circular paths (Gerhard & Binney 1985). If the nucleus is more massive, probably hosting a black hole, it can even shape the whole galaxy, leading to a rounder object. This was in fact predicted by Norman (1986) and confirmed through observations by BBJ (see their Appendix).

2.6 Summary and Conclusions

2.6.1 Surface photometry

We have carried out surface photometry (in B and R) and a detailed isophotal analysis (in R) for 25 early-type dwarf galaxies in the Virgo cluster. The sample considered mainly consists of nucleated dwarf ellipticals and has a mean absolute magnitude in B of $\langle M_{B_T} \rangle = -15.76$ and a mean colour of $\langle B-R \rangle = 1.27$.

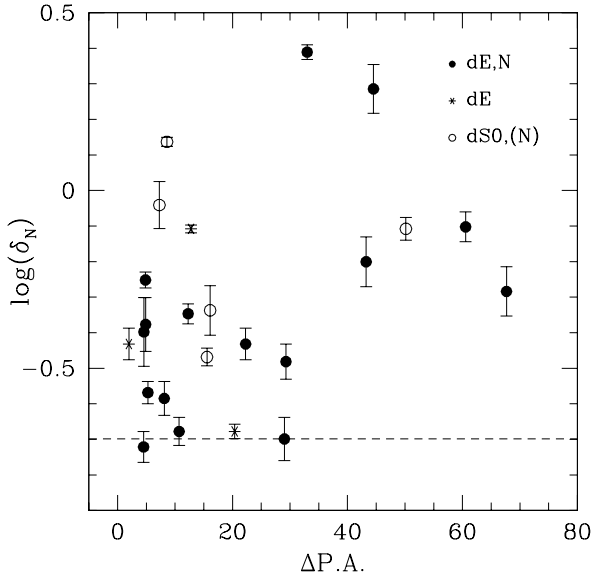

Abbildung 2.22: Isophotal twist, $\Delta P.A.$, versus the logarithm of δ_N. The dashed line indicates our lower detection limit of $0\farcs2$. The meaning of the symbols is indicated.

We provide surface brightness profiles in both filters and radial colour gradients. All profiles have been fitted by a Sérsic model and the corresponding parameters have been derived. Plotting these best fitting parameters together with the ones for giant ellipticals and local group dwarfs versus absolute magnitude (Fig. 2.13), we confirm the finding of Jerjen & Binggeli (1997) and jerjen, Binggeli & Freeman (2000) that the cluster dwarfs perfectly bridge the gap between giant ellipticals and dwarf spheroidals, indicating that there is *one, continuous family* of spheroidal stellar systems, provided the central few 100 pc of these galaxies is not considered. However, considering in detail the fits obtained, we find several profiles with rather large deviations from the models, in particular in the more central parts. By defining a mean, absolute residual, $\langle S_{res} \rangle$, taking into account also the errors of the profiles, we find that bright galaxies, having $\mu_{eff} < 22$ mag, show the strongest deviations from the Sérsic form. We suggest that in addition to the objects with disk structure (spiral or bar) signatures (Jerjen, Kalnajs & Binggeli 2000, Barazza et al. 2002) where strong residuals might be expected, some of the bright dwarfs may be quite complex in structure, possibly being two-component systems as well.

2.6.2 Isophotal analysis

By fitting ellipses to the isophotes, we have derived radial profiles for the ellipticity, position angle, major axis, and shape parameter a_4 (Fig. 2.12). For these parameters, as well as for the offsets of the nuclei we have determined mean (global), luminosity-weighted values (Table 2.3). Plotting ellipticity versus $a_4/a * 100$ we find a similar distribution as Bender et al. (1989) for giant ellipticals. However, as in the dE sample of Ryden et al. (1999) and in contrast to giant Es, there is no gap in the distribution between disky and boxy for highly flattened galaxies, i.e. there are highly flattened dEs that are perfectly elliptical. The meaning of a *mean* a_4-value is not so clear, however, as most of the galaxies have a a_4-profile that changes sign (from boxy to disky, or vice versa) along the galactocentric radius. Almost any behaviour

of the a_4 profile can easily be reproduced with multi-component (many parameter) models, but in lack of any knowledge about the inclination(s), i.e. the *intrinsic* shapes of the components, it seems impossible to construct *unique* models for the isophotal structure of these galaxies.

As most of the sample galaxies are nucleated, we have also searched for the presence of off-center nuclei. Most nuclei are indeed slightly off center. Defining δ_N as the offset of the nucleus from the center of the overall light distribution, we have looked for systematic relations between nuclear offsets and other galaxy properties. We confirm the existence of a relation between δ_N and the effective surface brightness, which was first suggested by Binggeli et al. (2000): galaxies with fainter effective surface brightnesses tend to have larger nuclear offsets. A similar relation is found to hold between δ_N and the effective radius. The most plausible explanation of the phenomenon is that the nuclei are simply oscillating about the centers in the shallow potential wells of these galaxies, as suggested by numerical simulations (Miller & Smith 1992, Taga & Iye 1998). The shallower the potential well (the lower the surface brightness), the higher the expected amplitude of the oscillations.

In addition, we determined isophotal twists, i.e. the largest changes of the position angles of the major axes within the range used for the isophotal analysis. We find a clear dependence of the twists measured on ellipticity in that large twists occur only in galaxies with $\epsilon < 0.3$. On the other hand, most of these galaxies are likely intrinsically more flattened, as the distribution of intrinsic ellipticities has a maximum at ~ 0.3. Assuming that the objects are intrinsically triaxial ellipsoids, we suggest that the twists observed, always being accompanied by changing axis ratios, are caused by projection effects.

In view of the results of the isophotal analysis we conclude that *less compact dwarf galaxies generally tend to have stronger irregularities* like off-centered nuclei or twisted isophotes, than more compact systems. However, with the available data we cannot decide whether these properties are caused by external perturbations or are due to the presence of substructures in these objects. Moreover, projection effects may play a crucial role in producing certain isophotal properties. Assuming that dwarf elliptical galaxies are intrinsically triaxial systems, the twists observed could be explained in terms of projection effects caused by changing axial ratios in apparently round galaxies that are intrinsically more flattened.

3
More evidence for hidden spiral and bar features in bright early-type dwarf galaxies

Abstract

Following the discovery of spiral structure in IC3328 (Jerjen et al. 2000), we present further evidence that a sizable fraction of bright early-type dwarfs in the Virgo cluster are genuine disk galaxies, or are hosting a disk component. Among a sample of 23 nucleated dwarf ellipticals and dS0s observed with the Very Large Telescope in B and R, we found another four systems exhibiting non-axisymmetric structures, such as a bar and/or spiral arms, indicative of a disk (IC0783, IC3349, NGC4431, IC3468). Particularly remarkable are the two-armed spiral pattern in IC0783 and the bar and trailing arms in NGC4431. For both galaxies the disk nature has recently been confirmed by a rotation velocity measurement (Simien & Prugniel 2002). Our photometric search is based on a Fourier decomposition method and a specific version of unsharp masking. Some "early-type" dwarfs in the Virgo cluster seem to be former late-type galaxies which were transformed to early-type morphology, e.g. by "harassment", during their infall to the cluster, while maintaining part of their disk structure.

3.1 Introduction

The physical nature and origin of early-type dwarf (essentially dE) galaxies is still largely unknown (for a review see Ferguson & Binggeli 1994). According to their apparent flattening, which is similar to the one measured for giant ellipticals (Binggeli & Popescu 1995; Ryden & Terndrup 1994), early-type dwarfs seem to be spheroids. This is supported by the fact that most of these systems are not rotation-supported (Ferguson & Binggeli 1994; de Rijcke et al. 2001; Geha et al. 2001). On the other hand, it has always been suspected that a considerable number of early-type dwarfs might be disk galaxies. In fact, around 20 bright early-type dwarfs in the Virgo cluster are classified dS0 because of their S0-like morphology, exhibiting a lens, a bar, or high flattening (Sandage & Binggeli 1984; Binggeli & Cameron 1991). In certain evolutionary scenarios, like ram-pressure stripping (Gunn & Gott 1972; Abadi et al. 1999) or galaxy harassment (Moore et al. 1998), dwarf ellipticals are believed to have originated from late-type spirals or irregulars, hence some of them might have retained their disk nature. In addition, Ryden et al.

(1999) showed that many early-type dwarfs have "disky" isophotes, similar to giant ellipticals.

Recently, Jerjen et al. (2000) discovered a weak spiral structure in the seemingly normal dwarf elliptical galaxy IC3328 by means of deep VLT-photometry. This is unambiguous evidence for the presence of a disk in this galaxy, supporting the conjecture that the number of (hidden) disk galaxies among bright early-type dwarfs could be quite high.

Following the work of Jerjen et al. (2000), we carefully searched a larger sample of dEs observed with the VLT for additional indications of spiral or bar structure. We first applied the same techniques as for IC3328, i.e. relying on residual images and Fourier analysis. Among the 23 dEs studied we found seven promising candidates for hidden disk structure. However, when we further explored these objects we realized that the observed spiral and bar features which we took as disk signatures are accompanied, and could actually be *caused*, by a specific behaviour of the ellipticity and position angle profiles. By performing a set of simulations with artificial galaxies we convinced ourselves that the interplay between photometric parameters can indeed produce amazingly spiral-like twisting isophotes and thus mimic a genuine spiral structure. Hence, although the particular parameter combinations found in many galaxies are remarkable in themselves, they cannot unambiguously be interpreted as signs of disk structure.

Fortunately, the ambiguity can be solved by applying an unsharp masking technique, which is a model-free method to amplify *local* image residuals. Only four of the seven candidates mentioned (two of which are already classified as dS0), in addition to IC3328 (Jerjen et al. 2000), withstood the scrutiny of unsharp masking: IC0783, IC3349, NGC4431, and IC3468. These are the galaxies focused on in the present paper. Although none of the four discovered cases is as spectacular as IC3328 with its tightly wound spiral, they show that the fraction of disk galaxies among bright early-type dwarfs, at least in the Virgo cluster, is 20% or larger. We recall that the situation is quite similar to classical (non-dwarf) elliptical galaxies, where also some Es turned out to be barred S0s, or to contain such a component, as betrayed by inner isophotal twists (Nieto et al. 1992).

The rest of the paper is organized as follows. In Sect. 3.2 we give some observational background and put this investigation into context with our more general project. In Sect. 3.3 we employ, and present the results of, a Fourier analysis of the galaxy images. Sect. 3.4 contains a brief account of the application of unsharp masking, which is the decisive detection tool. In Sect. 3.5 we discuss our findings and what they could mean, case by case. A summary is given in Sect. 3.6. Throughout this paper we assume a distance to the Virgo cluster of $D = 17$ Mpc, corresponding to $(m - M) = 31.15$.

3.2 Observational background

This work is part of a larger project aimed at the determination of distances to dwarf elliptical galaxies in the Virgo and Fornax clusters by means of the Surface Brightness Fluctuations method, and a detailed photometric analysis of their brightness distributions. The galaxies were primarily selected by their morphological appearance, i.e. early-type dwarfs (dE, dS0), and by their apparent size, i.e. an isophotal radius $r_{B,25} > 30''$. So far, 25 objects have been observed in two runs at the Very Large Telescope at ESO Paranal Observatory in service mode. Details of the observations are to be reported elsewhere (Jerjen et al., in preparation). The important parameters of the four galaxies considered in this study are listed in Table 3.4. The columns of the Table are as follows: *columns* (1) and (2): identification of the observed galaxy; *column* (3): morphological type in the classification system of Sandage & Binggeli (1984), taken from Binggeli et al. (1985); *column* (4): total R-band magnitude, corrected for galactic extinction (from Barazza et al., in preparation); *column* (5): absolute R-band magnitude; *column* (6): total colour index $B - R$; *column* (7): heliocentric radial velocity in km s^{-1} (from the NED); *columns* (8) and

Tabelle 3.4: Basic data of the early-type dwarfs considered in this study

VCC (1)	Name (2)	Type (3)	R_T (4)	M_{R_T} (5)	$B-R$ (6)	$v_\odot$ (7)	ϵ (8)	pa (9)
0490	IC0783	dS0(3),N	12.63	-18.52	1.34	1293	0.25	130
0940	IC3349	dE1,N	13.56	-17.59	1.25	1563	0.22	14
1010	NGC4431	dS0(5),N	12.47	-18.68	1.39	913	0.38	168
1422	IC3468	E1,N:	12.64	-18.51	1.16	1372	0.17	150

(9): ellipticity $\epsilon = 1 - \frac{b}{a}$, where a and b are the major and minor axis, and position angle pa (from top counterclockwise), respectively, determined at an isophotal level of $\sim 25\mathrm{mag}/\Box''$ in R.

Direct R-band images of the galaxies are shown in the left column of Fig. 3.23. The image reduction and the determination of the standard photometric parameters have been performed with ESO's image processing package MIDAS. The detailed results of the photometry, like surface brightness profiles, effective radii, colour gradients etc., as well as best-fitting Sersic parameters will be presented elsewhere (Barazza et al., in preparation). Using the MIDAS application FIT/ELL3 we fitted ellipses to the isophotes of the galaxies and, hence, determined their centers, ellipticities and position angles. The ellipticities and position angles of the fitted ellipses versus the equivalent radius, $r = \sqrt{ab}$, are shown in the top two panels of Fig. 3.24. The variations of these two parameters are indicative of the asymmetric features we are interested in.

3.3 Residual images and Fourier expansion

In a first approach we subtracted the deprojected and azimuthally averaged light distribution of a galaxy from the original image. More precisely, we reconstructed a galaxy using the measured surface brightness profile with *fixed* ellipticity and position angle, as given in cols. 8 and 9 of Table 3.4, and subtracted this model from the original. The results derived in this manner are shown in the second column of Fig. 3.23. Strong residuals are evident in the inner parts of all four galaxies.

IC0783 and NGC4431 show the most striking features; in both cases weak signs of spiral or bar structure can be discerned, or guessed, already in the direct images (left column). The spiral arms of IC0783 are beautifully traced by the oscillations in the ellipticity and position angle profiles plotted in Fig. 3.24. The residual of IC3349, which otherwise is a normal, almost round dwarf elliptical with a bright nucleus, shows an extended and seemingly lumpy structure along the major axis. The bright knot about $10''$ south-east of the center is caused by a luminous background galaxy. NGC4431 is certainly the most interesting case. In the northern and southern part of its R-band image two dark arcs are visible (unfortunately barely so in the printed version). The residual shows that these arcs are at the end of a bar, forming the outer edges of a spiral-like feature, probably the trailing arms of the rotating bar.

Finally, in the residual of IC3468 we note a prominent hourglass-like feature. This is in fact what is expected to appear whenever the ellipticity in the central part of a galaxy significantly changes with radius, and it was observed in more than these four galaxies (cf. Sect. 3.1). Indeed, by inspecting Fig. 3.24 (top row), we see that the ellipticity profile shows an inner peak in all four cases. Moreover, if an ellipticity change is combined with only a slight change of position angle (twisting isophotes), the residual,

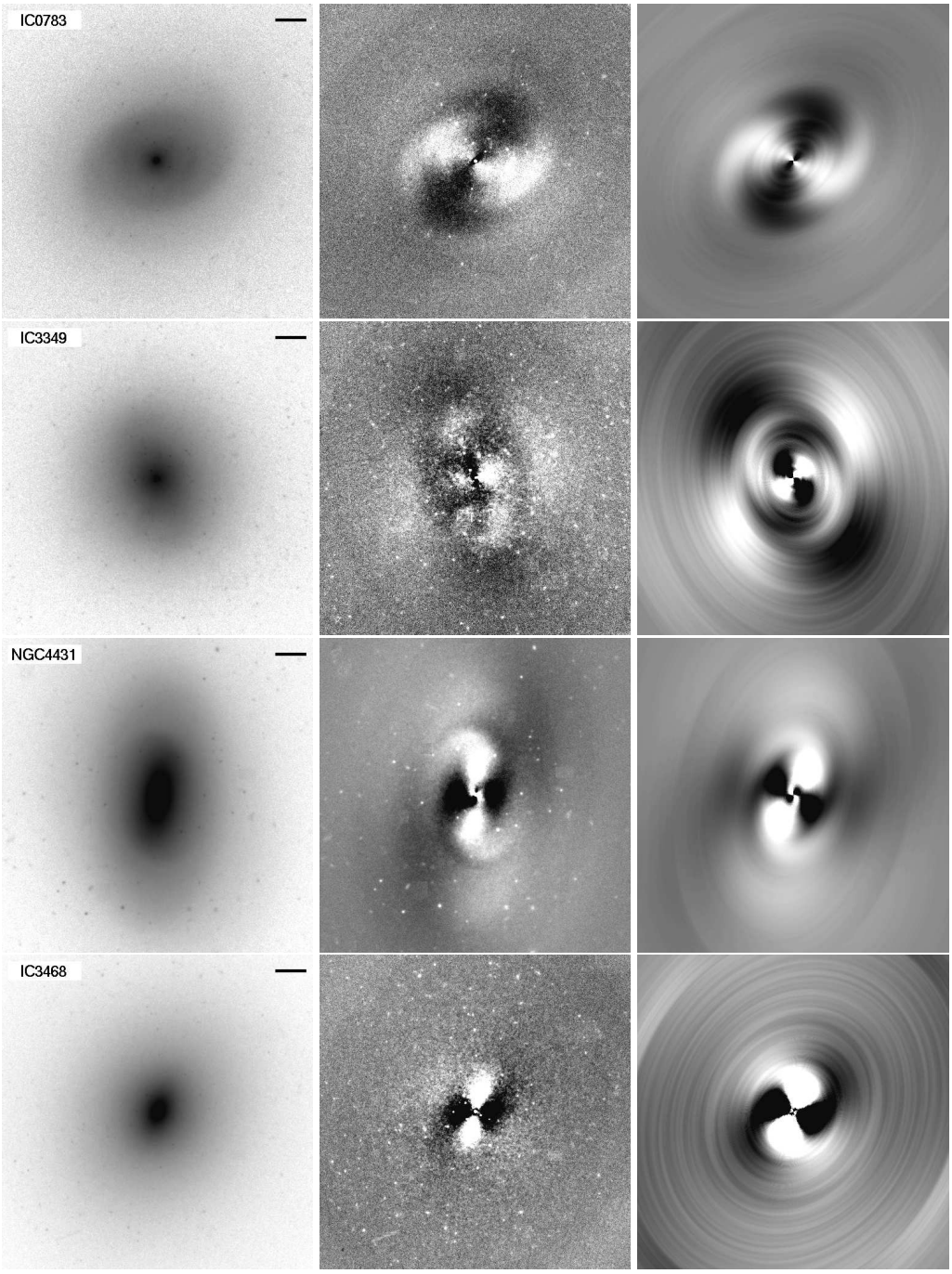

Abbildung 3.23: Left column: R-band images of the galaxies. The bar in the upper right corner corresponds to $10''$ (~ 1 kpc). Middle column: residuals obtained by subtracting the mean, deprojected surface brightness profile, corresponding to the first Fourier coefficient I_0 from the R-band image. Right column: representation of the third Fourier coefficient (Fourier map), see text. Image size: $1\farcm7 \times 1\farcm7$. North is up and east to the left.

as a means of amplification, can additionally show (sometimes dramatic) spiral structure. Again we note

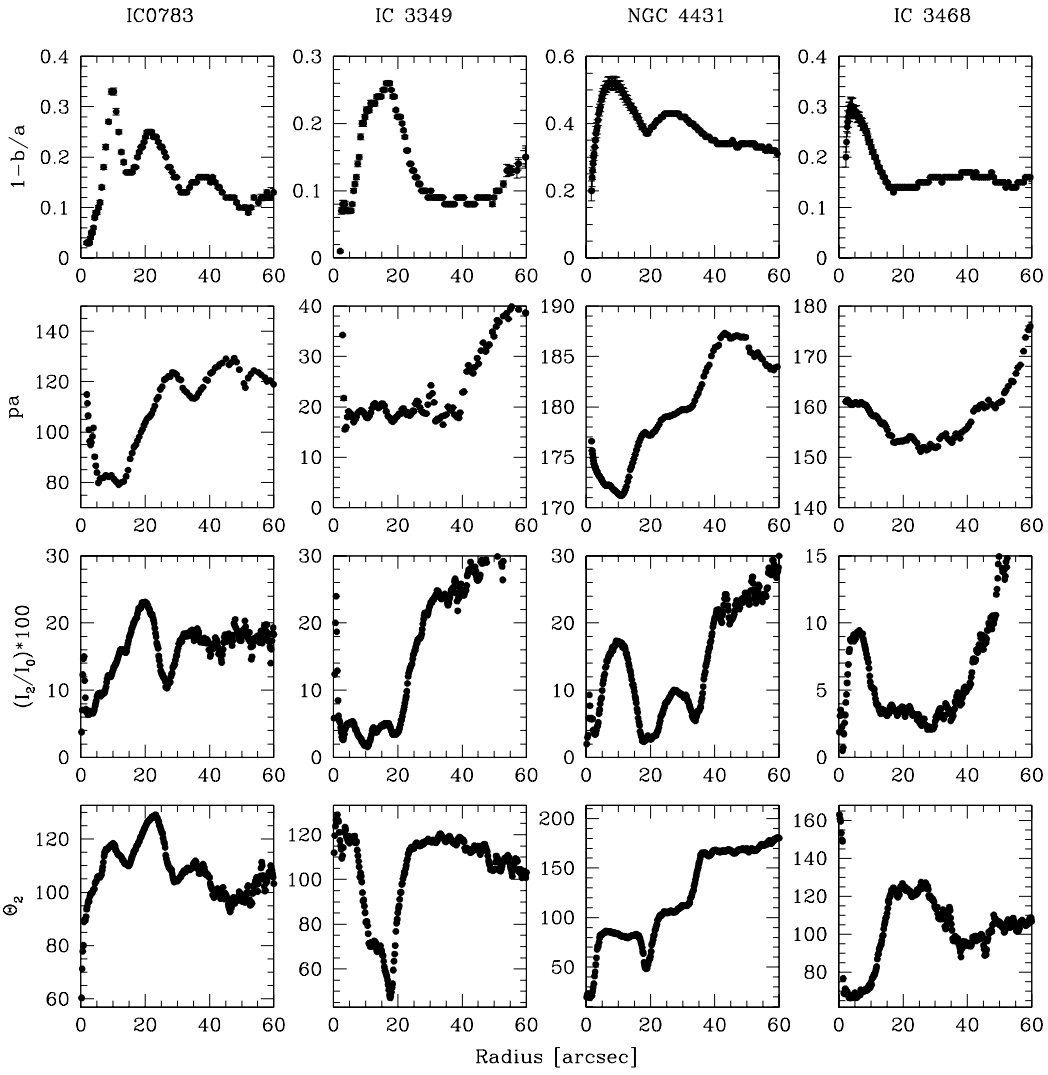

Abbildung 3.24: First row: ellipticity profile; second row: position angle profile. Third row: relative strength, in percent, of the third Fourier coefficient I_2 relative to I_0. Fourth row: profile of the phase angle Θ_2 of the third Fourier coefficient. All parameters are plotted against the equivalent galactocentric radius.

in Fig. 3.24 (second row from top) significant position angle changes in IC0783 and NGC4431, where we found traces of spiral arms. As ellipticity changes and twisting isophotes are quite commonly found in spheroidal galaxies, possibly as a result of their intrinsic triaxiality (e.g. Kormendy 1982, Binney & Merrifield 1998), it is thus clear that hourglass-like and spiral-like features found in residual images of the kind shown in Fig. 3.23 must not, at face value, be taken as indication for the presence of a true bar or true spiral structure (i.e. disk structure). However, as mentioned in the introduction and as demonstrated in the following section, the residual features in our four dwarfs clearly persist when scrutinized with an

unsharp masking method. Their strength makes it difficult to explain these features as mere artifacts produced by such parameter combinations; it is more likely that they indicate the presence of a real disk (bar and/or spiral) structure that is naturally accompanied by a systematic change in ellipticity and position angle when ellipses are fitted to the surface brightness distribution.

To analyse the residual features found in a more quantitative manner, we then Fourier decomposed the direct images. This technique has frequently been used in the past to quantify non-axisymmetric structures in disk galaxies (Grosbol 1987; Elmegreen et al. 1989; Rix & Zaritsky 1995, Vera-Villamizar et al. 1998). We used the Fourier expansion in the polar form, with azimuthal angle Θ. To this end we had to determine the centers of the galaxies first. Since we did not measure a considerable offset for any of the nuclei, we derived the centers by fitting a Gaussian to them. The pixel positions could then be expressed in polar coordinates. All isophotes were subsequently deprojected using the ellipticities and position angles from Table 3.4, and represented by 128 pixels uniformly distributed over each isophote. Finally, the corresponding intensities, $I(r, \Theta)$, were expanded in the Fourier series:

$$I(r,\Theta) = I_0(r) + I_1(r)\cos[\Theta - \Theta_1(r)] + I_2(r)\cos 2[\Theta - \Theta_2(r)] + ... \quad (3.6)$$

The zeroth order Fourier coefficient, I_0, only depends on the radius and is therefore equivalent to the mean surface brightness of the galaxy. Actually, converting I_0 in magnitudes and plotting it versus radius yields the mean surface brightness profile. The first order Fourier coefficient, I_1, characterises the offset of the isophote with respect to the chosen center. Hence, this parameter is a measure of the lopsidedness of a galaxy and the associated phase angle, Θ_1, indicates the direction of the offset. It could also be used to measure the offset of the nucleus from the center of the brightness distribution. The next coefficient, I_2, is associated with even-numbered asymmetries, e.g. structures like bars or an even number of spiral arms. Since the residuals in Fig. 3.23 show structures of this kind, we plotted the relative strength of I_2, expressed as $(I_2/I_0) * 100$, in the third row of Fig. 3.24 (intensity profile). The values shown therefore indicate the strength of the structures in percent of the underlying luminosity. In the fourth row the corresponding phase angle, Θ_2, is shown. This angle points to the position of the signal on the isophote. With respect to the radius it remains constant for a bar, indicating its position angle (e.g. NGC4431), and rises/decreases linearly for a spiral pattern (as beautifully seen in IC3328; cf. Jerjen et al. 2000).

However, the interpretation of this phase angle profile is not always so clear. We have therefore developed a method to map the third term of the Fourier expansion, i.e. $I_2(r)\cos 2[\Theta - \Theta_2(r)]$. Since each pixel belongs to an ellipse around the center, we can expand this specific ellipse in the given Fourier series and transform the pixel intensity according to

$$I_{x,y}(r,\Theta) = I_2(r)\cos 2[\Theta_{x,y} - \Theta_2(r)] \quad (3.7)$$

where x, y are the pixel coordinates. This procedure yields a visual representation of the information contained in the plots of the third and fourth row in Fig. 3.24. In the following, we denote these representations as "Fourier maps". The results for the sample galaxies are shown in the third column of Fig. 3.23. The Fourier maps are very similar to the residuals (middle column of Fig. 3.23), confirming that the structures shown by the residuals are of the symmetric type, giving a strong signal in I_2.

Let us now go through our sample galaxies, case by case. Considering the direct image and the ellipticity profile, IC0783 is clearly showing spiral structure. Unfortunately, the residual and the Fourier map, as well as the phase angle profile are not equally revealing. The reason for this might be the existence of an inner ring: its phase angle would be undefined and could cause the observed hump between $10''$ and $15''$. IC3349 is rather puzzling. The residual image of this galaxy in Fig. 3.23 shows an elongated,

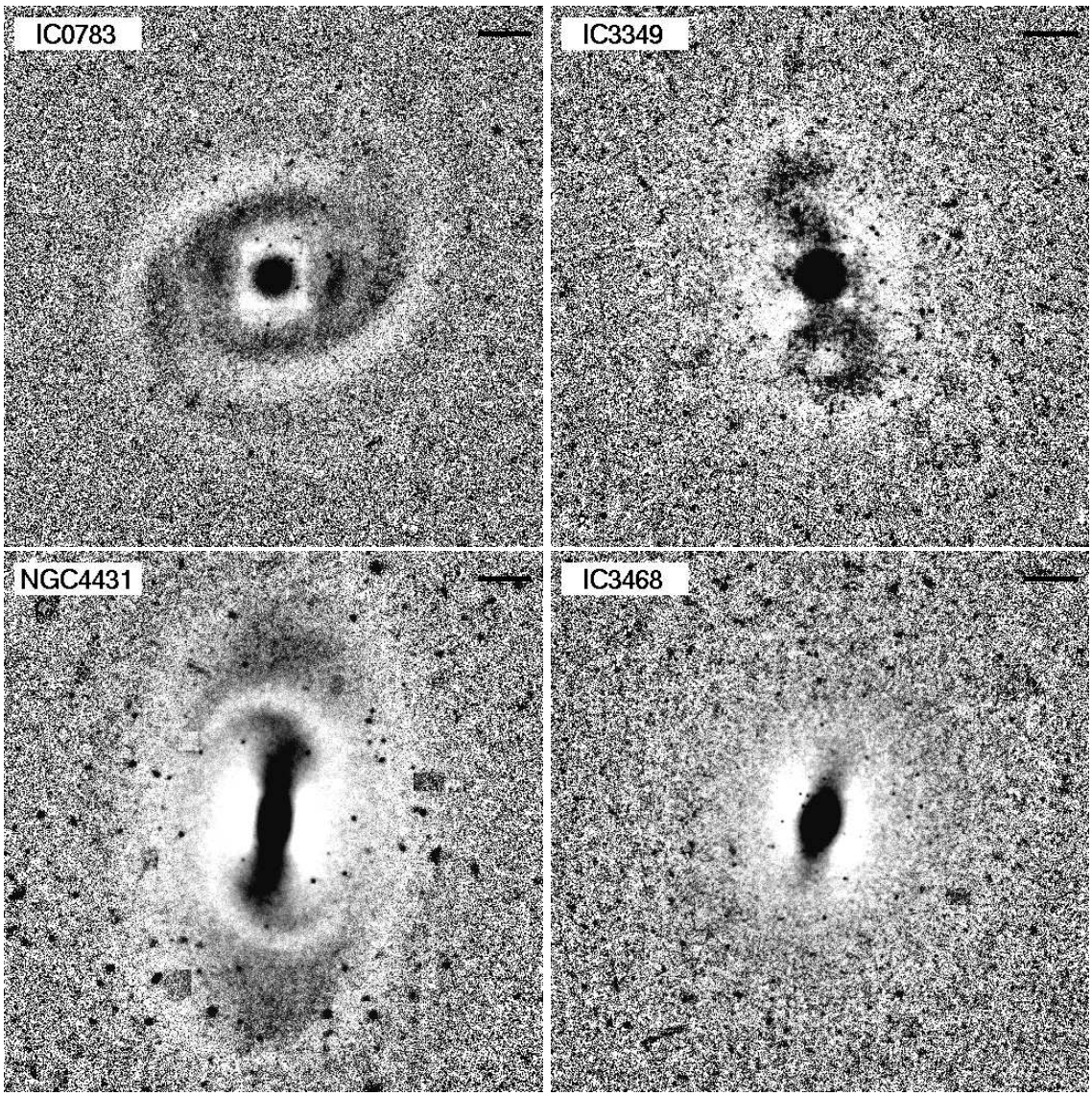

Abbildung 3.25: Result of unsharp masking for the four galaxies. The images are negatives. Size and orientation as in Fig. 3.23.

bar-like structure which is also evident in the ellipticity profile, where it appears as a prominent maximum around $20''$, and in the position angle, which is more or less constant in the same range. However, this does not appear in the Fourier parameter plots. The phase angle is strongly varying and the intensity profile shows almost no signal in this region. In contrast, NGC4431 is a clear case. The phase angle remains nearly constant between $4''$ and $17''$, the I_2 profile shows a corresponding luminosity excess of $\sim 18\%$, and the ellipticity profile is considerably peaked: all of this clearly points to the presence of a bar. The case of IC3468 is similar to this, but on a much smaller scale and with lower intensity. A sharp peak in the ellipticity and intensity profile, along with a constant phase angle are again pointing to a bar, whose length and intensity reach about half the values shown by NGC4431.

3.4 Unsharp Masking

A well-known method to uncover hidden structures that is independent of the Fourier analysis, and that also has the advantage that no assumptions are required, is unsharp masking. This method, which is also applicable to photographic plates (Malin & Zealey 1979), was widely used in the search for hidden inner structures in different objects. It was successful in investigating the fine structures in elliptical galaxies (Schweizer & Ford 1985), dust features in globular clusters (Mendez et al. 1989), and the true nature of bars in disk galaxies (Buta & Crocker 1993). Recently, Colbert et al. (2001) investigated the morphological differences between elliptical galaxies in different environments using, among other methods, unsharp masking.

The method essentially consists of deconvolving the optical image with an appropriate function. Often a point spread function, like a Gaussian, is used. We chose an even simpler approach: we produced a smoothed image by replacing each pixel intensity with the average intensity in a certain area around that pixel. The optimal size of this area obviously depends on the extension, or scale of the structure to be uncovered. We fixed this size simply by trying different smoothing lengths until the result was satisfactory. Applying the MIDAS task FILTER/SMOOTH, we obtained the best results with a smoothing radius of 30 pixels, corresponding to $6''$. Hence, each pixel intensity was set to the average intensity in a square of 31×31 pixels. The original image was then divided by this smoothed version. The result of this procedure for our four galaxies is shown in Fig. 3.25.

All four objects show very strong residual features – we will discuss them in detail in the following section. What was guessed before on the basis of "global" residual images and a Fourier analysis now appears with utmost clarity. It is important to note again that *no assumptions* are required here. We do not have to assume a global ellipticity and position angle in advance, to which the residuals refer – with unsharp masking we determine the residual light with respect to the *local* environment based on the observed brightness distribution alone.

Whenever residual features are uncovered in otherwise perfectly spheroidal galaxies, the presence of dust has to be considered as a possible cause (dust lanes in the cores of bright ellipticals are quite common; cf.,e.g., Binney & Merrifield 1998). Dust can be detected by its reddening of the colour. However, the $B - R$ colour maps of our galaxies do not show any conspicuous features other than a slight symmetric colour gradient (to be reported elsewhere). The only possible exception is NGC4431 whose colour map reveals that the bar may be slightly redder than the rest of the galaxy. In particular, IC3349, where dust could be suspected because the bar-like feature appears somewhat lumpy, is perfectly smooth in colour as well. This means that the residual brightness features reflect density enhancements in the distribution of stars – which of course is the case with true bars and spirals.

3.5 Discussion

The disk nature of **IC0783** has been conjectured before and this object has therefore been classified as dS0 (Sandage & Binggeli 1984; Binggeli & Cameron 1991). The possible presence of two spiral arms has already been reported (Barazza et al. 2001; Jerjen et al. 2001). This finding is clearly confirmed by our results. To what kind of central structure these arms are connected is not so evident, however. Since the phase angle is not constant in the central part, the presence of a bar is not very likely. We rather suggest the existence of an inner ring, as mentioned in Sect. 3.3. The strongest luminosity excess is observed at the locations where the spiral arms start, i.e. the connection points between the ring and the arms. This can be seen in the Fourier maps and also in the intensity profile, which reaches a relative excess of $\sim 24\%$.

During the refereeing stage of this paper, Simien & Prugniel (2002) have published a rotation curve of IC0783 (the authors classify this galaxy as SAB(rs)0/a in the de Vaucouleurs system, which is in agreement with our own new classification). Not surprisingly, as judged from the spiral morphology, the galaxy does show rotation, though only with a observed maximal radial velocity of v_{max} = 22 km s^{-1}, or v_{rot} = 33 km s^{-1} in the plane of the disk, if we assume that the galaxy's apparent ellipticity of 0.25 (Table 3.4) reflects the disk's inclination only. The observed central velocity dispersion is even a bit larger with σ = 36 km s^{-1} (however, the uncertainties, also for the inclination, are considerable).

IC0783 is situated in a region of rather low density within the Virgo cluster. The distance to the cluster center, i.e. M87, is quite large. In fact, this galaxy is probably a member of a group around the giant Sbc galaxy M100. The projected distance between M100 and IC0783 is ~ 100 kpc and the radial heliocentric velocities are $v_\odot = 1571$ km s^{-1} and $v_\odot = 1293$ km s^{-1} for M100 and IC0783, respectively (all velocities from the NED). IC0783 could therefore be bound to M100. The whole group is believed to have fallen into the cluster recently (Binggeli et al. 1987). Even if the group were falling in for the first time, IC0783 could already have been stripped of its gas and stopped star formation, in accord with its rather red colour of $B - R = 1.34$ and the non-detection of the spiral structure in the colour map.

IC3349 has been classified as dE1,N; it is very round and has a bright nucleus. The image from unsharp masking reveals an elongated structure almost along the major axis of the galaxy. As mentioned in Sect. 3.3, the knot lying south-east of the nucleus is caused by a background galaxy. Therefore, the feature is quite symmetric. The best photometric evidence for the structure is provided by the ellipticity profile, which shows a pronounced maximum at $\sim 20''$. Despite its weakness (the luminosity excess amounts only to $\sim 5\%$), the structure clearly resembles a bar. Its thick, dumb-bell-like ends are in fact reminiscent of the classical SB0$_3$ Hubble type. There is even a slight hint for rudimentary spiral/trailing arms as in NGC4431 (though much less clearly). In any case, the presence of a bar suggests that IC3349 is a rotating disk galaxy. There is no kinematic data available yet to confirm this. IC3349 is located in the Virgo M87 subcluster as well, i.e. in the densest region of the cluster. It is more or less between M87 and M86, but closer to the latter, and does not seem to be associated with a giant galaxy.

The most impressive discovery is the beautiful bar in **NGC4431**. This galaxy has been classified as dS0 before, though without acknowledging the presence of a bar (Sandage & Binggeli 1984); we now would call it a dSB0/a. Its twisting isophotes have been pointed out by Ryden et al. (1999), where a contour plot of a V-band image is shown. Also Gavazzi et al. (2001) observed this galaxy in the B- and V-band and performed a profile decomposition.

In the unsharp masked image in Fig. 3.25 the bar and the trailing arms of NGC4431 are very striking. The whole morphology is reminiscent of the results of a bar simulation presented by Patsis & Athanassoula (2000). The gas density distribution plotted in Fig. 5 of that paper shows exactly the same features. In particular, the authors draw attention to the typical "T-structure", consisting of the bar, the trailing arms plus short density enhancements on the leading side of the bar. Even the gaps beyond the outer edges of the trailing arms, followed by another pair of denser filaments, are much the same in NGC4431 and the simulation. Given this similarity, we can assume that the bar in NGC4431 is rotating clockwise. However, we should also note a difference in size: the bar in the simulation has a length of ~ 10 kpc, whereas the observed one measures only ~ 3 kpc. But just this smallness may provide another interesting aspect: As dwarf galaxies are believed to contain large amounts of dark matter, and as the pattern speed of a bar is governed by the mass distribution via dynamical friction (Debattista & Sellwood 1998, 2000), objects like NGC4431 might offer new possibilities to put constraints on the dark matter content of dwarf galaxies.

The pattern speed of the bar in NGC4431 is still unknown, but its solid body rotation has been measured: the rotation curve determined by Simien & Prugniel (2002) nicely shows the expected linearity

over the scale of the bar. The maximum rotational velocity for NGC4431 is listed as v_{max} = 60 km s^{-1}. As the galaxy is apparently strongly flattened (ϵ = 0.38, Table 3.4), meaning its disk is strongly inclined, this transforms into a mere v_{rot} = 76 km s^{-1} in the plane of the disk – barely larger than the measured central velocity dispersion of σ = 55 km s^{-1}.

NGC4431 is close to the center of the Virgo cluster; its projected distance to M87 is ~ 300 kpc. It is therefore located in a rather dense region and belongs to subcluster A (Binggeli et al. 1987). In fact the dwarf-like SBa galaxy NGC4440 and another dS0 type, NGC4436, lie within a projected radius of ~ 40 kpc (see image in Sandage & Binggeli 1984). However, the radial velocities of these galaxies are quite different. NGC4431 itself has $v_\odot = 913$ km s^{-1}, the closest neighbors (in projection), NGC4436 and NGC4440, have $v_\odot = 1163$ km s^{-1} and $v_\odot = 724$ km s^{-1}, respectively. A physical grouping of these dwarfs is therefore unlikely

Finally, a small, bar-like feature is evident in the unsharp masked image of **IC3468**. The peak in the ellipticity profile is very narrow and the relative intensity reaches almost $\sim 10\%$. Note that the galaxy has been classified E1,N instead of dE1,N – precisely on the basis of the high-surface brightness central core that was found to be indicative of a classical (non-dwarf) elliptical. It is not clear whether we see a small disk nearly edge-on embedded in an almost round (dwarf) elliptical, or a very short bar embedded in a disk galaxy almost face-on. Judging from the pointed (lemon-shaped) isophotes of the residual feature (as confirmed by a "disky" value of $a_4/a \sim 0.01$ in the inner 15"; see below), a disk component within a spheroid would seem more likely. Surprisingly, however, Simien & Prugniel (2002) were not able to measure any appreciable rotation in IC3468, listing $v_{max} < 9$ km s^{-1} for this galaxy (along the correct position angle of the elongated inner feature). An embedded edge-on disk can therefore be excluded. But a bar in an almost face-on disk is a difficult interpretation as well, because with ϵ = 0.17 (Table 3.4) the deprojected velocity of $v_{rot} < 16$ km s^{-1} would still be much smaller than the central velocity dispersion σ = 36 km s^{-1}. With v_{max}/σ = 0.25, IC3468 appears to be a typical anisotropic (non-rotation-supported) dwarf elliptical. One might argue, though, that the maximum of the rotation curve was not reached by Simien & Prugniel (2002); their measurements indeed cover only the innermost (barred) part of the galaxy. We think the case – for or against the presence of disk structure in this galaxy – is left open. As to its position in the cluster, IC3468 is situated between the A subcluster, dominated by M87, and the M49 subcluster in the south of Virgo and is therefore in a region of rather low density.

We have also done an isophotal analysis for all our Virgo dwarfs observed with the VLT, the results of which will be reported elsewhere (Barazza et al., in preparation). In such an analysis one is looking for systematic deviations of the isophotes from pure ellipses, again by means of a Fourier method. The fourth Fourier coefficient, a_4, determines whether the isophotes are "disky" ($a_4 > 0$) or "boxy" ($a_4 < 0$). This parameter is believed to be sensitive to weak disk or bar components in elliptical galaxies, depending on the inclination angle (Carter 1987; Bender & Möllenhoff 1987; Rix & White 1990; Ryden et al. 1999). Our disk/bar dwarf candidates do show some correlation with the a_4 parameter. We have already mentioned the inner diskyness of IC3468. While IC0783 does not show a coherent a_4 signal, NGC4431 is slightly boxy, as is IC3349 slightly disky (surprisingly), in the central residual region. However, in general we think the meaning of a_4 is difficult to interpret; different combinations of components can produce the same a_4 profile. In particular, disky isophotes need not necessarily mean that there is a true disk component embedded in the galaxy. We are currently exploring the principal possibilities to model a_4 profiles.

The best evidence for the presence of disk components in dwarf ellipticals or dS0s can be expected to come from kinematic studies. These difficult observations are now underway for a large number of early-type dwarfs in the Fornax and Virgo clusters (de Rijcke et al. 2001; Geha et al. 2001). So far, the majority of dwarfs have turned out to be non-rotating spheroids. However, a few are rotation-supported and may

plainly be disk galaxies (Simien & Prugniel 1998). Interestingly, this holds only for Virgo cluster dwarfs; no rotators were found so far among Fornax dEs, nor did any of them exhibit the kind of spiral or bar features reported in the present paper (de Rijcke, private communication).

Our findings support the conjecture that a rather large number of bright, early-type dwarf galaxies, at least in the Virgo cluster, are disks or at least possess a disk component. These systems might formerly have been late-type disk galaxies which, by interactions with the cluster, were transformed to the systems we observe today. Such processes are described for example in the harassment scenario developed by Moore et al. (1998). In this picture, galaxies falling into the cluster lose all of their gas and most probably transform to a spheroid by gravitational interactions with the other cluster members. However, massive late-type galaxies might preserve their disk nature, at least for some time. The galaxies discussed could therefore be transient remnants of the harassment process. Also with respect to this scenario, the Fornax cluster may be a different galaxy environment because it is more isolated in space. The Virgo cluster is surrounded by clouds of late-type galaxies that seem to be fed into the cluster at a constant rate (see, e.g., Binggeli et al. 1987). Perhaps the high frequency of hidden disks in dEs is unique for the Virgo cluster environment.

3.6 Summary and Conclusions

Following the discovery of spiral structure in a early-type dwarf galaxy classified as dE,N by Jerjen et al. (2000), we searched our whole VLT-sample of bright Virgo dEs and dS0s for further photometric disk signatures. The principal search tools applied were (1) looking for inner residual features by subtracting a model image of the galaxy based on its mean surface brightness profile, but with fixed ellipticity and position angle, from the observed image; (2) a Fourier expansion of the galaxy image in polar form, where the lowest order of non-axisymmetry is indicating the presence of a bar or two-armed spiral structure; and (3) unsharp masking, where the original image is divided by an appropriately smoothed one to enhance any local “irregularities”. Unsharp masking turned out to be the most reliable method to uncover hidden structures. The first method can give misleading results, if the inherent assumptions on global symmetry, as well as the high sensitivity of the outcome to slightly varying position angles are not taken into account. But once the clear-cut choice by unsharp masking is made, the first two methods are useful to visualize and quantify the symmetric residual structures found.

In addition to IC3328 (Jerjen et al. 2000), we found photometric traces of a possible disk component in four more early-type dwarfs out of a sample of 23:

IC0783: The two spiral arms of this “dS0” galaxy are already evident in the direct optical image. Obviously this is a disk galaxy, which now is also confirmed by the measurement of its rotation (Simien & Prugniel 2002). The central structure of this galaxy remains unresolved; we think there could be an inner ring.

IC3349: Fourier analysis and unsharp masking reveal a long and elongated (if only weak) structure in the central part, which we interpret as a bar in a nearly face-on disk. A revised type for this “dE” galaxy would be dSB0.

NGC4431: The quite strong bar present in this galaxy is the most striking discovery and clearly reveals the disk nature of this dwarf – again nicely confirmed by its measured rotation (Simien & Prugniel 2002). Besides the bar we clearly note trailing arms and two dense regions on the leading side of the bar. This so-called T-structure is very similar to the results of a simulation presented by Patsis & Athanassoula (2000). A more fitting type for this “dS0” galaxy would be dSB0/a.

IC3468: In the very center of this dwarf elliptical we either observe a rather short bar in a nearly

face-on disk, or a small disk seen edge-on in a spheroid. Surprisingly, Simien & Prugniel (2002) found essentially zero rotation along the position angle of this structure, which renders a clear interpretation of what we see impossible at present.

We emphasize that none of these objects is comparable to IC3328. The weak and uniformly wound spiral structure in this galaxy seems to be truly unique, constituting a particular class of dwarf galaxies; at least we did not find an additional example.

Our findings confirm previous suggestions that a sizeable fraction of all bright early-type dwarfs in the Virgo cluster are disk galaxies. In a possible scenario for their evolution they are former late-type disk galaxies which have been transformed to the systems we observe today during their infall to the cluster. The discovery of more objects of this kind in the Virgo cluster, but also in other clusters, could therefore further constrain possible models for the formation and evolution of early-type galaxies in general.

4
Colour properties of early-type dwarf galaxies

4.1 Introduction

The most fundamental colour property of early-type stellar systems is the Colour-Magnitude relation (CMR) first discussed by Faber (1973) and Sandage & Visvanathan (1978) (see also Caldwell 1983, Mould 1984, Caldwell & Bothun 1987) and further established for giant ellipticals by Bower et al. (1992) (see Figure 1.11 for an example). The CMR is commonly explained in terms of metallicity: the more luminous (massive) galaxies are more metal rich, hence redder. A typical feature of the CMR is the increase of its scatter in the range $-14 \gtrsim M_B \gtrsim -18$, the domain of the early-type dwarfs. This scatter is related to the ellipticity (see appendix D) and shows a weak correlation with age (Rakos et al. 2001). However, the dwarf spheroids of the local group, which generally have $M_B \gtrsim -14$, follow the CMR. With respect to the CMR for spheroidal stellar systems the cluster early-type dwarfs therefore show the largest deviations. This suggests that their colour is not only determined by their luminosity (mass) but is influenced by at least one additional property (flattening).

The colour gradient, as a more detailed measure than the total colour, might provide further clarification in this context. It is again interesting to compare the corresponding values for giant and dwarf ellipticals. Most of the giants exhibit a negative colour gradient, i.e. they become bluer towards the outer parts (Peletier et al. 1990, Idiart et al. 2002). This is commonly interpreted in terms of a metallicity gradient, since the metal abundance is higher in the center due to a longer period of star formation that led to a stronger enrichment with heavy elements (Saglia et al. 2000). In contrast, Vader et al. (1988) find that most of the dwarfs in their sample exhibit a positive colour gradient, i.e. a reddening with larger radii. The authors assign this result to an age gradient, since galactic winds will have removed most of the enriched material, erasing the metallicity effect. The colour gradient is therefore due to a younger stellar population, resulting from a more centrally concentrated star formation. More recently, Pierini (2002) in his sample finds slightly more dwarfs with a negative colour gradient than objects with a positive gradient (using B and H colours). Moreover, he finds a relation between the gradients and the total colour indices: redder galaxies show a reddening with larger radii, whereas bluer objects become bluer towards the outer parts.

Obviously, it is difficult to develop a consistent explanation for the colour properties of early-type dwarfs found so far. In the following, we will reassess this issue. In particular, we discuss the rather tight total colour versus colour gradient relation found in our sample and, hence, confirm the findings by Pierini (2002). Furthermore, we will specifically focus on the question whether the colours of early-type

dwarfs are stronger influenced by stellar populations of different age or metallicity.

4.2 Samples, Observations, and Photometric Procedures

The sample of 22 early-type dwarf galaxies in the Virgo cluster observed with the VLT in B and R and extensively discussed in the previous chapters also constitutes the main basis for our study of the colour properties. (Please refer to chapter 2 for details of the observations and reduction processes.)

However, in order to get a second colour we performed additional observations in the U-filter (supplemented by the B- and R-filters) for the same sample of objects. The U-band was chosen, since it might provide indications of a possibly present young stellar population as well as help to constrain the metallicity of the dwarfs observed. For instance, in some dSphs of the local group evidence for the presence of an intermediate age stellar population have been found already (Sarajedini et al. 1997, Held et al. 1999, Saviane et al. 2000). The corresponding data have been collected with the 1.54-m Danish Telescope at the European Southern Observatory on La Silla, between May 18, 2001 and May 22, 2001. We used the DFOSC 2048×2048 CCD camera. We took three 20 min exposures in U, three 10 in exposures in B and three 5 min exposures in R for each of the seven Virgo fields, containing two to seven objects. The field of view is $13\farcm3 \times 13\farcm3$ with a resolution of $0\farcs39$ per pixel. The gain was set to $0.77e^-$ per ADU,

Tabelle 4.5: Total colour indices of the objects observed with the 1.5 m-Danish Telescope

VCC	Name	B_T	$U-B$	$B-R$		VCC	Name	B_T	$U-B$	$B-R$	
0490	IC0783	14.38	0.52	1.46		0942		19.69	-0.20	0.68	
0510	UGC7425	15.62	0.07	1.52		0959		19.90	-0.09	1.57	
0545	IC0783A	15.84	0.29	1.46		0962		17.03	0.10	1.50	$\star$
0779		17.52	0.31	1.40	$\star$	0965	IC3363	15.53	0.11	1.29	$\star$
0793		16.78	-0.23	0.85		0974		16.72	0.09	1.33	$\star$
0810		16.73	0.21	1.21	$\star$	0998		18.28	-0.19	1.24	
0815		15.86	-0.03	1.25	$\star$	1010	NGC4431	13.95	0.14	1.21	
0833		17.48	0.41	1.33	$\star$	1014		20.40	-0.71	0.89	
0839		18.41	0.22	1.66		1015		19.39	0.70	1.00	
0846		16.18	0.43	1.26	$\star$	1036	NGC4436	14.09	0.02	1.13	
0850		18.56	0.79	1.24		1069		16.58	-0.01	1.28	$\star$
0856	IC3328	15.00	0.30	1.14		1070		19.14	0.02	0.68	
0920		17.90	0.01	1.25		1077		19.19	-0.05	1.18	
0928		16.15	0.03	1.25	$\star$	1104	IC3388	15.49	0.04	1.27	$\star$
0929	NGC4415	13.56	0.37	1.35	$\star$	1122	IC3393	14.95	0.09	1.24	$\star$
0940	IC3349	14.84	0.26	1.29	$\star$	1129		17.87	-0.04	1.15	$\star$

Only the data of galaxies marked with $\star$ have been used in the analysis.

and the CCD was read out with a readout noise of $3.11e^-$. Seeing was between $0\farcs8$ and $2\farcs3$.

The weather conditions during the observing run were not satisfactory, we lost half a night due to clouds and had to repeat several exposures. Even though we observed 32 objects, we remained with usable data only for 15 galaxies. Hence, performing a colour study of early-type dwarfs we had primarily to rely on our VLT-data.

The data reduction procedures adopted for the La Silla sample are essentially the same as for the VLT sample and are described in chapter 2. The only difference concerned the flat-fielding. The available sky- and dome-flats already allowed an accurate elimination of the intensity gradients, without fitting higher order polynomials to the background. Hence, the background intensity of all frames could be subtracted in terms of a tilted plane. The basic photometric parameters of the La Silla sample are given in appendix B. Table 4.5 just shows the total apparent magnitude and the two colour indices which have been partly used in the following analysis. All values have been corrected for galactic extinction using the maps of Schlegel et al. (1998).

4.3 Colour gradients

A colour gradient is commonly defined as the slope of a line which has been fitted to the radial colour profile of the galaxy. This procedure can lead to ambiguous results in the case of dwarfs, in particular of nucleated dwarfs, since the radial range appropriate for the fit might be rather small. On the one hand the central parts have to be excluded to avoid the nuclei, on the other hand the surface brightness of dwarfs reaches low values already at rather short radii leading to large errors of the colour gradients. The slopes of the fits can therefore be quite inaccurate.

A possibility to circumvent these uncertainties is to use the ratio of the effective radii in the corresponding colour bands instead. This parameter is well defined and easy to determine even for observations of lower resolution. However, the ratio of the effective radii is essentially a measure for the colour gradients only for the central parts of the galaxies, where half of the luminosity is accumulated and contains little information about the outer parts. Hence, we have to assume that the slopes of the gradients do not change strongly towards larger radii. Yet, this is not a drawback, since the method of fitting a line to the colour gradients is based on the same assumptions. In fact, taking the ratio of the effective radii is a more general approach, since it is essentially model-free.

Almost all dEs in our sample are nucleated and several of them have rather low surface brightnesses so that the determination of the colour gradients would be quite inaccurate using the fitting method in these cases. In order to derive meaningful data of comparable accuracy for *all* objects in the sample, we used, therefore, the ratios of the effective radii in the corresponding filters as indicators of the colour gradients in the following considerations.

4.3.1 The relation between total colour and colour gradient

In Figure 4.26 (left) the relation between total colour and r^R_{eff}/r^B_{eff} (the colour gradient) is shown. Obviously redder galaxies tend to have $r^R_{eff}/r^B_{eff} > 1$ (i.e. they become redder towards the outer parts), whereas bluer ones rather have $r^R_{eff}/r^B_{eff} < 1$. The same is evident in Figure 4.27, where the corresponding data of the La Silla sample in U and B are shown. In BR-colours a weak dependence on luminosity is evident in the sense, that the relation for the fainter objects is slightly shifted towards bluer colours, whereas in UB no such effect is obvious. The same relation, though weaker, has already been found by Pierini (2002) in B and H colours, using a sample of early-type dwarfs in Virgo as well. Moreover, the

fact that a majority of the objects are redder in their centers than in the outer parts is surprising. Dwarf galaxies in general are expected to have either almost no colour gradient or to show a reddening towards larger radii. The particularity of the cluster dEs in terms of colour gradients becomes evident in the right panel of Figure 4.26, where they are compared to dEs in nearby groups and to dwarf irregulars in the field. In the colour range $1 \leq (B-R) \leq 1.3$ the colour gradients of group dEs almost completely differ from the ones of cluster dEs. However, it is important to stress the fact that early-type dwarfs in clusters are different from their counterparts in groups, in particular due to a difference in their luminosity functions. The bright nucleated dEs which dominate the dwarf population in the centers of clusters are not found in groups of galaxies, where rather faint not-nucleated dwarf spheroidals outnumber the dwarf population. This difference is for instance reflected in the mean luminosities of the two samples: the group dEs have $\langle M_B \rangle = -13.17$ mag, the dEs in Virgo have $\langle M_B \rangle = -15.76$ mag. Hence, the different distributions of group and cluster dEs in Figure 4.26 (right panel) is similar to the apparent shift of the relation between bright and faint objects in Figure 4.26 (left panel).

4.3.2 The relation between ellipticity and colour gradient

The three dimensional shape of a galaxy, statistically accessible by the apparent ellipticity, might have a strong influence on certain properties reflected by colour (see appendix D). In fact, Figure 4.28 indicates a relation between the apparent flattening and the strength of the colour gradient. What concerns cluster dEs (left panel) strong colour gradients are only exhibited by rather round objects. Among the six galaxies outside the range $1.1 > r^R_{eff}/r^B_{eff} > 0.9$ five have ellipticities $\epsilon < 0.2$. In addition, gradients showing a reddening towards the outer parts can only be found in round objects as well. Both findings do not

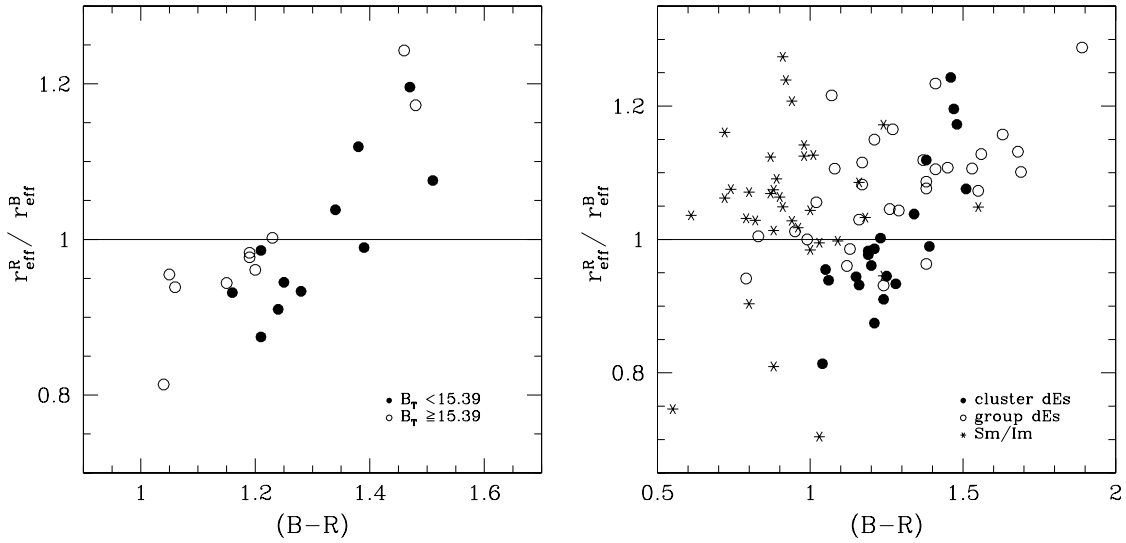

Abbildung 4.26: (*left*) Total colour versus the ratio of the effective radii in R and B, respectively. The sample has a mean total apparent magnitude of $\langle B_T \rangle = 15.39$ mag. (*right*) Comparison of cluster dEs with dEs in nearby groups (data from Bremnes et al. 1998, 1999, 2000, Jerjen et al. 2000, Barazza et al. 2001, Parodi et al. 2002) and field dwarf irregulars (data from Barazza et al. 2001, Parodi et al. 2002) in the same parameter space. Note: the mean error of the total colours is of the order of ≈ 0.15 mag.

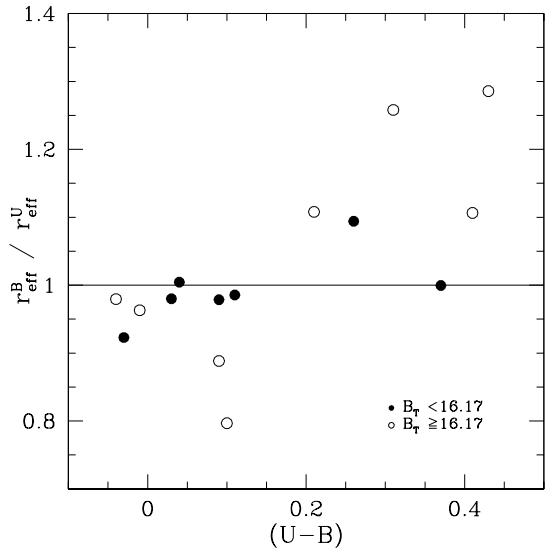

Abbildung 4.27: Total colour versus the ratio of the effective radii in U and B, respectively, for the dEs of the La Silla sample which has a mean total apparent magnitude of $\langle B_T \rangle = 16.17$ mag. Note: the mean error of the total colours is of the order of ≈ 0.15 mag.

apply to the group dEs, which however tend to be more flattened than the cluster dEs with $\langle \epsilon \rangle_{group} = 0.32$ instead of $\langle \epsilon \rangle_{cluster} = 0.28$. The right panel of Figure 4.28 reveals an ellipticity versus gradient strength relation also for giant elliptical galaxies which, however, seems to be different from the dwarf relation. Like expected almost all giants have a red central region compared to their outer parts, but the corresponding gradients are the stronger the rounder the galaxies are. The relation is very weak using the $(B - R)$ gradient, however since colour gradients in giant ellipticals are commonly interpreted in terms of metallicity, we might expect to find any possible relation in particular in $(U - B)$, which is the better tracer for metallicity. However, the findings should be interpreted differently for the two galaxy classes (see below) and they have therefore to be confirmed using for instance metallicity gradients.

In view of a possible relation between colour properties of dwarfs and their shapes, represented by the apparent ellipticity, we also check for a potential correlation with the deviation of the isophotes from pure ellipses, expressed in the a_4-parameter. As described in chapter 2, this parameter is a measure for the manner of isophotal deviation, termed either disky ($a_4 > 0$) or boxy ($a_4 < 0$). In Figure 4.29 a_4 is plotted versus the colour gradient. Since round galaxies tend to have $a_4 \sim 0$ (see Figure 2.17) the upper part of the plot is consistent. On the other hand it is striking that galaxies with disky isophotes predominantly have $r^R_{eff}/r^B_{eff} < 1$, i.e. a red central part and a bluer outer parts. Assuming that disky isophotes are indicative of a disk component, we would indeed expect to observe such colour gradients. However, from the five objects for which the presence of a disk has been suggested adopting image processing methods (see chapter 3 and references therein), only two lie in the lower right quadrant (IC3349, IC3468), whereas two exhibit the "correct" colour gradient, but are slightly boxy (IC3328, NGC4431). The fifth candidate for a disk component (IC0783) is the only object in the upper right quadrant. Again it is important to keep in mind that the values of a_4 are the mean of a_4 profiles which frequently alternate between the disky and boxy regime. Probably the best example of a misleading mean a_4 is NGC4431, where the boxyness is caused by the central bar dominating the bright parts of the galaxy which is certainly a disk. Nevertheless, despite the truism that each galaxy is an individual, a trend like the one presented can indicate a general relation which might be valid for the majority of the dwarf galaxy population.

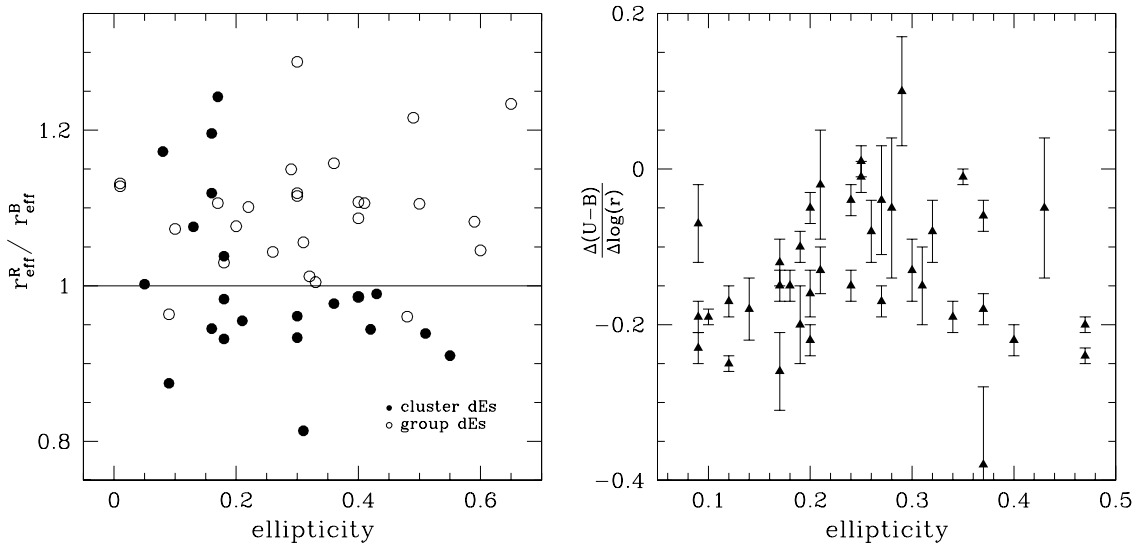

Abbildung 4.28: (*left*) The ellipticity defined as $1-(b/a)$, where a and b are the major- and minor-axis, respectively, versus the colour gradient for cluster and group dEs. The samples are the same like in Figure 4.26 (right panel). Note: errors are of the order of the plot symbols. (*right*) The ellipticity-colour gradient relation for giant ellipticals. Data are from Peletier et al. (1990). Note: the $(U-B)$ colour gradient has been determined fitting a line to the colour profile.

4.4 The $(U-B)$ - $(B-R)$ relation

With our UBR-data from the La Silla sample we are able to analyse the colour-colour relation for dEs and thus compare them to other types of spheroidal stellar systems. This is done in Figure 4.30, where the $B-R$ colour index is plotted versus the $U-B$ colour index. We only show the 15 objects with

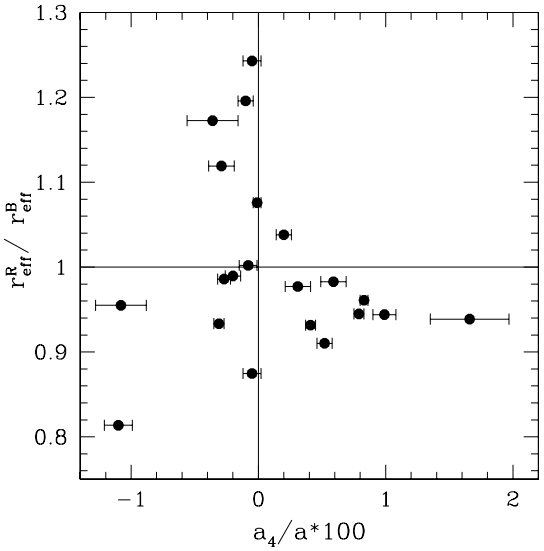

Abbildung 4.29: The colour gradient versus $a_4/a * 100$. The value of a_4 is the luminosity weighted mean over a large fraction of the radial profile (see chapter 2 for details).

reliable colour determinations (filled circles) together with the data for giant ellipticals from Peletier et al. (1990, filled triangles) and a sample of galactic globular clusters (GC) from Harris (1996, crosses). The GCs have been restricted to objects with small galactic extinctions, i.e. $E(B-V) < 0.15$, in order to limit uncertainties due to reddening. In addition, we show the theoretical positions of single stellar populations (SSPs, open squares) using the synthetic models of Worthery (1994) together with the alternate stellar evolutionary isochrone library of Alongi et al. (1993). The three different types of stellar systems constitute roughly a continuous sequence, though with large scatter. In particular the early-type dwarfs cover quite a large range in $U-B$, which obviously stems from the metallicity-flattening relation (see appendix D). However, the location of the bluest dwarfs (i.e. $U-B < 0.2$) with respect to the GCs is difficult to interpret. Whith regard to the theoretical models, we would have them expected to show the best consistency with the GCs, since they represent single stellar populations. Yet, following these models the GCs should have an age of ~ 2 Gyr, which is obviously wrong. A similar plot is provided by Ferguson (1994, Figure 2), using $B-V$ instead of $B-R$. The large scatter of dEs is not evident in these data. However, the samples used, stemming from Caldwell (1983) and Caldwell & Bothun (1987), mostly consist of rather round galaxies, with $\epsilon_{max} = 0.36$.

4.5 Discussion

Since colour properties in general can be regarded in terms of age or metallicity the interpretation of correlations like the ones just presented is not straightforward. Moreover, the presence of dust can affect the colours of stellar systems. In spite of the fact that the problem might be easier to tackle in the case of dwarf galaxies, where at least the influence of dust can be neglected, some unknown mixture of effects between the ages of the stellar populations and their metallicities might be the origin of the colours observed in these objects. Since we cannot disentangle a possible connection between these two contributions using photometric three-colour data alone, we will discuss the influence of different stellar populations and different heavy element abundances separately, in order to see whether a single effect can account for the relations found.

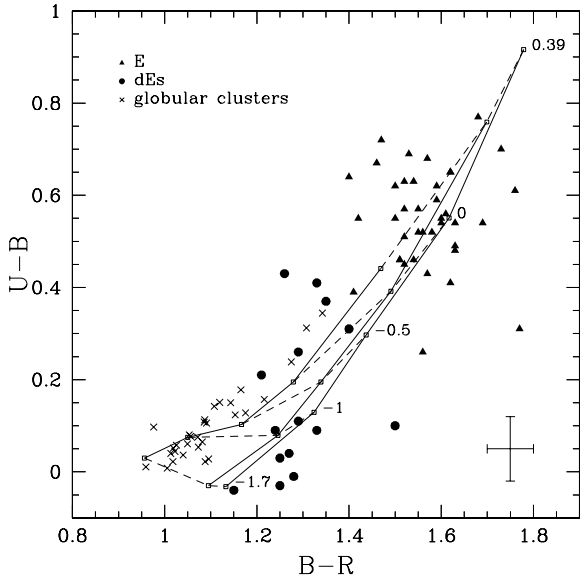

Abbildung 4.30: The $(U-B)$-$(B-R)$ relation for Es from Peletier et al. (1990, filled triangles), the 15 dEs with reliable colour data from the La Silla sample (filled circles) and a sample of galactic globular clusters (GC) from Harris (1996, crosses). The open squares give the positions of single stellar populations (SSP) using the models of Worthey (1994) together with the isochrone library of Alongi et al. (1993). The solid lines connect populations with the same age, but different metallicities. From right to left: 12 Gyr, 6 Gyr, 2 Gyr. The dashed lines connect populations with the same metallicity, but different ages; the corresponding metallicity is indicated on the right side.

To simplify the discussion, we number the relations described as follows: (1) total colour vs. colour gradient; (2) ellipticity vs. colour gradient; (3) a_4 vs. colour gradient; (4) $(U-B)$ vs. $(B-R)$.

4.5.1 Different stellar populations/ages

In general, dwarf galaxies, regardless of their environment, will have experienced a more or less complex star formation history, leading to the presence of stellar populations of different ages and metallicities. Assuming for the moment that only these different stellar populations (and not metallicity) are responsible for the colour properties in early-type dwarf galaxies, we would expect them to exhibit a reddening towards larger galactocentric radii. This specific colour gradient would be due to the fact that the last burst of star formation is believed to occur in the center of a spheroidal stellar system, leaving behind a slightly younger (bluer) stellar population in the inner parts surrounded by an older (red) stellar component (irrespective of the presence of a nucleus). In this picture the gradients should be the stronger the more recent the last star formation event took place, i.e. the bluer in integrated colour the galaxy is, since the colour difference between the populations decreases with time. However, considering relation (1) this scenario can obviously not explain the correlation found. Most of the galaxies, in particular the bluer ones, show an opposite colour gradient. This behavior might be understood assuming a disk component in these objects which dominates in luminosity over the spheroidal part. Like in spiral galaxies the disk could be composed of younger stars surrounding an older central part, equivalent to the bulge in giant disks. The fact that four of the five objects, for which a disk component has been observed (chapter 3) indeed have $r^R_{eff}/r^B_{eff} < 1$ supports this view, not explaining relation (1) itself, however. Moreover, relations (2) and (3) provide further evidence for the hypothesis of dominant disk components. (2) shows that more flattened objects always become bluer towards larger radii, whereas the rounder objects can have either gradient, yet keeping in mind that we only observe apparent ellipticities and that therefore round objects might be intrinsically flatter. Relation (3) reveals that our candidates for disk components tend to have disky isophotes, commonly regarded as an indication of an embedded disk, at least for giant ellipticals. Hence it strengthens the foundation of our conjecture. However, except for the objects for which a disk component could be observed directly, such a structure can not be claimed for the other galaxies, having only the observations presented available. In particular, we would need kinematical data, which only exist for two of the galaxies in question: NGC4436 exhibits a slow rotation and IC3468 does not rotate at all (Simien & Prugniel 2002).

It remains therefore an open question whether all galaxies showing a redder center with respect to the outer parts host a disk component or whether metallicity effects have to be considered as well.

4.5.2 Implications of the metallicity

The colour properties of giant ellipticals are believed to be due to metallicity. It is not clear however, below which luminosity/mass the dominance of the metallicity ceases and the influence on the colour of the ages of the stellar populations takes over. This transition has not implicitly to coincide with the one from giant to dwarf galaxies. Since most of our sample members are rather bright (or massive), metallicity effects might play an important role in these specific cases as well.

The metallicity effect in giant ellipticals causes them to become bluer from the center towards the outer parts. This colour gradient is due to the fact that most of the gas will be accumulated in the center leading to a longer duration of star formation and hence to a stronger enrichment of heavy elements. Assuming that the same process accounts for some of the gradients in dwarfs, we would expect a relation with luminosity, but this is not observed. In general, the properties which seem to be correlated with

the colour gradient (total colour in (1), ellipticity in (2), a_4 in (3)) do not strongly depend on absolute magnitude.

However, a metallicity effect is evident for dwarf ellipticals: rounder objects are more metal rich than flatter systems (appendix D). Hence, the red objects in relation (1) should be rather round which is confirmed by (2). We might therefore interpret relation (2) as consequence of (1) and the metallicity-flattening relation. Even relation (3) could be understood in terms of this connection. Relation (1) as well as the metallicity-flattening relation do not apply to giant ellipticals, whereas relation (2) does: the colour gradient is stronger for rounder galaxies. Their potential depth might prevent Es, in contrast to dEs, from significant mass losses through galactic winds. However, a central star burst will affect the surrounding and might therefore disperse the heavy elements within the main body of the galaxy. If the efficiency of this redistribution depends on ellipticity, the existence of a colour/metallicity gradient-flattening relation is quite plausible.

The rather continuous sequence of relation (4) is believed to be caused mainly by metallicity. The three different stellar systems shown have more or less the same age, but differ in their metal abundances due to their different masses. The large scatter exhibited by the dwarfs, in particular in $(U-B)$, can again be attributed to the metallicity-flattening relation, which causes a large scatter in their metal abundances. The almost vertical distribution of the dEs might be due to the fact that the rounder (redder) objects were able to maintain their star formation for a longer period and that a younger population of stars therefore influences their colours and shifts them to bluer values. However, the location of the metal poor dEs with respect to the globular clusters is puzzling. At first view they could be considered to be older than the globular clusters, but this is very unlikely. No clarification is provided by the predictions of theoretical models. In particular the metal poor (blue) part considerably deviates from the observations, assigning the unreasonable age of ~ 2 Gyr to the globular clusters, for which a better consistency would be expected, since the models are based on single stellar populations. This fact shed some doubt on the reliability of these models (or, less likely, on the reliability of the GC data).

4.6 Conclusions

Besides the fact that bright early-type dwarf galaxies only appear in clusters and cannot be found in small groups like the Local Group, relation (1) indicates that there are more systematic differences between these two populations. A possible explanation accounting for the deviations found is the existence of dEs stemming from transformations of late-type disk galaxies during their infall into the cluster. In this picture the early-type dwarf population in clusters is composed of “normal” dEs, which can also be found in the Local Group and former late-type disk galaxies which might have maintained some properties of their earlier “life”. Candidates for this type of objects have already been discovered (Jerjen et al. 2000, chapter 3). Since the galaxy density in groups is much lower than in clusters the corresponding population of dwarf ellipticals is therefore composed differently. The different colour properties of cluster dEs with respect to nearby dEs as well as the large range of colour gradients exhibited by these objects can be understood under this assumption. Nevertheless, the origin of relation (1) for cluster dEs still remains an open question.

The fundamental metallicity-flattening relation (appendix D) should obviously also leave behind its traces in the colour properties. In fact, relation (2) can be understood as a secondary effect caused by relation (1) and the metallicity-flattening relation. The latter might even be responsible for relation (2) found for giant ellipticals, which are not significantly affected by galactic winds. Nevertheless, the effect of a central star burst might redistribute the heavy elements in the galaxy depending on its flattening. This

seems to be plausible interpreting the $U - B$ colour gradient in terms of metallicity. The large scatter of the dwarf galaxies in relation (4) is another indication of the influence of the metallicity. The large range of $U - B$ colours reflects the range of exhibited ellipticities and therefore the efficiency of galactic winds in removing enriched material from the galaxy. However, it is difficult to see how this effect alone can account for the location of the bluest dwarfs, in particular with respect to the globular clusters. Due to their strong mass loss they might have experienced only one major star burst, which should make them comparable to GCs. Hence, we would expect them to have similar colours. Interestingly enough the locations of the theoretical models, which are based on single stellar populations, better agree with the dwarfs than with the GCs. Altogether, we might understand the distribution of the dEs and GCs individually in the colour-colour plot, but the relation among each other remains unclear.

To sum up, we may state that besides the metallicity-flattening relation, which is responsible for some of the features found, the very different colour properties exhibited by our sample are due to the existence of two subgroups constituting the early-type dwarf populations in clusters. The majority of cluster dEs might be the counterparts of the dEs and dSphs in the local group sharing similar properties. On the other hand, there is strong evidence that transformed late-type disk galaxies, which could maintain some of their earlier structures, account for a substantial fraction of the early-type dwarf population in clusters. However, to really assess the strength of the influence of the ages of the different stellar populations as well as of the metallicity on the colour of an objects, quantitative models are needed which provide detailed star formation histories for every location in the galaxy.

5
Concluding remarks

Dwarf ellipticals are the most numerous galaxies in the universe. However, dEs seem not to constitute a homogeneous class of galaxies. The most obvious evidence for this suggestion is the discovery of disk components in several dEs in the Virgo cluster. Since there are five such objects in our sample of 25 galaxies (chapter 3, Jerjen et al. 2000) they might account for a considerable fraction of the whole dE population. In addition, the surface brightness profiles of the brighter objects are not well represented by a Sérsic model. Again an indication for a greater complexity of these galaxies. The fact that we find colour gradients of either sign in our sample is also a surprising result, which suggests that the dEs, at least in clusters, might have different origins.

To sum up, it can be stated that only a part of the dE population in the Virgo cluster consists of spheroidal stellar systems with an almost homogeneous distribution of stars and, in some cases, a nucleus as the only possible substructure. This was the usual characterisation of dEs so far and might be denoted as *classical* dE. A rather large fraction of the dEs, however, are different, exhibiting the features described above. Since we have only studied dEs in the Virgo cluster, we cannot extend these considerations to other clusters or even to dEs in groups. On the contrary, the results of the analysis of the colour properties as well as all the knowledge we have about the well studied dEs in the local group suggest that only *classical* dEs can be found in small groups. Whether *non-classical* dEs are present in other galaxy clusters has still to be discovered.

The origin of the dEs is rather unclear so far. A reasonable scenario, in particular for the dEs with disk component, is that they stem from transformation processes of infalling late-type disk galaxies. For instance, a spiral galaxy entering a cluster will start to interact with the cluster galaxies lying close enough to its path. The resulting *harassment* (Moore et al. 1998) will cause the spiral galaxy to lose a substantial amount of gas and to transform its shape into a spheroidal. If it is furthermore assumed that these transformation processes will induce a burst of star formation using up all the remaining gas, the results might be dEs obeying the metallicity-flattening relation (appendix D). On the other hand, it seems to be unlikely that this process can account for all the differences found among the dE population. However, the general influence of the cluster environment might become apparent in the specific properties of the *non-classical* dEs. They might indeed be the real cluster dEs, which can only be found in regions of high galaxy density and whose morphology has been shaped by the cluster. Whereas the *classical* dEs can be found in different environments, in loose groups as well as in dense clusters, and whose origin is, therefore, not immediately connected to their environment.

Appendix A
The bar in IC779 and simulations of Fourier transformations

A.1 The bar in IC779/UGC7369

During the work on the colour properties of dEs, which also comprises nearby dwarfs in groups, a disk feature similar to the ones discussed in chapter 3 was found in IC779 (UGC7369). Despite the fact that this object is classified as E, its low surface brightness together with its rather small radial velocity of $333\ \mathrm{km\,s^{-1}}$indicate that it is more likely a dE. Therefore it was included in the photometric study of dwarfs in the Canes Venatici cloud by Bremnes et al. (2000, details about the observations and the data reduction as well as all relevant informations about IC779 can be found in this paper) and ended up in our sample of field dEs. Applying the same techniques as described in chapter 3, evidence for the presence of central bar arises. This can be seen in Fig. A.1, where the R-band image (left) and the result of unsharp

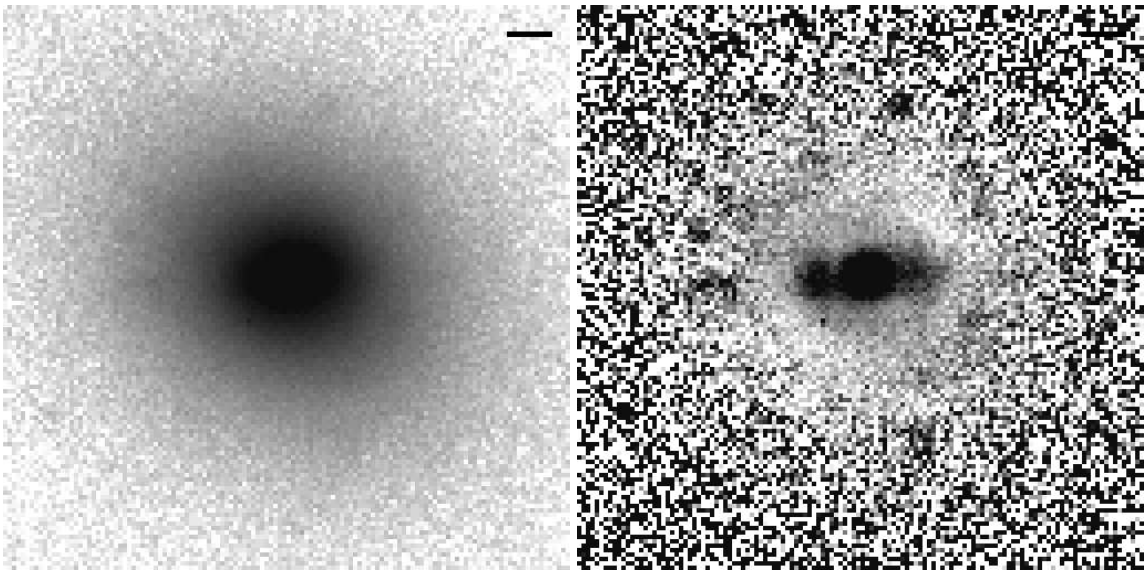

Abbildung A.1: *(left)* R-band image of IC779. The bar in the upper right corner corresponds to $\approx 7''$. *(right)* The result of unsharp masking (see chapter 3). The size of both images is $1\farcm4 \times 1\farcm4$.

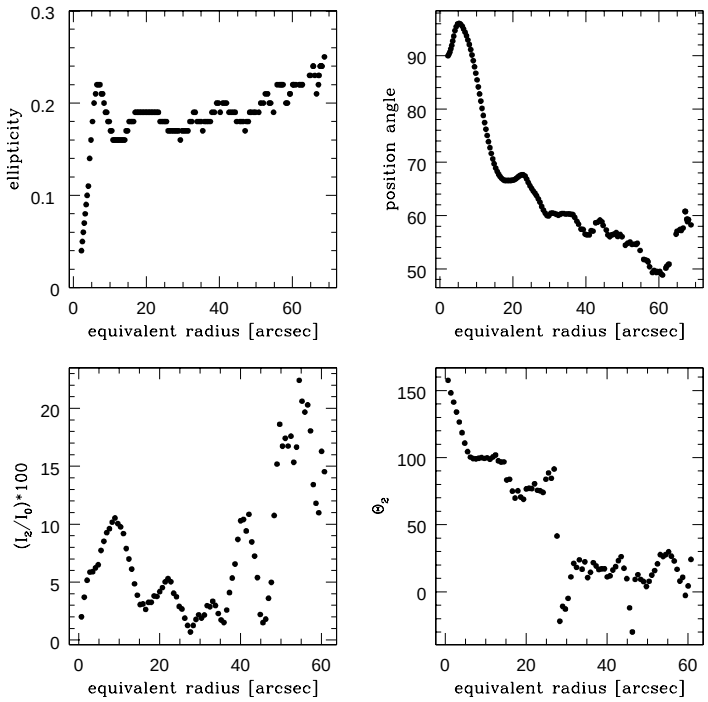

Abbildung A.2: *(upper left)* ellipticity profile; *(upper right)* position angle profile. *(lower left)* relative strength, in percent, of the third Fourier coefficient I_2 relative to I_0. *(lower right)* profile of the phase angle Θ_2 of the third Fourier coefficient. All parameters are plotted against the equivalent galactocentric radius.

masking (right) are shown. The unsharp masked image reveals a bar within the bright and, for a nucleus, too large central region. It is oriented almost horizontally and therefore shifted by $\approx 40^\circ$ with respect to the major axis. This is also shown in the profile of the position angle of the major axis plotted in Fig. A.2: inside the central $15''$ an according twist is obvious. It is also quite striking to compare the profiles of the ellipticity of IC779 with the one of NGC4431 in chapter 3. Irrespective of the extent and the strength of the scatters, the two profiles are almost identical. Moreover, the Fourier analysis yields an excess of $\approx 11\%$ in the central parts for the third order Fourier coefficient (lower left in Fig. A.2).

In contrast to the dEs in the Virgo cluster discussed in chapter 3, IC779 lies in an environment of low galaxy density. Therefore, the transformation processes believed to be the origin of the features found in the Virgo dwarfs unlikely account for the bar in IC779. However, in galaxy aggregates like the Canes Venatici cloud mergers might be quite common. It is therefore plausible that the bar as well as the unusually bright and extended central region of the galaxy are evidence for an earlier merger event.

A.2 Simulations

Besides the four galaxies discussed in chapter 3, three other objects (IC3303, IC3381, NGC4482) exhibited disk features, which, however, were only apparent in the Fourier decomposition, but could not be

confirmed applying unsharp masking. This suggests that for certain galaxies the Fourier decomposition can be a valuable method to determine the shape and the strength of hidden disk structures. However, projection effects seem to be able to deceive this method and to lead to wrong conclusions in some cases. If certain combinations of parameter profiles always mimic disk structures in the Fourier analysis, this method *alone* is not sufficient and has to be accompanied by other means. Therefore, the three galaxies mentioned have been excluded from the analysis in chapter 3. But their specific parameters have been taken as basis for the construction of models used to carry out simulations of the Fourier decomposition, in order to get a better handle on the differentiation between projection effect and genuine inner structure. NGC4482 was used as prototype, with regard to luminosity and size of the nucleus. This basic model

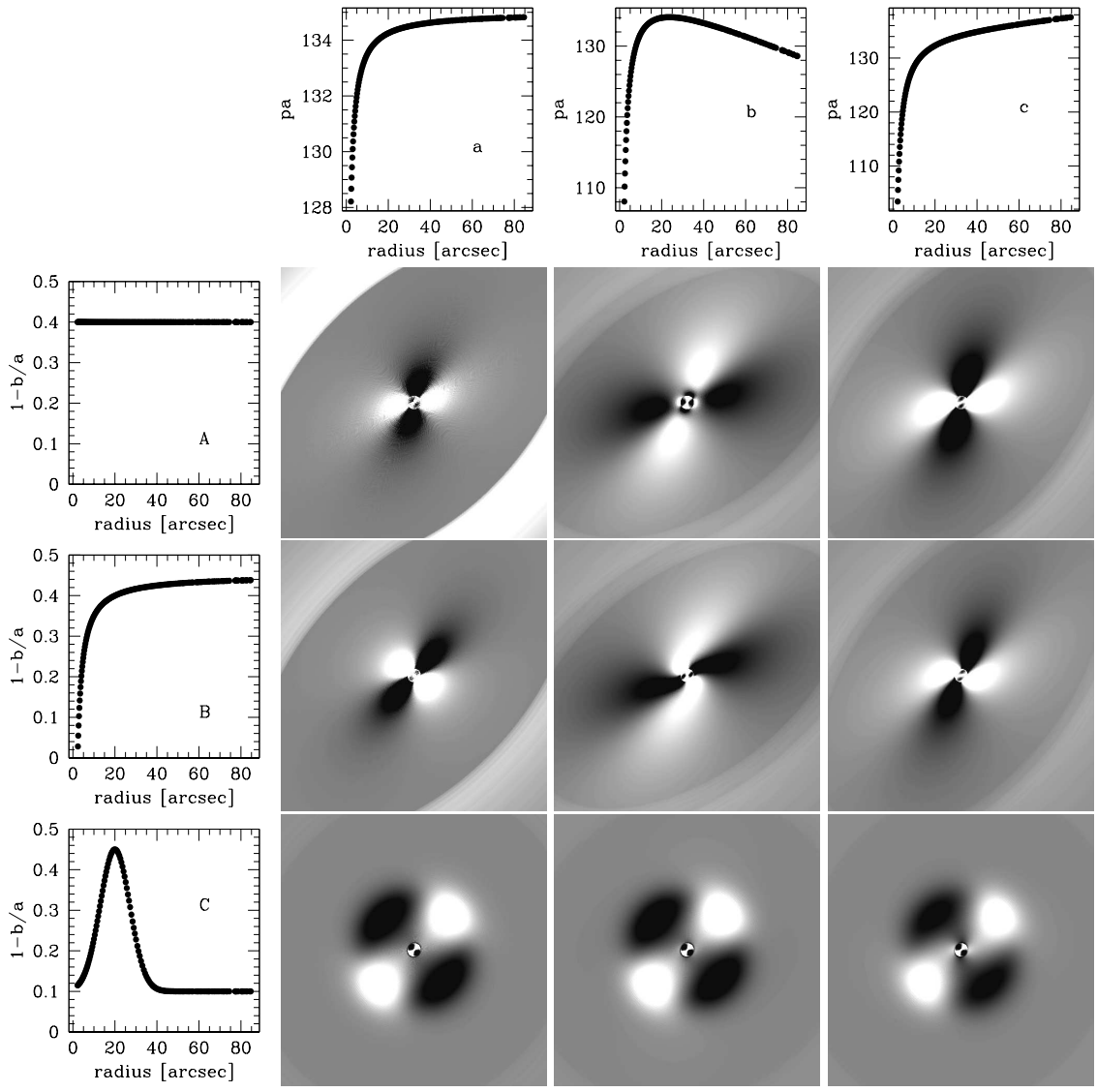

Abbildung A.3: Residuals resulting from the simulations, combining the input position angle profiles shown on top with the ellipticity profiles shown to the left. Image size: $1\farcm7 \times 1\farcm7$.

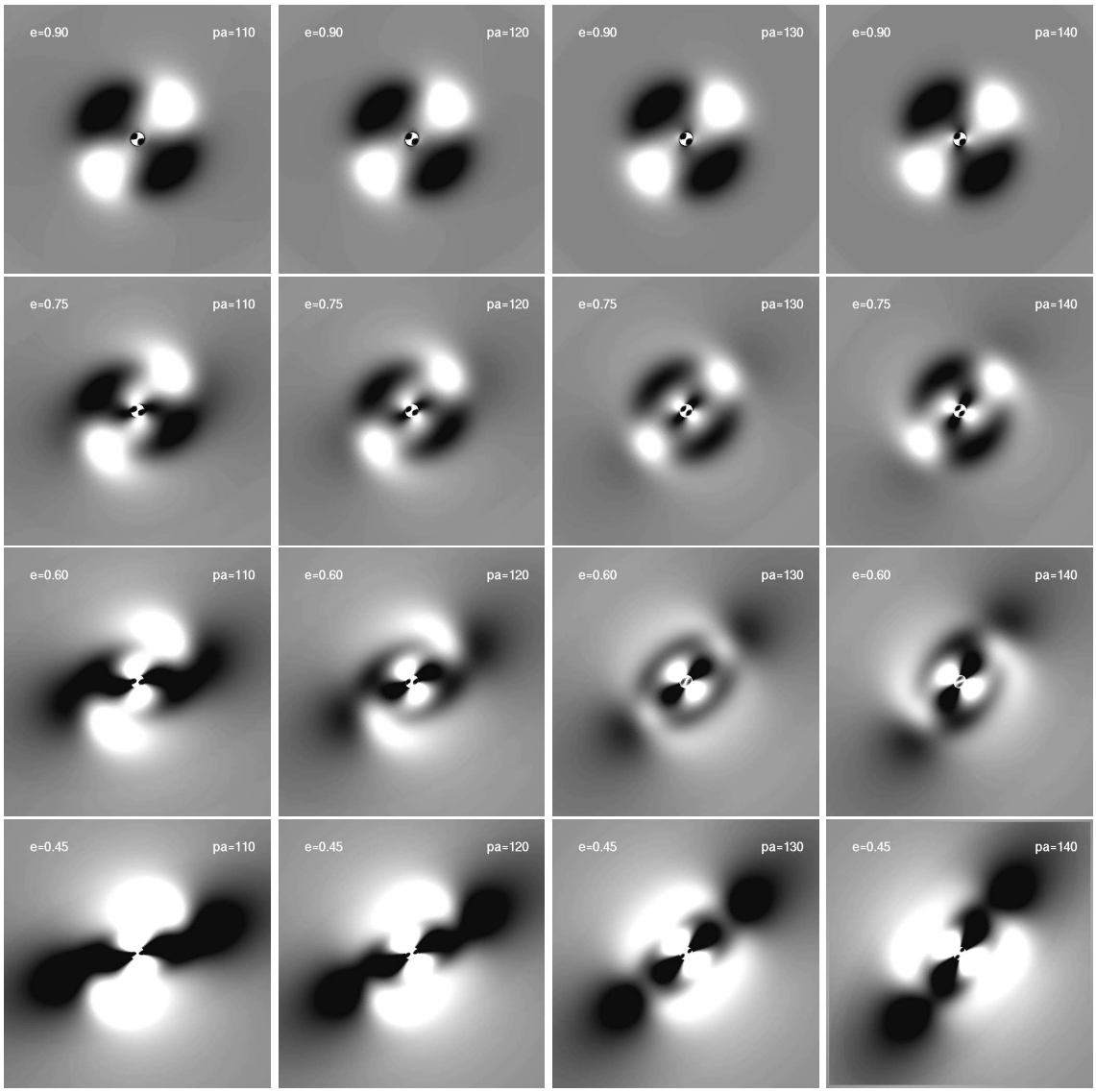

Abbildung A.4: Residuals of model (b,B) of Figure 3 ($e = 0.56, pa = 125°$) by varying the input parameters systematically. The used axis ratios, $e = \frac{b}{a}$, and position angles, pa, are indicated in the upper left and upper right corners, respectively.

was then configurated with different ellipticity and position angle profiles. The plots in the top row of Fig. A.3 show the input isophotal twists (a,b,c). They reproduce qualitatively the observed profiles for these three galaxies: NGC4482 → a, IC3381 → b, IC3303 → c. These profiles were combined with the ellipticity profiles shown in the left margin of Fig. A.3 (A,B,C). A constant profile, A, was chosen in order to find out whether an isophotal twist alone can lead to a spiral structure in the Fourier map. Profile B corresponds qualitatively to the observed ones, which are more or less the same in all three galaxies, and profile C characterises a central bar (e.g. IC3349). Since the residuals do not deviate strongly from the Fourier maps, Fig. A.3 only shows the results after having subtracted the first Fourier coefficient, I_0,

from the model galaxy. Each ellipticity profile has been combined with each position angle profile.

The residuals of models with a constant ellipticity profile ($pa =$ a, $1 - b/a =$ A / b,A / c,A) indicate that an isophotal twist alone cannot cause a clear spiral pattern, at least with twist strengths shown by our galaxies. However, result (a,B) has similarities to the residual of NGC4482 and result (b,B) is very close to the residual of IC3381. Hence, we are able to nearly reproduce the observed residuals by applying simple profile shapes. On the other hand the results in the bottom row are not very suggestive for a bar, even though the ellipticity profile C corresponds to such a structure. Probably the sharp rise of the position angle profiles is the reason for this result, since such a behavior is not shown by any of the objects with similar ellipticity profile and bar feature in the residual (e.g. IC3349, IC3468).

The interpretation of these simulations is not straightforward. There seems to be only a certain number of possible parameter combinations which lead to the appearance of a spiral structure. We could indeed reproduce the observed patterns, but only by remaining very close to the observed profiles. Fig. A.3 shows that the *combination* of the parameters is the crucial point and that randomly chosen combinations never lead to a spiral or bar structure. Therefore, it is quite surprising that three galaxies have exactly the parameter combinations causing spiral features and we could argue that these features are genuine. On the other hand, the observed variations in ellipticity and position angle can also be explained by other effects. Consider for example the profiles of IC3381 in Fig. 3.24. Since this galaxy is nucleated (like all galaxies in question) the rise in the ellipticity profile might be caused by the massive central object (see above). If this galaxy is triaxial, the variation of the intrinsic ellipticity can lead to a considerable isophotal twist, depending on our viewing direction. Hence, we can explain the observed parameters in a simple way, without the assumption of a exceptional spiral structure in a dwarf elliptical galaxy.

The latter argument is even more strengthened when we take into account the strong sensitivity of the result with respect to the chosen input parameters. As mentioned in the last section, we have to *deproject* the light distribution before applying the Fourier expansion. Hence, we have to find the correct inclination and position angle of the galaxy. Usually, these parameters are determined in the outer parts of the galaxy (see above). Taking a look at the ellipticity profiles of IC0783, IC3328 or NGC4431 this choice has to be questioned. It is clear that in general only photometric parameters determined in the *outer* parts provide reasonable values to characterize the whole galaxy. However, it is not clear whether these parameters are appropriate to uncover inner structures as well. The profile of NGC4482 offers, in this sense, at least two possibilities: we could choose the "standard" value in the outer parts (~ 0.38) or the maximum value of the profile (~ 0.44). That this makes a difference is shown in Fig. A.4. We took model (b,B) of Fig. A.3 and varied the ellipticity and the position angle in a systematic way: the axis ratio from 0.45 to 0.90 in steps of 0.15 and the position angle from 110° to 140° in steps of 10°.

It is evident that the input parameters have a strong influence on the result of the Fourier decomposition and subsequently on the residuals. None of the residuals in Fig. A.4 is similar to the one for the same model (b,B) shown in Fig. A.3, even though the parameter intervals bracket the "standard" values used for model (b,B) ($e = 0.56, pa = 125^\circ$). Of course, it has to be kept in mind that some of the input parameters applied in Fig. A.4 are not very reasonable. Nevertheless, the fact that we have to *assume* vital characteristics of the galaxies for the Fourier decomposition turns out to be a drawback. Given the strong sensitivity on the input parameters, the reality of the residual structure cannot be taken as face value but must be backed by other methods.

Appendix B
Basic data and photometric parameters of the La Silla sample

In the following table the basic data and photometric parameters of the La Silla sample are given. A part of the sample has been included in the analysis of the colour properties of early-type dwarfs in chapter 4, where also the total colour indices $U-B$ and $B-R$ are given (see table 4.5). All values in magnitudes are corrected for galactic extinction using the maps of Schlegel et al. (1998). The columns are as follows:
columns (1) and (2): identifications of the galaxies; for the coordinates see VCC
column (3): morphological type in the classification system of Sandage & Binggeli (1984), taken from the VCC
column (4): absolute B-band magnitude, based on the apparent magnitude given in column 6 (middle line) and a mean Virgo cluster distance of 17 Mpc
column (5): heliocentric radial velocity in $\mathrm{km\,s^{-1}}$ from the VCC and Binggeli et al. (1993)
column (6): total apparent magnitude in U (upper line), B (middle line) and R (lower line)
column (7): effective radius in arcsec [$''$] in U (upper line), B (middle line) and R (lower line)
column (8): effective surface brightness in [mag/$\Box''$] in U (upper line), B (middle line) and R (lower line)

VCC	Name	Type	M_{B_T}	$v_\odot$	U_T B_T R_T	r_e^U r_e^B r_e^R	μ_e^U μ_e^B μ_e^R	
(1)	(2)	(3)	(4)	(5)	(6)	(7)	(8)	
0490	IC0783	dS0(3),N	-16.77	1293	14.90	22.74	23.68	$\approx$
					14.38	28.82	23.67	
					12.92	24.94	21.90	
0510	UGC7425	dE3,N	-15.53		15.69	25.93	24.75	$\approx$
					15.62	21.05	24.23	
					14.10	19.25	22.52	
0545	IC0783A	dE2,N	-15.31	1159	16.13	12.98	23.69	$\approx$
					15.84	13.64	23.51	
					14.38	11.98	21.77	

VCC	Name	Type	M_{B_T}	$v_\odot$	U_T B_T R_T	r_e^U r_e^B r_e^R	μ_e^U μ_e^B μ_e^R	
(1)	(2)	(3)	(4)	(5)	(6)	(7)	(8)	
0779		dE0,N	-13.63		17.83	10.66	24.96	
					17.52	13.41	25.15	
					16.12	13.71	23.80	
0793		ImIII-IV,N?	-14.37	1910	16.55	8.28	23.13	≈
					16.78	8.71	23.48	
					15.93	9.73	22.87	
0810		dE0,N	-14.42	-340	16.94	8.90	23.68	
					16.73	9.86	23.69	
					15.52	9.42	22.38	
0815		dE2,N	-15.29	-700	15.83	16.73	23.94	
					15.86	15.44	23.80	
					14.61	16.09	22.64	
0833		dE0,N	-13.67		17.89	7.52	24.27	
					17.48	8.32	24.07	
					16.15	8.15	22.70	
0839		dE0:	-12.74		18.63	12.74	26.15	≈
					18.41	13.44	26.05	
					16.75	20.62	25.29	
0846		dE1,N:	-14.97	-730	16.61	9.94	23.59	
					16.18	12.78	23.71	
					14.92	12.62	22.42	
0850		dE,N	-12.59		19.35	5.91	25.20	≈
					18.56	8.38	25.17	
					17.32	9.33	24.16	
0856	IC3328	dE1,N	-16.15	972	15.30	17.87	23.56	≈
					15.00	17.48	23.21	
					13.86	17.30	22.04	
0920		dE1?,N	-13.25		17.91	11.32	25.17	≈
					17.90	9.67	24.82	
					16.65	11.47	23.94	
0928		dE6,N	-15.00	-254	16.18	9.50	23.06	
					16.15	9.31	22.99	
					14.90	9.32	21.74	
0929	NGC4415	d:E1,N	-17.59	910	13.93	20.93	22.53	
					13.56	20.92	22.16	
					12.21	20.33	20.75	
0940	IC3349	dE1,N	-16.31	1563	15.10	17.32	23.29	
					14.84	18.95	23.22	
					13.55	18.25	21.85	
0942		dE4	-11.46		19.49	6.43	25.53	≈
					19.69	5.37	25.33	
					19.01	4.25	24.15	
0959		dE2	-11.25		19.81	7.31	26.18	≈
					19.90	8.62	26.57	
					18.33	11.59	25.64	

VCC	Name	Type	M_{B_T}	$v_\odot$	U_T B_T R_T	r_e^U r_e^B r_e^R	μ_e^U μ_e^B μ_e^R	
(1)	(2)	(3)	(4)	(5)	(6)	(7)	(8)	
0962		dE3	-14.12		17.13	21.84	25.82	
					17.03	17.40	25.23	
					15.53	20.52	24.09	
0965	IC3363	dE7,N	-15.62	791	15.64	13.84	23.34	
					15.53	13.64	23.20	
					14.24	14.05	21.97	
0974		dE3:,N	-14.43		16.81	9.23	23.63	
					16.72	8.20	23.28	
					15.39	8.79	22.10	
0998		dE4,N:	-12.87		18.09	10.02	25.09	≈
					18.28	9.72	25.21	
					17.04	10.49	24.14	
1010	NGC4431	dS0(5),N	-17.20	913	14.09	17.64	22.32	≈
					13.95	17.12	22.11	
					12.74	16.86	20.87	
1014		dE2?	-10.75		19.69	7.55	26.07	≈
					20.40	4.29	25.55	
					19.51	4.30	24.67	
1015		dE:	-11.76		20.09	5.12	25.63	≈
					19.39	8.67	26.07	
					18.39	9.15	25.19	
1036	NGC4436	dE6/dS0(6),N	-17.06	1163	14.11	16.44	22.18	≈
					14.09	14.65	21.91	
					12.96	13.97	20.68	
1069		dE6,N	-14.57		16.57	8.95	23.32	
					16.58	8.62	23.25	
					15.30	8.72	22.00	
1070		dE,N	-12.01		19.16	8.73	25.86	≈
					19.14	9.11	25.93	
					18.46	7.87	24.93	
1077		dE0,N	-11.96		19.14	6.26	25.15	≈
					19.19	6.10	25.11	
					18.01	6.14	23.95	
1104	IC3388	dE5,N	-15.66	1704	15.53	11.48	22.82	
					15.49	11.53	22.79	
					14.22	11.93	21.60	
1122	IC3393	dE7,N	-16.20	436	15.04	11.22	22.28	
					14.95	10.98	22.15	
					13.71	10.59	20.83	
1129		dE3	-13.28		17.83	7.78	24.28	
					17.87	7.62	24.27	
					16.72	7.17	22.99	

The values of the galaxies marked with a ≈ are uncertain.

Appendix C
Off-center nuclei in dwarf elliptical galaxies

Abstract

We have searched for off-center nuclei in 78 "nucleated" dwarf elliptical (dE,N) galaxies, drawing on digitized photographic images from a previous study of Virgo cluster dwarfs. The search is based on a simple algorithm which compares the center coordinates of a series of outer elliptical isophotes with the position of the galaxy's nucleus. Monte Carlo simulations of the measuring procedure are used to assess random and systematic errors. Roughly 20% of all dwarf nuclei in the sample (neglecting uncertain cases) are found to be signifi cantly off-centered. The typical displacement is $1''$, or 100 pc (assuming a Virgo cluster distance of 20 Mpc), corresponding to 0.5 to 1 effective radii of the dwarf galaxy. There is a tendency of the nuclear off-center displacement to increase with decreasing surface brightness of the underlying galaxy. A similar trend was found with normal elliptical galaxies before. If real, the effect could mean that a nucleus can oscillate about the galaxy center with larger amplitude in a shallower (less cuspy) gravitational potential.

In an appendix we present evidence for the existence of a strong, unambiguous relation between the nuclear *magnitude* and the ellipticity of dE,N galaxies. If a nucleus is comprising 4% or more of the total light of the underlying galaxy, that galaxy is nearly always round, i.e. ellipticity less than 0.15 (dE0, dE1). This effect was predicted qualitatively long ago as the result of box orbit disruption caused by a central massive compact object (black hole).

C.1 Introduction

Since many, if not most non-active galactic nuclei are suspected to harbour a black hole (e.g. Kormendy & Richstone 1995), interest in these nuclei is no longer peripheral. Aside from their black hole "attraction", the nuclei are likely telling us something about the star formation history and the dynamics of the innermost part of galaxies. Among the most intriguing nuclei are those in dwarf elliptical (dE) galaxies (for a review on dEs see Ferguson & Binggeli 1994). Due to the low surface brightness of the underlying galaxy, the dE nuclei are not only popping out most clearly, their very formation in a low-density environment is a riddle. The most nearby dE nucleus is that of the Andromeda satellite NGC 205, which is of course known at least since Baade (1944). The universality of the dwarf nucleus phenomenon became clear with the Las Campanas survey of the Virgo cluster (Binggeli et al. 1985, preceded by Reaves 1983) where ≈400 nucleated dEs (out of ≈800 dEs in total) were identified. The morphology of "dE,N"

galaxies is illustrated in the dwarf galaxy atlas of Sandage & Binggeli (1984).

The nature of the dE nuclei is still unclear, but most likely they are massive compact star clusters (like the nuclei in M33 and other low-luminosity spirals; Kormendy & McClure 1993, Phillips et al. 1996, Matthews et al. 1999) constituting separate dynamical entities, but without being totally decoupled from the rest of the underlying galaxy. Their formation is still more speculative. One plausible scenario regards the dE nuclei as the fossils of the last bursts of star formation in the evolutionary transition from dwarf irregulars (or blue compact dwarfs, BCDs) to dwarf ellipticals (Davies & Phillipps 1988; however, see, e.g., Durrell 1997 and Miller et al. 1998 for the shortcomings of the Irr to dE scenario).

In this paper we address the question of *how central* the dwarf nuclei are. The nuclei have of course to be *fairly* central to be noticed as such, but still they could be significantly off-center relative to the radially symmetric, global light distribution of the parent galaxy. Why should this be interesting? Suppose the nuclei were formed secularly by the merging of globular clusters through dynamical friction, or evolved from non-central star burst regions in dwarf irregulars, as in the Davies & Phillipps scenario mentioned above. Depending on the age of the nucleus we might expect them to be off-center to various degrees. Miller & Smith (1992) have shown that even old nuclei would not patiently sit in the center of a galaxy. Such a state would be dynamically unstable; a nucleus is bound to oscillate in the potential of a galaxy. Taga & Iye (1998), performing N-body simulations of a rotating spherical galaxy with a central black hole, have found that the amplitude of oscillation depends on the mass of the black hole (or the nucleus) relative to the mass of the underlying galaxy. The simulations suggest that the amplitude will also depend on the central mass density of the underlying galaxy. These things have still to be worked out in detail by further numerical experiments.

In any case, there are enough hints from theory that off-center nuclei should be widespread, and that a quantification of the nuclear offsets might help us to put constraints on the formation, mass, and dynamics of the nuclei and the inner region of galaxies. Several off-center nuclei have been discovered by the *HST* survey of the centers of giant elliptical (E) galaxies (Lauer et al. 1995). However, part of these nuclear offsets in Es could be artifacts due to dust obscuration, or be caused by unresolved off-center sources. Spectacular cases of such off-center sources are the apparent double nuclei in the bulge of M31 and the compact elliptical NGC 4486B (Lauer et al. 1993, 1996), which are most plausibly modelled by an eccentric nuclear disk (Tremaine 1995).

The present paper is a first attempt to find off-center nuclei in dwarf elliptical galaxies, and to quantify the nuclear off-center distances, based on a homogeneous sample of 78 nucleated Virgo cluster dEs.

The rest of the paper is organized as follows. In Sect. C.2 we define our sample of nucleated dwarfs, and in Sect. C.3 we describe the procedures adopted to measure off-center positions. Some individual cases of off-center nuclei, illustrating the phenomenon and the measuring procedure, are shown and discussed in Sect. C.4. To get reliable statistics for off-center nuclei we had to account for systematic and random errors of the measuring procedure, which we did by running Monte Carlo simulations with artificial galaxies, as described in Sect. C.5. The statistical results are then presented in Sect. C.6, showing the general trends for the whole sample. Our conclusions are given in Sect. C.7.

In an appendix we address the relation between nuclear brightness and ellipticity. This feature is related to our main topic of off-center nuclei insofar as it may also have some bearing on the mass of the nuclei and the possibility that they harbour a black hole.

C.2 Sample

The present investigation draws on the photometric study of $\approx$ 200 Virgo cluster early-type dwarf galaxies by Binggeli & Cameron (1991, 1993, hereafter BC91 and BC93, respectively), which itself is based on digitized photographic plates from the Las Campanas survey of the Virgo cluster (Binggeli et al. 1985, hereafter VCC = Virgo Cluster Catalog). For our purpose of measuring nuclear dwarf positions digitized (deep & high-resolution) photographic images are as well suited as modern CCD images. We have selected a subsample from the BC91 sample by the following constraints: (1) the dwarf object had to be classified as nucleated, i.e. dE,N or dS0,N, and (2) the apparent magnitude was required to be brighter than $B_{\rm T}$ = 18 mag, corresponding to an absolute blue magnitude of -13.5 by assuming a distance to the Virgo cluster of 20 Mpc. Note that the dS0 type is a slight, and for the present purposes insignificant, variant of the dE class (see Sandage & Binggeli 1984, and BC91). – This sample amounted to 109 objects. Due to bright stars in the central areas of the galaxies and other technical difficulties we lost about 30 images. Without introducing strong biases, this left us with a final, representative sample of 78 nucleated dwarfs. The sample galaxies with some of their fundamental photometric parameters (all from BC93) are listed in Table C.6. The **columns of Table C.6** are as follows:

column (1): VCC number of the galaxy;

column (2): dwarf type classified in the system of Sandage & Binggeli (1984);

column (3): total apparent blue magnitude $B_{\rm T}$;

column (4): mean surface brightness within the effective radius $r_{\rm eff}$ that contains half of the total light, $\langle\mu\rangle_{\rm eff}$ (in B arcsec^{-2}).

The remaining columns (5)–(7) of Table C.6 are defined in Sect. C.3 further below.

Constraining the sample to objects explicitly classified as "nucleated" is of course not without problems. Besides a bias against very faint nuclei that simply went undetected in the photographic survey of Binggeli et al. (1985), a nucleus had to be sufficiently *central* to be considered and classified as such, to begin with. A "nucleus" very far off the center is indeed a contradiction in terms. Consider, e.g., VCC1857 depicted in Fig. C.1 (also reproduced, as IC3647, in Sandage & Binggeli 1984, Fig. 2, Panel 5). There is a bright star-like object on top of the galaxy, but so much off-center that it might be a foreground star or a background galaxy rather than the type of nucleus seen in the center of "dE,Ns"; hence the classification "dE,N?". This galaxy still happens to be included in our sample, albeit as "uncertain case" (see below).

A potential problem is the presence of globular clusters in the dwarfs. Deep *HST* images of Virgo dwarf ellipticals (dEs and dE,Ns) by Miller et al. (1998) show many globulars. The distinction between a faint nucleus and a globular may become impossible at this level of high resolution. However, our data do not go deep enough for this to be of any concern.

C.3 Measurement of nuclear off-center positions

The procedure we adopted for the determination of the offset distance of a nucleus to the center of the galaxy is straightforward. Our basic tool was the image processing package MIDAS provided by ESO. Within the context SURFPHOT we used the algorithm FIT/ELL3 to fit a series of ellipses to the surface brightness distribution of a galaxy. The important point with the fitting procedure FIT/ELL3 is that the center coordinates of the fitted ellipse are kept as free parameters. Any difference between the calculated ellipse center and the actual position of the nucleus is then giving an off-center distance of the nucleus.

The galaxy images had already been background-subtracted, cleaned from disturbing foreground stars, and calibrated from BC93 (where also all details concerning the photometry can be found). The

Tabelle C.6: Basic data and nuclear off-center displacements of 78 dE,N and dS0,N galaxies in the Virgo cluster

VCC	Type	B_T	$\langle\mu\rangle_{eff}$	δr_N	$\sigma_{\delta r}$	$\frac{\delta r_N}{r_{eff}}$	VCC	Type	B_T	$\langle\mu\rangle_{eff}$	δr_N	$\sigma_{\delta r}$	$\frac{\delta r_N}{r_{eff}}$
		[mag]	$[B/\Box'']$	$['']$	$['']$				[mag]	$[B/\Box'']$	$['']$	$['']$	
(1)	(2)	(3)	(4)	(5)	(6)	(7)	(1)	(2)	(3)	(4)	(5)	(6)	(7)
0109	dE3,N	16.06	23.41	0.76	0.06	0.065	1122	dE7,N	14.60	22.42	0.90	0.18	0.062
0235	dE0:,N	16.87	24.81	2.56:	0.10:	0.165:	1164	dE6,N	16.66	24.94	0.88	0.29	0.048
0389	dS0(4),N	14.21	22.16	1.09	0.17	0.070	1167	dE0,N	15.91	23.53	0.96	0.34	0.073
0554	dE2,N:	17.11	24.90	1.19:	0.44:	0.082:	1172	dE5,N	16.23	22.85	0.54	0.12	0.065
0684	dE0,N	16.04	23.16	0.20	0.06	0.019	1185	dE1,N	15.68	22.93	0.23	0.06	0.020
0753	dE0,N	16.37	24.46	0.72	0.14	0.043	1207	dE0,N	17.55	24.72	0.50	0.06	0.047
0765	dE1,N	16.49	22.16	0.30	0.01	0.054	1210	dE0,N	17.65	24.24	0.54	0.06	0.065
0779	dE0,N	17.67	25.00	0.92:	0.34:	0.078:	1213	dE0,N	16.42	24.08	0.41	0.08	0.030
0781	dS03(5),N:	14.72	21.80	0.68:	0.09:	0.065:	1254	dE0,N	15.51	22.90	0.44	0.08	0.036
0810	dE0,N	16.95	23.67	0.26	0.06	0.030	1264	dE0,N	17.31	24.52	0.35	0.07	0.032
0812	dE1,N	17.03	24.43	0.34	0.10	0.028	1308	dE6,N	15.64	22.35	0.16	0.01	0.018
0815	dE2,N	16.10	23.48	0.69:	0.05:	0.057:	1348	dE0,N pec	15.87	22.29	0.33	0.02	0.042
0854	dE8,N	17.69	24.67	0.89:	0.20:	0.089:	1386	dE3,N	14.32	24.18	1.70	0.46	0.046
0856	dE1,N	14.25	22.36	0.41	0.21	0.025	1389	dE2:,N	15.91	22.84	0.27	0.04	0.028
0870	dS0(5),N	15.52	22.51	1.01	0.11	0.101	1399	dE5,N	16.49	24.16	0.68	0.14	0.049
0871	dE4,N	15.79	24.01	0.28	0.05	0.016	1407	dE2,N	15.49	22.46	0.37	0.07	0.037
0872	dE0,N	17.00	23.65	0.08	0.03	0.009	1420	dE4,N	16.41	23.19	0.22	0.04	0.024
0896	dE3,N	17.96	24.60	1.72	0.21	0.202	1444	dE8,N:	16.05	23.46	0.64	0.12	0.053
0916	d:E1,N:	16.04	21.41	0.28	0.02	0.060	1446	dE0,N	16.00	23.55	0.56:	0.06:	0.043:
0931	dE2,N	16.43	24.11	0.53	0.04	0.038	1451	dE5:,N	16.47	23.56	0.23	0.08	0.022
0933	dE2,N	17.00	23.14	0.64	0.10	0.056	1491	dE2,N	15.24	21.98	0.37	0.05	0.041
0936	dE1,N	15.81	23.34	0.31	0.05	0.024	1496	dE5,N:	17.92	24.21	0.36	0.02	0.050
0940	dE1,N	14.72	23.05	0.81	0.10	0.043	1509	dE0,N	16.42	24.05	1.05	0.11	0.078
0949	dE4,N	15.48	23.78	0.40	0.05	0.022	1523	dE0,N	17.64	24.19	0.70	0.12	0.086
0974	dE3:,N	16.11	22.62	0.19	0.06	0.024	1539	dE0,N	15.68	23.85	0.47:	0.10:	0.027:
0992	dE0,N	16.81	23.87	0.44	0.08	0.043	1561	dE0,N:	15.82	25.03	4.48:	0.57:	0.163:
1010	dS0(5),N	13.68	21.88	0.33:	0.08:	0.019:	1563	dE3,N	16.11	24.38	0.97	0.20	0.053
1036	dS0(6),N	13.68	21.94	0.19	0.04	0.011	1567	dS0(5),N	14.52	23.56	0.86	0.16	0.033
1044	dE5,N	16.98	23.71	0.16	0.05	0.018	1661	dE0,N	15.97	24.06	0.69	0.18	0.041
1075	dE4,N	15.08	23.32	0.37	0.09	0.021	1711	dE3,N	16.48	23.68	0.22	0.06	0.020
1076	dE0,N	17.36	24.85	0.63	0.29	0.050	1767	dE5,N	16.45	24.08	1.01	0.10	0.075
1079	dE2,N	16.95	25.14	1.11:	0.67:	0.064:	1773	dE5:,N:	16.16	24.18	0.22	0.05	0.014
1093	dE0,N	16.85	24.48	0.55	0.11	0.041	1796	dE5:,N:	16.52	24.15	1.41	0.08	0.104
1095	dE,N	17.93	24.65	0.51	0.03	0.058	1812	dE3,N	17.78	23.73	0.52	0.10	0.084
1099	dE4,N	17.71	23.99	0.20	0.06	0.028	1826	dE2,N	15.70	21.72	0.57	0.03	0.088
1101	dE6,N	15.78	24.12	1.18:	0.05:	0.063:	1857	dE4:,N?	15.07	23.89	6.92:	0.09:	0.295:
1104	dE5,N	15.22	22.67	0.53:	0.19:	0.043:	1886	dE5,N	15.49	23.09	0.69	0.07	0.052
1119	dE4:,N:	17.36	24.20	0.95	0.39	0.102	1896	dSB01(2),N	14.82	22.58	0.49	0.12	0.035
1120	dE2,N	17.17	24.18	0.70	0.08	0.070	2045	dE6:,N	16.33	23.27	1.68	0.15	0.172

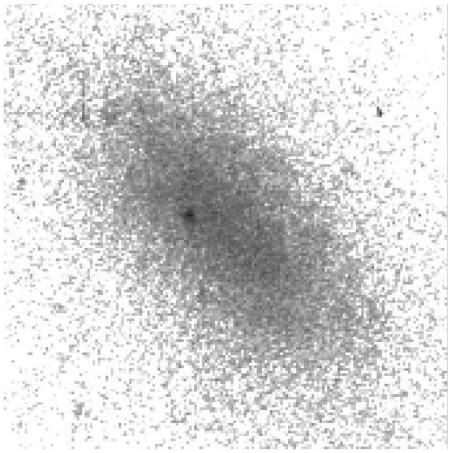

Abbildung C.1: The dwarf elliptical VCC1857 (=IC3647) classified as "dE,N?". Note the very large off-center position of the bright quasi-stellar object, rendering its nuclear status uncertain. Compare with the more ordinary (only slightly off-centered) nuclei shown in Fig. C.2. The image is 1.2 arcmin on a side.

pixel size of the digitized images corresponds to 40μ, or $0.43''$, which has to be compared with the typical FWHM of $1.2''$ for the stellar images on the photographic plates. The position of a nucleus was simply taken as the center of the brightest pixel, resulting in a geometrical mean error of the nuclear position of $0.16''$. For the ellipse fitting the images were slightly smoothed with a running 5×5 pixel mean. This degree of smoothing was found experimentally to be optimal for our purposes.

Ellipses were then fitted to five isophotes in the surface brightness range 24–25 B arcsec^{-2} with steps of $\Delta\mu$ = 0.25 mag, i.e. at the isophotal levels of 24, 24.25, 24.5, 24.75, and 25 B arcsec^{-2}. The fainter surface brightness boundary at 25 B arcsec^{-2} was arbitrarily chosen to avoid the noisy outer parts of the galaxy images. The brighter surface brightness boundary at 24 B arcsec^{-2}, on the other hand, was dictated by the inclusion of faint dEs that have a surface brightness of 24 B arcsec^{-2} already close to the center of the galaxy (underlying the nucleus). This simple and convenient procedure guarantees that all dwarfs are treated in a homogeneous way. We have also experimented with individually different surface brightness ranges within which to determine the nuclear position but found no difference, in the statistical results, to the present procedure.

For each isophotal level in the adopted surface brightness range we calculated the distance of the nucleus to the ellipse center as well as the position angle of the nuclear offset with respect to the major axis. Averaging over the five points in the surface brightness range we derived a mean off-center distance of the nucleus, δr_N, with a 1σ standard deviation, $\sigma_{\delta r}$. To account for the differing sizes of the dwarf galaxies we have also calculated *relative* nuclear off-center distances by dividing δr_N by the "effective" (half-light) radius r_{eff}. All of these data are given in **Table C.6** as follows:

column (5): mean off-center distance of the nucleus, δr_N (in arcsec);

column (6): standard deviation of the nuclear displacement, $\sigma_{\delta r}$ (in arcsec);

column (7): relative nuclear off-center distance, $\frac{\delta r_N}{r_{eff}}$.

Columns (1)–(4) of Table C.6 are defined in Sect. C.2 above.

The δr_N values in arcsecs can be transformed to linear distances by adopting a Virgo cluster distance. A convenient scaling is provided by $D_{Virgo} \approx 20$ Mpc, where an angle of $1''$ just corresponds to 100 pc at the Virgo cluster.

In a number of cases the strong scatter, or generally inconsistent behaviour of the nuclear off-center distance in the surface brightness range 24–25 B arcsec^{-2} was found to cast strong doubt on the calculated mean δr_N. A clear sign of an unreliable mean nuclear offset was also the inconsistency of the offset *position angles* for the different isophotal levels. A significant off-center distance is accompanied by a robust value for the position angle. Uncertain cases in this sense are flagged with a colon in columns (5) to (7) of Table C.6 and they are shown with open symbols in Figs. C.5–C.7 below.

C.4 Illustration of individual cases

The large uncertainties involved call for a statistical treatment of the subject, which is carried out below. First we show, in Fig. C.2, a few cases with significant nuclear off-center displacements, to illustrate the phenomenon as such and to show how the procedure to determine a mean nuclear offset in the isophotal range 24–25 B arcsec^{-2} works. All six dwarfs have an average nuclear offset of $1''$ or more (for the exact values see Table C.6), which is larger than what could be explained by systematic and random errors alone (as explained below), i.e. the displacements are very likely real. In fact, in all cases but one (VCC1386) the displacements are easily recognized by eye.
Notes on individual galaxies (see Fig. C.2):
VCC389: This is a bright dwarf S0 galaxy, classified as such because of a distinct and clearly visible two-component structure: there is an inner, lens-like feature of high surface brightness, with a fairly sharp edge, on top of a more extended low-surface brightness part (for the morphology of dS0s, see Sandage & Binggeli (1984) and BC91). If we look how the nuclear distance to the center correlates with the surface brightness level at which the center was determined from fitting an ellipse, we see that the nucleus is quite central (only insignificantly displaced) in the inner part, but then jumps to $\delta r_N \approx 1''$ beyond $\mu \approx$ 24 B arcsec^{-2}. Obviously, the nucleus is central with respect to the inner "lens", while the whole lens seems to be displaced with respect to the rest of the galaxy.
VCC870: Again a bright dS0,N with a lens-like structure in the inner part. In contrast to VCC389, however, the nucleus is clearly displaced already within the lens and it remains so, albeit with a strange bump in the $\delta r_N - \mu$ relation, with respect to the outer part. Such cases, where the nucleus is shifted against the *whole* galaxy, including the inner part, seem to be rare.
VCC1386: This is an ordinary, bright dE,N. A nuclear displacement sets in at $\mu \approx 24$ B arcsec^{-2} and rapidly increases towards fainter surface brightness. Nevertheless, the effect is very hard to see by eye.
VCC1563: A fainter dE,N with a "well-behaved" and easily visible off-center nucleus.
VCC1767: Similar to VCC1563. However, the nucleus is clearly peculiar, being irregular in shape. The whole galaxy appears somewhat lumpy.
VCC1796: This dwarf is again slightly peculiar as dE, having explicitly been classified as "dE5:, N:" (the colon means uncertainty). Yet the nuclear offset is obvious.

C.5 Error estimation

The standard deviation $\sigma_{\delta r}$ of the mean off-center distance within the adopted surface brightness range, of the order of $0.1''$, is of course only a lower limit to the true uncertainty of any measured δr_N value. The adopted procedure, when applied to a noisy galaxy image, is likely producing large systematic and random errors in δr_N. To get a handle on these errors, we have run Monte Carlo simulations of the measuring procedure with artificial galaxies. We have chosen a typical dE with B_T = 16 mag and ellipticity 0.25 (between E2 and E3) and formed a purely exponential model galaxy from its measured

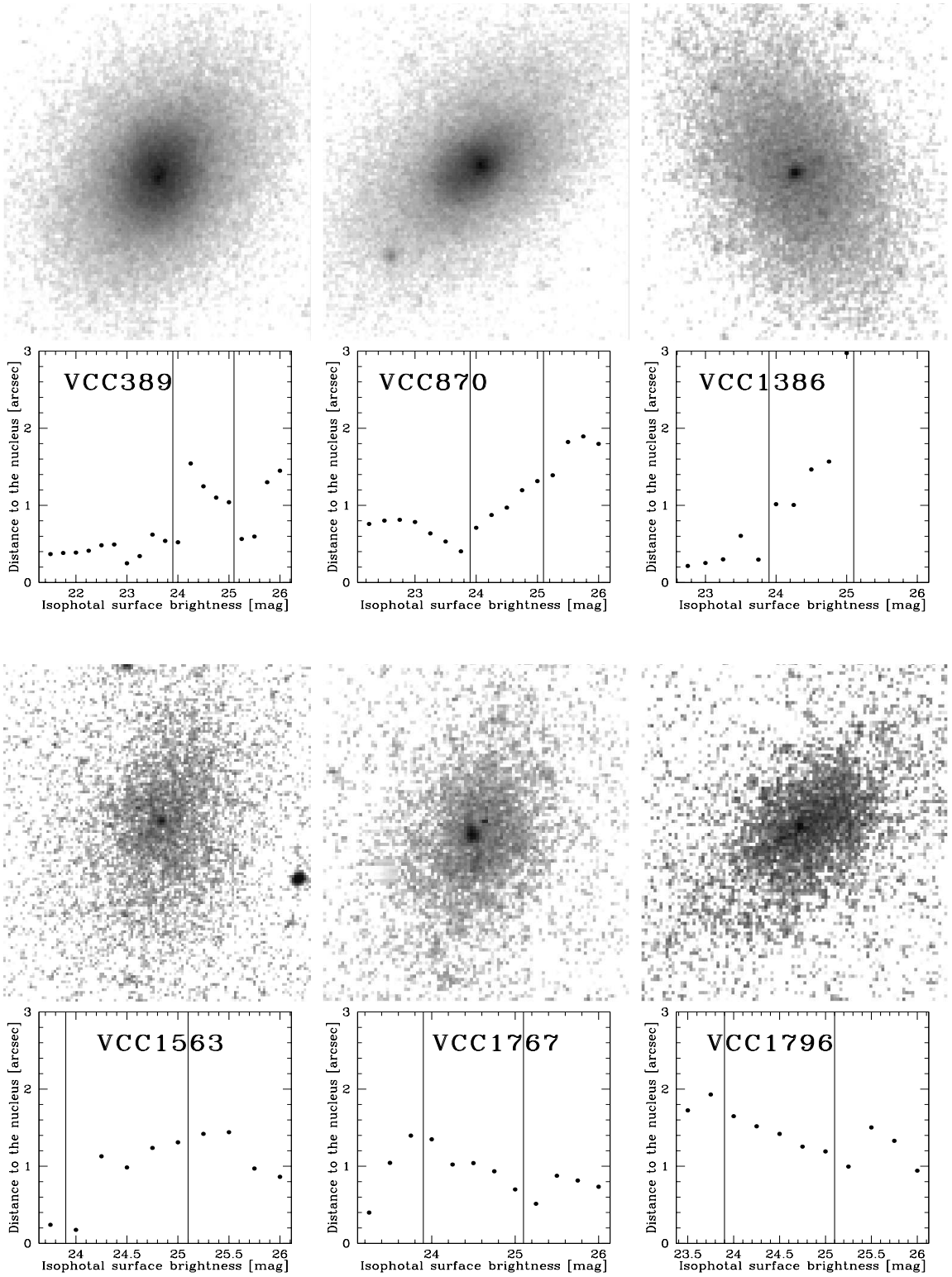

Abbildung C.2: Six individual cases of dwarfs with off-center nuclei. For each galaxy we display a direct image on top of a plot showing the nuclear off-center displacement (in arcsecs) as function of the surface brightness level (in B arcsec^{-2}) at which an ellipse was fitted and a center defined. The thin vertical lines are indicating the boundaries of the surface brightness range 24–25 B arcsec^{-2} within which an average nuclear offset was determined. The objects can be identified from the VCC numbers given in the plots. Each image is 45 arcsecs on a side, except VCC1563 which is 1 arcmin. A detailed description is given in the text (Sect. C.4).

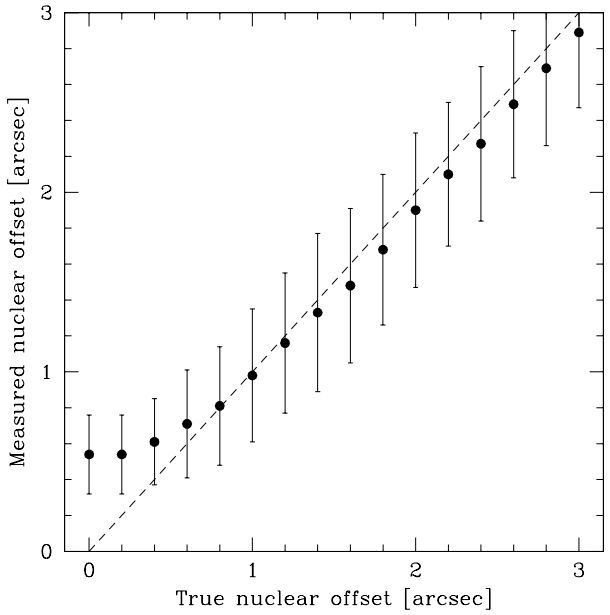

Abbildung C.3: Measured nuclear offset δr_N as a function of the true nuclear offset given as input parameter for an artificial dE,N galaxy with B_T=16 mag and an exponential light profile. Each point is the mean from 500 random (Monte Carlo) representations of the same galaxy. The error bars give the uncertainty for a single case. The broken line is the locus of identity between true and measured nuclear offset.

exponential scale-length and central surface brightness as given in BC93. Having added a suitable sky background and Gaussian nucleus at a certain off-center distance (to be varied), a Poissonian pixel-to-pixel noise was mimicked by a Gaussian sigma weighted with the square root of the local total intensity, and then again added to the artificial image.

Using that Gaussian sigma as a probability distribution, a single artificial galaxy was produced, pixel by pixel, with a random number generator. Then, we determined its nuclear off-center distance δr_N exactly in the same way as with a real galaxy, i.e. according to the procedures described in Sect. C.3 (including a convolution of the model galaxy with a Gaussian seeing function and 5×5 smoothing). For a given (true, input) displacement of the nucleus from the center of the underlying (exponential) galaxy, this application was repeated for 500 representations of the galaxy, and a mean (output) δr_N and its associated standard deviation were calculated. The results of such a Monte Carlo run are shown in Fig. C.3, where we have varied the input nuclear offset – along the major axis in this case – in steps of $0.2''$.

The main characteristics of this simulation are as follows. Exactly central and nearly central (up to about $\delta \approx 0.5''$) *true* nuclear positions, when measured with our procedure, appear *systematically* larger, i.e. displaced from the center. The more central a nucleus truly is, the more displaced it appears. There is a minimal apparent displacement of $\approx 0.5''$. This result of image noise had to be expected. In the process truly displaced nuclei can get more *or* less displaced, but truly *central* nuclei can get *only* more displaced. On the other hand, large true nuclear displacements ($\delta \geq 1''$) get systematically, but insignificantly too small. The *random* errors for a given single case, shown as error bars in Fig. C.3, are quite large – again

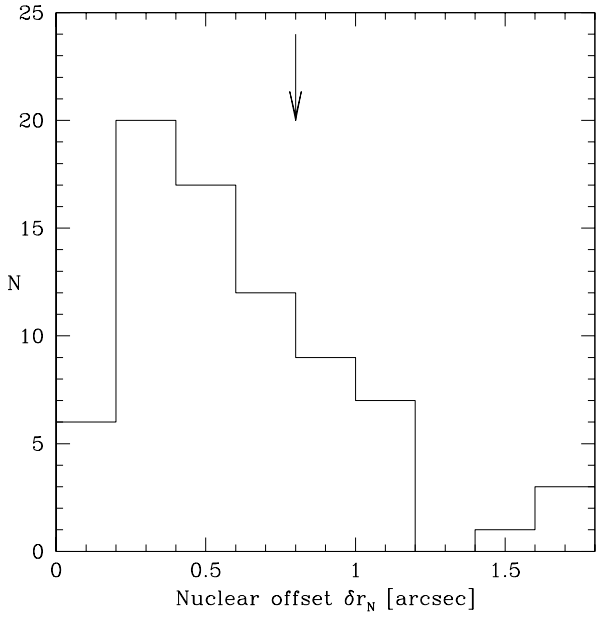

Abbildung C.4: The frequency distribution of measured nuclear offsets δr_N. There are three very large (however uncertain) nuclear offsets beyond the bounds of the figure. The arrow at δr_N = 0.8″is indicating a critical line above which a nuclear offset can be regarded as real (see text).

as expected – : from 0.22″ at δ = 0″ up to $\approx$ 0.4″ at larger displacements (note that the errors of the means would be $\sqrt{500}$ times smaller).

We have of course also varied the total magnitude, and hence surface brightness and exponential scale length (see BC91) of the artificial galaxy, but found rather little variance in the Monte Carlo results, except that for bright dwarfs with B_T = 14 mag (which are in the minority, however), both random and systematic errors are significantly smaller. Also, displacing the nucleus along the minor, rather than the major axis, as well as altering the ellipticity of the galaxy made little difference. As there is a degeneracy of δr_N for small true nuclear displacements, and in view of the generally large random errors, any correction of the measured δr_N for an *individual* galaxy is infeasible. We therefore, in the following, take resort to a very rough and global, statistical accounting for the uncertainties in δr_N, drawing on the results for an artificial typical dE,N (B_T = 16 mag, ellipticity E2.5) shown in Fig. C.3.

C.6 Statistical trends

From Fig. C.3 it is clear that, if most nuclei are truly central, we should expect to see, in the frequency distribution of measured nuclear offsets, a strong peak around $\delta r_N \approx 0.5''$. This is indeed what is observed, as shown in Fig. C.4. However, what is also quite evident from this distribution is the existence of a tail of large δr_N-values; the distribution is strongly skewed towards large measured offsets, and this is clearly hinting at a population of dwarfs with *true* nuclear offsets. How can we quantify this? First, we note that the peak is centered on δr_N = 0.4″, rather than 0.5″(or 0.54″, as is the precise value from Fig. C.3). This means that we have apparently slightly overestimated the systematic errors with our Mon-

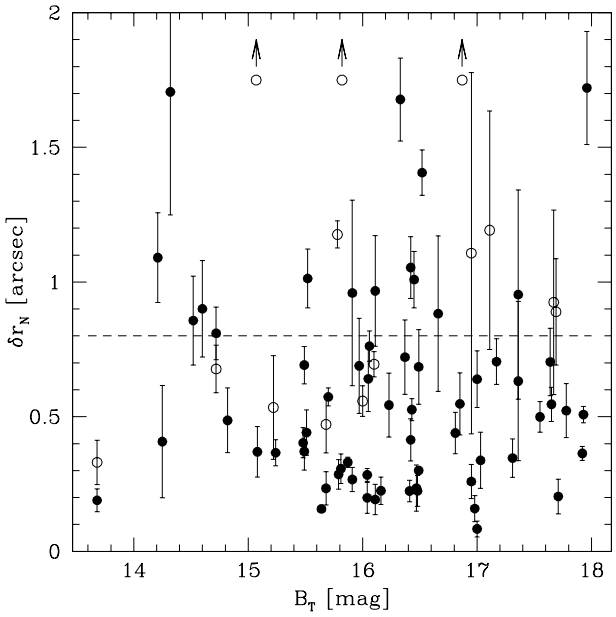

Abbildung C.5: Nuclear off-center distance δr_N versus total galaxy magnitude B_T. Open symbols indicate uncertain offset distances, three of which are larger than $2''$(arrows). The error bars are standard deviations of the mean δr_N-values. The broken line at δr_N is the fiducial division line between dwarfs with central and non-central nuclei.

te Carlo simulation. It should be noted that the observed peak, at $\delta < 0.5''$, must almost certainly stems from a population of dwarfs with central nuclei; at least we see no other explanation for it. Judged from the width of this peak towards smaller offsets (to the left), we estimate a Gaussian sigma of $\approx 0.2''$ (as compared to $0.22''$ from our simulation; Fig. C.3). Assuming, then, a Gaussian distribution with mean and sigma as $0.4'' \pm 0.2''$ for a population of perfectly central nuclei, any measured nuclear offset larger than $2\sigma = 0.8''$ is very likely real (with a probability of 95%). There will be some true nuclear offsets among those with $\delta r_N < 0.8''$, but for an individual case we cannot tell. Above $0.8''$ we should be on the safe side and be allowed to take the measured δr_N for granted, albeit with a large random error of $\approx 0.4''$. We therefore adopt a very rough division line at $\delta r_N = 0.8''$ (the arrow in Fig. C.4) in the sense that most dwarf nuclei with $\delta r_N < 0.8''$ are regarded as central, while those with $\delta r_N > 0.8''$ are regarded as truly displaced from the galaxy center.

In Fig. C.5 we have plotted the nuclear offset δr_N versus the total galaxy magnitude B_T. The nuclear offset distances are shown with their formal r.m.s. errors from averaging the five offsets determined at five isophotal levels. As discussed above, the true uncertainties are usually much larger, of order $0.4''$, without considering the systematic errors (see Fig. C.3). However, it is evident that even these formal errors can be considerably large for dwarfs with $\delta r_N > 0.8''$. Truly "uncertain" or inconsistent cases (cf. Sect. C.3.) – indicated by colons in Table C.6 and flagged with open symbols in Figs. C.5–C.7 – are also more common above the division line of $\delta r_N = 0.8''$.

No systematic trend of δr_N with B_T is obvious from Fig. C.5. A few bright dwarfs with off-center nuclei are popping out, but this is caused by the large size of the parent galaxies (see below). The fraction of dwarfs above the chosen division line at $\delta r_N = 0.8''$ compared to the total, given as percentage of

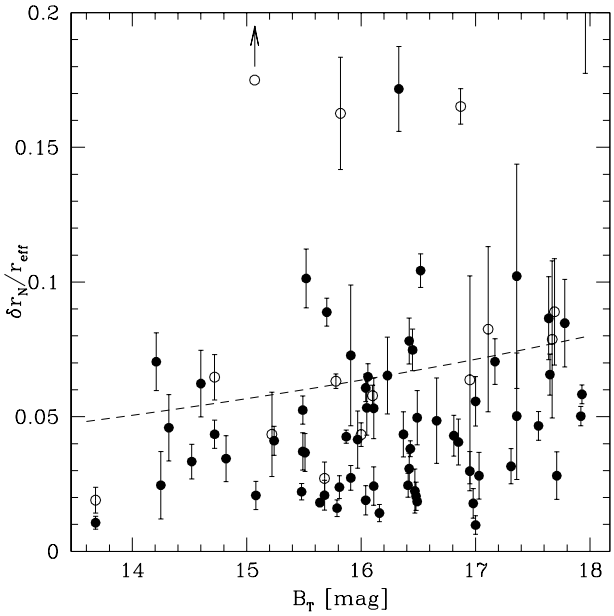

Abbildung C.6: Same as Fig. C.5 but now plotting the dimensionless ratio $\delta r_N/r_{eff}$ (nuclear offset divided by effective radius) versus total magnitude B_T. The broken line is the mean locus of δr_N = 0.8″(see text).

dwarfs with off-center nuclei, is 29% (23 out of 78) if uncertain cases are included, or 23% (15 out of 64) if uncertain cases are excluded. Overall, it seems fair (and conservative) to state that *roughly 20% of all nucleated dwarf ellipticals have off-center nuclei.*

So far we have given the nuclear off-center distances in absolute units of arcsecs. However, as the size of the dwarf galaxies varies, one might suspect that a *relative* measure of nuclear off-center distance, i.e. relative to some characteristic radius of the parent galaxy, is physically more meaningful. We have therefore plotted, in Fig. C.6, the ratio $\delta r_N/r_{eff}$ versus B_T, to see whether we get a different picture.

One obvious change is that the large nuclear offsets in some bright dwarfs (see Fig. C.5) are strongly reduced in relative units, i.e. the nuclear offsets in those dwarfs are large in distance but are *relatively* small as the dwarfs themselves are large in size. Less luminous dwarfs tend to have larger relative nuclear offsets. But where do we now have to draw the critical line between significant and non-significant nuclear offsets?

It turns out that this line does not strongly depend on B_T, simply because the metric (effective) radius of dE galaxies does not. This is also expressed by the basic $\mu - L$ relation of dEs, where the surface brightness is systematically decreasing with decreasing luminosity. To show this, we use the formula for the observed scaling law of Virgo cluster dEs given in BC91:

$$\langle\mu\rangle_{eff} \approx 0.75\, B_T + 11.5\,, \tag{C.1}$$

where $\langle\mu\rangle_{eff}$ is in B mag arcsec^{-2}, and the identity:

$$\langle\mu\rangle_{eff} = B_T + 5\,\log\, r_{eff} + 2\,, \tag{C.2}$$

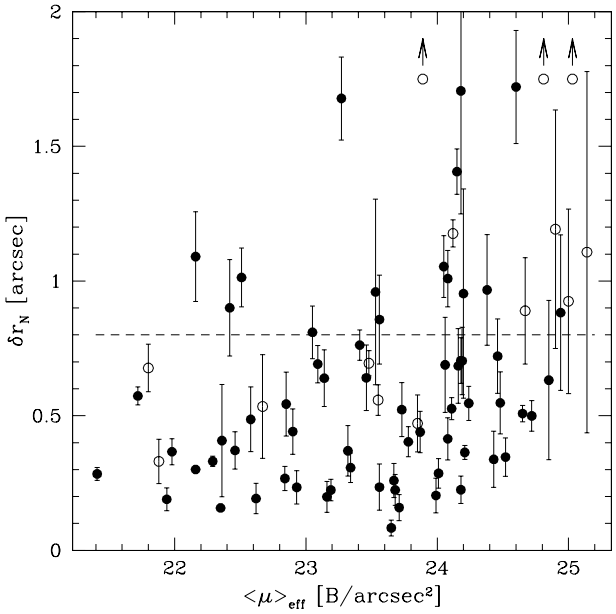

Abbildung C.7: The nuclear off-center distance δr_N (in arcsecs) versus the effective mean surface brightness $\langle\mu\rangle_{eff}$ (in B mag arcsec^{-2}) of the parent galaxy. Otherwise as Fig. C.5.

to derive the equation (r_{eff} always in arcsecs):

$$r_{eff} = 10^{1.9-B_T/20}\,. \tag{C.3}$$

Equ. (3) and $\delta r_N = 0.8''$ now define a critical *relative* nuclear offset $\delta r_N/r_{eff}$, which is shown as broken line in Fig. C.6. Obiously, using $\delta r_N/r_{eff}$ instead of δr_N does not make much difference, justifying *a posteriori* that we have worked with absolute nuclear offsets (in arcsecs or parsecs) from the beginning. Still, there is a hint that the offsets become more common in fainter dwarfs when they are measured in a relative way.

A most interesting and possibly real statistical trend of the nuclear offset distance with the mean effective surface brightness of the parent galaxy is shown in Fig. C.7. There is a clear tendency of δr_N to increase with decreasing surface brightness. Again, given the small sample and large errors, we cannot claim significance of the effect, but Fig. C.7 is certainly very suggestive. What is most striking, of course, is the apparent lack of high-surface brightness dwarfs with large nuclear offsets (the void region in the upper left of Fig. C.7). Remember that the *relative* offsets ($\delta r_N/r_{eff}$) for bright dwarfs, which on average also have higher surface brightness, would be even further reduced.

On the other hand, the apparent lack of very low-surface brightness dwarfs with small nuclear offsets (the void in the lower right in Fig. C.7) is probably an observational bias (incompleteness of the sample), or an artifact from unaccounted-for errors which grossly increase at such faint surface brightness levels. In this case the trend might be better described as an *increasing spread in the range of observed offsets with decreasing surface brightness*.

This spread might result from the nuclear oscillations seen in the simulations of Miller & Smith (1992) and Taga & Iye (1998). Its increase towards fainter surface brightness, *if real*, would then simply

mean an increase in the amplitude of oscillations. Although this was not explicitely explored by the simulations just mentioned, it appears quite plausible that a nucleus can oscillate more easily, i.e. with larger amplitude, in a galaxy of low surface brightness and hence shallow gravitational potential than in a deep, cuspy potential (high-surface brightness central part). Interestingly, the few normal elliptical galaxies with known nuclear displacements in the study of Lauer et al. (1995) all have *cores*, as noted by the authors themselves. *Core* ellipticals have lower central surface brightness than *cuspy* ellipticals, so this would be the same effect.

We have also looked for a trend with the "exponential" *central* surface brightness, μ_0^{exp}, which is one of the parameters of the exponential law that was fitted to the dwarf profiles by BC91/93, but found this relation to be much weaker than that with the mean effective surface brightness. This is actually not too surprising, as μ_0^{exp} is nearly constant (although with very large scatter) in the magnitude range B_T = 14-17 mag (see Fig. 9a of BC91). The reason for this is that the exponential law was fitted to the outer part of the dE profiles. As there is often an extended brightness excess above the fitted exponential, μ_0^{exp} does not represent the "true" central surface brightness of the parent galaxy underlying the quai-stellar nucleus (see BC91/93). A better measure for this would be the central surface brightness from the best-fitting King model (King 1966), but many dwarf profiles could not be fitted by a King model. Ironically, these are often those dwarfs that are found here to have an off-center nucleus. One reason for this could be that all dE,N profiles were automatically centered on their "central" nucleus. On the other hand, there are hints that a significant fraction of bright early-type dwarfs are rotating disk galaxies rather than King spheroids (e.g., Jerjen et al. 2000, and references therein). Rotation might, in fact, be the driving mechanism for the nuclear oscillations (see Taga & Iye 1998)!

We have looked for possible trends of δr_N with many other parameters, among them are – : (1) the flattening of the parent galaxy (with a slight hint that apparently flatter dEs have higher nuclear offsets; but see the appendix for a significant nucleus-ellipticity relation); (2) the angular distance of the parent galaxy from M87 (as the nuclear displacement might be influenced from the environment within the Virgo cluster); (3) the isophotal shape a_4/a of the parent galaxy (diskyness $\leftrightarrow$ boxyness, as given by Ryden et al. 1999); (4) the strength of the nucleus itself (as given by BC91/93 from their King profile fitting, but unfortunately, as mentioned above, only available for a subsample).

No clear trends were found with these parameters. But this is no proof of their absence, as our qualitative analysis of a very limited data set is necessarily blind for any subtle effects, if present. The most interesting, or most expected trend would be a relation between nuclear displacement and nuclear strength. Such a relation, in the sense that stronger nuclei should be less displaced from the center (oscillate with smaller amplitude), is in fact predicted (Taga & Iye 1998).

Finally, we have looked for any systematic trend of the nuclear offset position angle with respect to the galaxy major axis, and found none.

C.7 Summary and conclusions

With very simple means, by fitting ellipses to the outer galaxy part and measuring the distance of the nucleus to the ellipse centers, we have searched for the existence of off-center nuclei in a sample of 78 nucleated dwarf elliptical galaxies of the Virgo cluster. Simulating the measuring procedure with artificial galaxies showed that nuclear displacements of more than $0.8''$ can safely be regarded as real. Taking this into account, we found that roughly 20% of all nucleated dEs have off-center nuclei.

In search for a relation between the nuclear displacement and any kind of structural and environmental parameter of the underlying galaxy, we found a possible tendency of the nuclear displacement (or its

spread) to increase with decreasing surface brightness of the underlying galaxy. A similar trend (but even less significant, given the small number of objects involved) appeared in Lauer et al.'s (1995) study of the centers of normal elliptical galaxies. If confirmed to be real, the trend could simply mean that the nuclei are less strongly bound in a shallow gravitational potential, moving more easily away from, or oscillating with larger amplitude about, the center of the underlying galaxy (see Miller & Smith 1992, and Taga & Iye 1998), whatever the excitation or driving mechanism for this motion may be.

A typical off-center distance in a Virgo dE,N is $1''$, or 100 pc with D_{Virgo}=20 Mpc. With respect to the size of the dwarfs, this corresponds to 0.5 to 1 effective radii. But it has to be borne in mind that dwarfs with nuclei more displaced from the galaxy center than $\approx 2''$ are strongly selected against in our sample, because such objects, if they really exist, would not always have been recognized and classified as "nucleated" (dE,N).

We have used a fairly large and homogeneous data set of digitized photographic images of dE,N galaxies. Future studies of the subject, based on higher-resolution images, will undoubtedly allow much more precise measurements of the nuclear displacements. However, as exemplified beautifully by the *HST* imaging of Miller et al. (1998), high resolution also opens up *Pandora's box*, in that all bright globular clusters become detected as well, rendering the distinction, or even definition, of a fairly faint "central" nucleus non-trivial. But this kind of entanglement is quite natural, as globular clusters and "central" nuclei are related phenomena and may well have a common origin. Nevertheless, even with superior imaging, a large sample ($N \approx 100$) of dE,Ns will be needed to search for statistically significant trends of any nuclear property with the structure of the underlying galaxy, as has been attempted with archive data in the present paper.

Finally, the nuclear displacements, as well as the nuclear magnitudes in relation to galaxy shape (see appendix), will likely tell us something about, or at least allow us to put constraints on, the masses of the nuclei and the galaxy potentials in which they sit. But this is only possible based on quantitative models. Aside from the simulations of Miller & Smith (1992) and Taga & Iye (1998), we completely lack an adequate, realistic and quantitative modelling of off-center nuclei in galaxies.

C.8 Appendix: nuclear strength versus ellipticity

Although there is apparently no correlation between the nuclear offset distance and the ellipticity of the underlying galaxy (see above), there is clearly such a correlation between nuclear *strength* and ellipticity. The data are available since years, but the correlation has never been shown in the literature. As the nuclear strengths, just as the nuclear offsets, must have a bearing on the mass of the nuclei and the structure of the host galaxies, we show this in the present appendix.

By nuclear strength we mean the magnitude of the central luminosity excess of a nucleated dE above a suitable luminosity profile fitted to the underlying galaxy. Such nuclear magnitudes are provided by BC91/93 for a subsample of their dENs, where the galaxy luminosity profile was represented by a King model profile (King 1966). In Fig. C.8 we have plotted the ellipticity of the underlying galaxy (also taken from BC93) versus the nuclear magnitude, B_N, from the King model fitting of B93. B93 do not give a mean uncertainty for their nuclear magnitudes, but we estimate it to be as large as 0.5 mag. Recall first the absolute magnitude scale: with $(m-M)_{\rm Virgo}$ = 31.5 (D=20 Mpc) an apparent magnitude of B_N=20 corresponds to $M^{B_N} = -11.5$, which is roughly met by the very brightest globular clusters of M87 (however, being several magnitudes brighter than an ordinary globular cluster of the Milky Way galaxy; see BC91).

There is a rapid decline in the number of nuclei beyond B_N=21, which is most likely due to incom-

pleteness: fainter nuclei are obviously much harder to detect. The interesting part of Fig. C.8 is the bright end. We notice a pronounced tendency of the brightest nuclei (B_N <19.5) to live in *round* (ϵ <0.2) galaxies. In Fig. C.9 we show the same for the *relative* nuclear strength, i.e. the luminosity ratio L_N/L_T, which in magnitudes is simply $B_N - B_T$. A value of $B_N - B_T$=2.5 means that the nucleus comprises 10% of the total light of the galaxy; a value of 5 corresponds to 1% of the total galaxy, etc. There is clearly the same effect here in Fig. C.9: the relatively brightest nuclei are found in round galaxies. Nuclei that are brighter than 4% of the total galaxy light ($B_N - B_T$ <3.75) are found in galaxies with ellipticities $\epsilon < 0.15$ (there is only one outlier in Fig. C.9, VCC1826).

Nucleated dEs are known to be rounder than the non-nucleated dEs on average by about half an ellipticity class (Binggeli & Popescu 1995). What we have shown here is that this is probably due to the distinct roundness of the host galaxies of the very brightest nuclei. There are at least three possible explanations for this effect. (1) The more elongated dwarfs might have higher internal extinction towards the nucleus due to our viewing angle. This is rather unlikely, as there is no evidence for a great amount of dust in dwarf ellipticals. (2) The built-up of the nucleus could be linked to gas infall which, in turn, is likely governed by angular momentum and, if dEs are rotation supported, by ellipticity (e.g., Davies & Phillipps 1988). However, the very sparse kinematic data for dEs available so far seem to indicate that dEs are *not* rotationally supported (see Ferguson & Binggeli 1994; however, Jerjen et al. 2000). (3) the most plausible explanation is that the presence of the nucleus, if it is massive enough, has changed the orbital structure of the galaxy over a Hubble time. Norman et al. (1985) have calculated and simulated the effect of a black hole put in the center of a triaxial elliptical, with a mass of a few tenths of the core mass of the galaxy, and found a significant roundening of the underlying galaxy out to at least five core radii. The physical cause for this is the disruption of box orbits by scattering of stars off the central

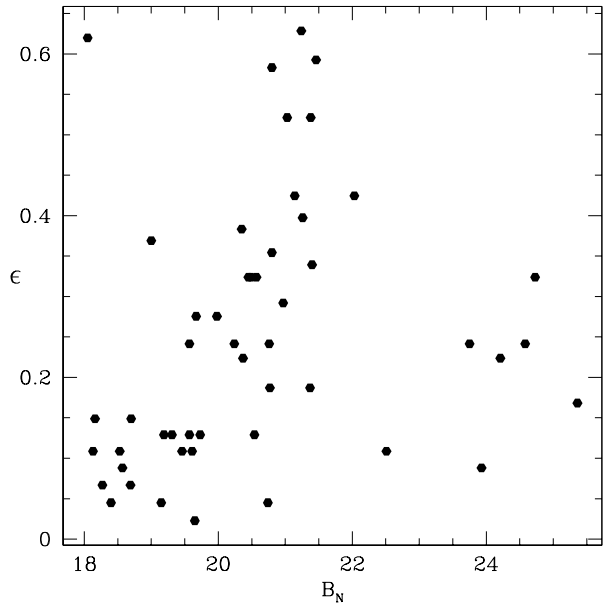

Abbildung C.8: Magnitude of the nucleus B_N, calculated as central light excess above a King model profile fitted to the underlying dE galaxy, versus the ellipticity ϵ of the underlying galaxy. Data taken from BC93.

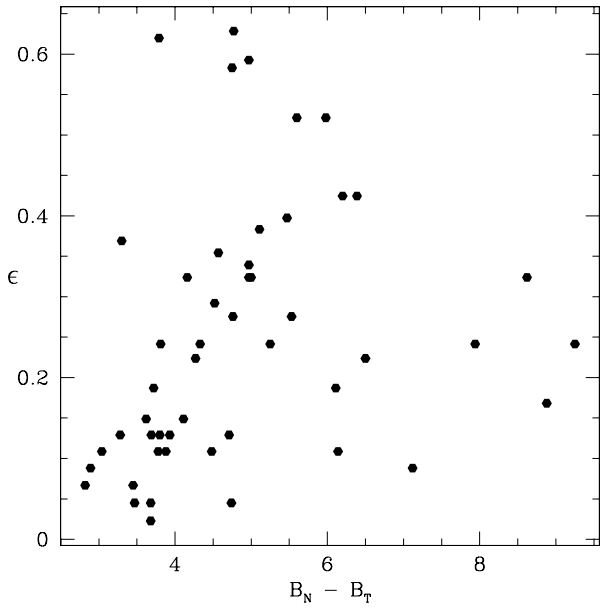

Abbildung C.9: Nuclear magnitude relative to the total galaxy magnitude (including the nucleus), $B_N - B_T$, versus the ellipticity ϵ of the underlying galaxy. Data taken from BC93.

density cusp. A similar result, with a less massive and less effective central compact object, was obtained by Gerhard & Binney (1985).

Based on the work of Norman et al. (1985), Norman (1986) actually predicted that nucleated dEs should be rounder than non-nucleated ones. This is certainly confirmed by our observations. Indeed, the effect that a nucleus of only a few percent of the total galaxy *light* should cause a nearly perfect roundness of the underlying galaxy out to a faint surface brightness of 26 B arcsec^{-2} (the level at which the ellipticities were determined in BC93) may appear even stronger than expected. Could it be that some of these nuclei harbour a black hole, thus comprising a more significant fraction of the total *mass* of the galaxy? Without further, detailed work on the dynamics of nucleated dEs, including the effects of dark matter, it is impossible to draw any quantitative conclusions.

Appendix D
A metallicity-flattening relation for dwarf elliptical galaxies

Abstract

It is shown that bright cluster dwarf ellipticals follow a relation between metallicity and apparent flattening. Rounder dwarfs tend to be more metal-rich. The evidence is based on colour as well as spectroscopic line-strength data from the literature. The large scatter of dEs around the mean metallicity-luminosity relation, usually ascribed to large observational errors, turns out to be an ellipticity effect. In the magnitude range $-14 \gtrsim M_B \gtrsim -18$ the metallicity of dEs depends more strongly on ellipticity than luminosity. A possible explanation is that galaxies with masses around $10^9\ M_\odot$ suffered a partial blowout of metal-enriched gas along their minor axis, rendering ellipticity a critical parameter for metallicity (De Young & Heckman 1994).

D.1 Introduction

Elliptical galaxies follow a well-known luminosity-metallicity relation, in the sense that more luminous ellipticals are observed to be globally redder, or have larger metallic absorption line strengths in their spectra than less luminous systems (Faber 1973, Visvanathan & Sandage 1977). Obviously this is a mass-metallicity relation, and its canonical interpretation is that less massive galaxies had more significant outflows of metal-enriched gas at an early evolutionary stage (Faber 1973, Mould 1984). The relation seems to hold for the entire luminosity range of spheroidal galaxies, down to the faintest dwarfs (Caldwell 1983, Brodie & Huchra 1991, Caldwell et al. 1992). However, there is also considerable scatter in the relation, and there have been attempts to find a *second parameter* which governs metallicity (mass being the primary parameter). A good candidate is the internal velocity dispersion (Terlevich et al. 1984, Efstathiou & Fall 1984), which even more strongly correlates with metallicity than mass (Bender et al. 1993).

The largest scatter in the luminosity-metallicity relation is observed in the magnitude range of bright cluster dwarf ellipticals ($-14 \gtrsim M_B \gtrsim -18$). While this scatter could plausibly be due to measurement errors, Rakos et al. (2001) find a weak correlation with age for a sample of Fornax cluster dwarfs observed in Stroemgren narrow-band colours.

In this letter we show that the scatter in metallicity for cluster dEs is largely explained by *apparent ellipticity* (flattening). At a given luminosity, *rounder dwarf ellipticals are more metal-rich*. There have

already been hints that ellipticity might act as a second parameter in normal elliptical galaxies (Terlevich et al. 1984). However, for dEs the effect is so strong that ellipticity appears to be the *primary* parameter. Such a metallicity-flattening relation for dEs is not implausible. The outflow of metal-enriched gas in stellar systems of intermediate mass ($M \approx 10^9\ M_\odot$) is preferentially occurring along the minor axis, rendering ellipticity a critical parameter for the metallicity of present day dwarfs (De Young & Heckman 1994). *Rounder dEs seem to have suffered less significant outflow*.

D.2 Colour versus flattening

We first show the evidence from multi-colour photometry, which is how we stumbled over the flattening effect. In Fig. D.1 we have plotted integrated colour versus apparent ellipticity for different samples of spheroidal galaxies. The filled circles are $U - B$ values for 15 Virgo dEs from our own photometry (Barazza et al., in prep.). There is a very clear trend appearing, in the sense that rounder dEs are redder than more flattened ones. Such a correlation is rather unexpected – see for comparison a sample of normal ellipticals from Peletier et al. (1990, triangles). However, our finding is corroborated by the $U - B$ data for Virgo and Fornax dEs (crossed circles) from Caldwell (1983) and Caldwell & Bothun (1987), and the Stroemgren $vz - yz$ data for Fornax dEs (open circles) from Rakos et al. (2001). In contrast, local dwarfs with colour data available (from Mateo 1998, asterisks) show no clear relation. All ellipticities used here are taken either from the references given for colour/metallicity data, or from LEDA.

Is the trend for cluster dEs real? Observational bias can be excluded: the samples were not selected

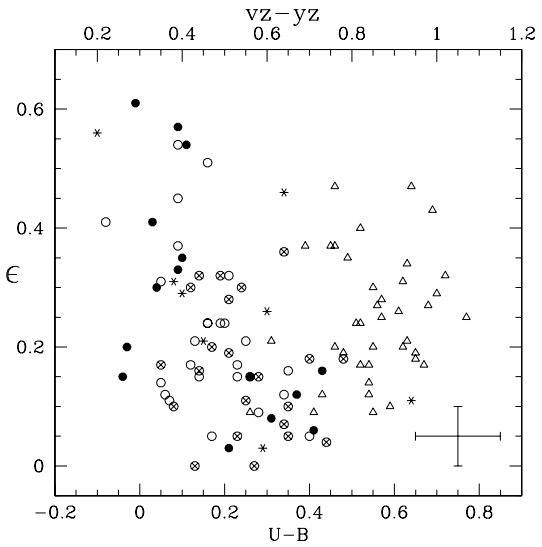

Abbildung D.1: Colour versus apparent ellipticity for cluster dEs (circles), local dEs/dSphs (asterisks), and normal ellipticals (triangles). Filled circles are Virgo dEs from our own photometry, crossed circles are Virgo and Fornax dEs from Caldwell et al., open circles are Fornax dEs from Rakos et al. (complete references given in the text). For the Rakos et al. data the colour plotted is $vz - yz$ (Stroemgren system), shifted by an arbitrary amount along the abscissa (scale on top). For all other samples the conventional $U - B$ colour is plotted (bottom scale). Typical error bars are shown in the lower right.

by colour or ellipticity. Nor is it conceivable that the photometric errors in colour somehow depend on the ellipticity of the whole galaxy. Another suspicion is that ellipticity is not an independent parameter: if ellipticity were correlated with absolute magnitude, we simply might have recovered the well-known luminosity-colour relation (e.g. Ferguson 1994). However, the ellipticity of dEs is not significantly related to luminosity, nor to surface brightness (Binggeli & Popescu 1995).

We take it for granted that colour is essentially indicating metallicity, as spheroidal galaxies are believed to be dust-free and old. Of course, metallicity can also be measured more directly. We now show that the colour-ellipticity relation is indeed a metallicity-ellipticity relation.

D.3 The luminosity-metallicity relation

Fig. D.2 shows the "universal" luminosity-metallicity relation for essentially the same galaxies as in Fig. D.1. Normal Es (small triangles) are represented by data from a more recent study (Kobayashi & Arimoto 1999). [Fe/H] values for local dwarfs (asterisks) are again from Mateo (1998). For bright cluster dEs ($-14 \gtrsim M_B \gtrsim -18$) we have three sources for [Fe/H]: 1) Brodie & Huchra (1991) give spectroscopically determined metallicities for nearly 40 Virgo and Fornax cluster dEs (essentially the Caldwell et al. sample) based on several different line indices. However, the estimated errors in [Fe/H] are considerable. Data with 1 σ errors less than 0.6 dex are plotted as filled circles, those with larger errors (but smaller than 1 dex) as filled squares. 2) Held & Mould (1994) provide spectroscopically measured

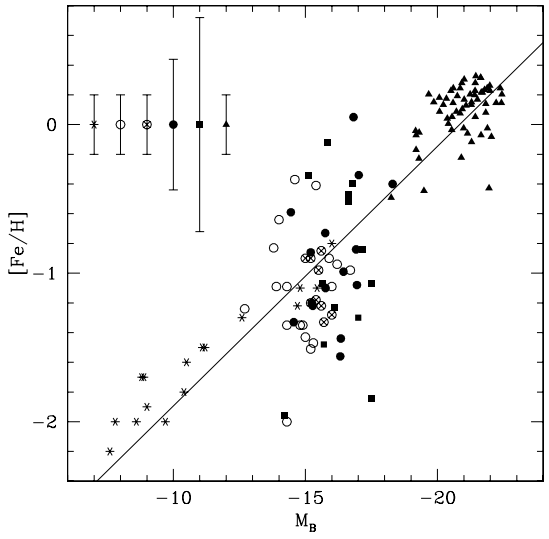

Abbildung D.2: [Fe/H] versus absolute blue magnitude for cluster dEs (circles and squares), local dEs/dSphs (asterisks), and normal Es (small triangles). Open circles are estimated [Fe/H] values for Fornax dEs based on Stroemgren colours (Rakos et al.), crossed circles are spectroscopically measured metallicities for Fornax dEs (Held & Mould). Filled circles and squares are [Fe/H] values for Virgo and Fornax dEs, spectroscopically determined as well (Brodie & Huchra), but with considerable errors. Mean errors for the different samples are shown as error bars in the upper left corner. Complete references are given in the text. The line is a fit to all data (equation given in text).

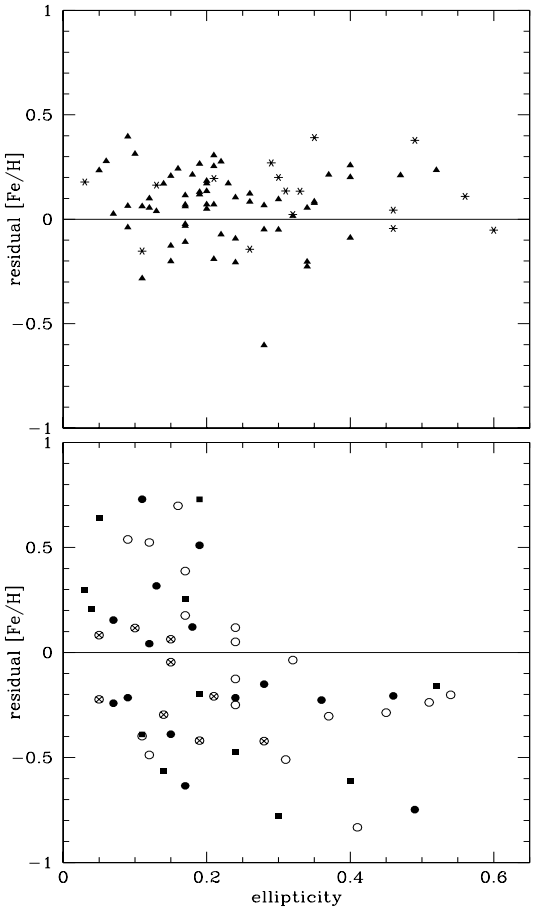

Abbildung D.3: Residual [Fe/H] with respect to the linear fit in Fig. D.2 versus apparent ellipticity for normal ellipticals and local dwarfs (upper panel), and for cluster dEs (lower panel). Symbols as in Fig. D.2.

[Fe/H] values, with much smaller estimated errors, for 8 nucleated Fornax dEs (crossed circles). 3) Finally, there are the Rakos et al. (2001) $vz - yz$ Stroemgren colours for Fornax dEs, appropriately transformed into [Fe/H] values (open circles), with a small mean error of 0.2 dex.

Naively fitting a line through all data plotted in Fig. D.2, we get an expression for the mean (universal) luminosity-metallicity relation: [Fe/H] = $-0.1747\,M_B - 3.6405$, which will be used for a residual analysis below. The local dwarfs follow the mean relation surprisingly well. In contrast, the cluster dEs in the intermediate range between normal Es and extreme dwarfs, while falling in place with the universal relation in the mean, show enormous scatter in their *individual* metallicities. The natural suspicion is that this is simply due to large errors in [Fe/H]. However, we now show that this scatter is systematically related to ellipticity, i.e. it must, at least partially, be real.

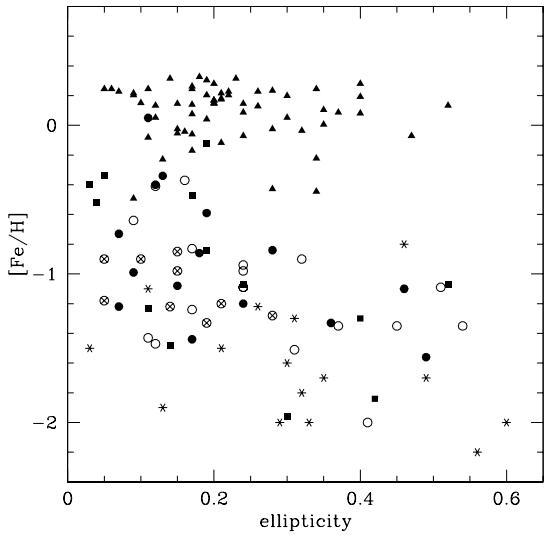

Abbildung D.4: [Fe/H] versus apparent ellipticity. Symbols as in Fig. D.2.

D.4 Flattening as second parameter

The residual metallicities with respect to the line shown in Fig. D.2 are plotted versus ellipticity in Fig. D.3. There is clearly no correlation for normal Es and local dwarfs (upper panel), whereas a relation is evident for cluster dEs (lower panel): dEs with positive residuals are throughout round, while highly flattened dEs have always negative residuals. At a given luminosity, rounder dEs tend to be more metal-rich.

Several points have to be noted. First, the trend is followed by *all* dE samples used, even those where large errors were claimed (the Brodie & Huchra data). Again it is not conceivable why these errors, were they real, should correlate with ellipticity (we believe the errors are simply overestimated). Second, we have tested that the metallicity residuals do not correlate with other parameters, such as effective radius, i.e. there is no other "second" parameter than ellipticity. Third, the true physical relation behind this effect will involve *intrinsic* ellipticity. Due to random projection this relation should even be *stronger* than what we see with apparent ellipticity. The distribution of points in Fig. D.3 (lower panel) is in accord with what we expect from projection effects: apparently round galaxies with positive residuals will also be intrinsically round, while some of the apparently round galaxies with negative residuals will intrinsically be more flattened (i.e. would be shifted to the right).

D.5 The metallicity-flattening relation

In Fig. D.4 we have plotted metallicity directly versus ellipticity, to get an equivalent to the colour-ellipticity diagram of Fig. D.1. As expected, no correlation is seen for giant Es, while dwarf objects evidently follow the suspected relation: rounder galaxies tend to be more metal-rich than flatter ones. Owing to some outliers, the trend is less evident for the local dwarfs (no correlation at all was seen in the residual plot). Conceivably, local (*field*) dwarfs are systematically different from *cluster* dwarfs (see Sect. D.6).

In general, the flattening-metallicity relation is not as striking as the residual plots in Fig. D.3. This is because luminosity now acts as a hidden parameter, adding scatter. In Fig. D.5 we have plotted metallicity versus logarithmic ellipticity for only cluster dwarfs, which provides an almost linear relation. A linear fit yields [Fe/H]=$-0.72\log(\epsilon) - 1.56$, or in terms of abundance: $Z/Z_\odot \propto \epsilon^{-0.72}$. Including the absolute magnitude and fitting a plane to the cluster dwarfs in the parameter space defined by [Fe/H], ϵ and M_B, we get $Z/Z_\odot \propto \epsilon^{-0.70} L^{-0.20}$, which clearly shows that ellipticity is in fact the *primary* parameter, having a stronger effect on the metallicity of dEs than the luminosity.

D.6 Discussion of a possible explanation: outflow of metal-rich gas along the minor axis

The mass-metallicity relation of spheroidal galaxies, evident in Fig. D.2, is most likely the result of early chemodynamical evolution. The central idea is gas loss by a galactic wind, which is believed to be particularly metal-enhanced (Vader 1986, 1987). Certainly, the mass (i.e. potential depth) of a galaxy must be a key parameter for the loss of gas (hence metals), and this explains the mass-metallicity relation. However, it has been pointed out by De Young & Heckman (1994) that the shape (i.e. flattening) of a galaxy may play a crucial role as well. These authors show that galaxies of intermediate mass ($M \approx 10^9 M_\odot$) would not lose almost all of their ISM in a central starburst, but would preferentially undergo a blowout event, having gas flowing out in the direction of their minor axis. The important point is that the strength of such an outflow would critically depend on the intrinsic flattening of the ISM distribution, i.e. the galaxy. Our cluster dwarfs showing a metallicity-flattening relation have masses precisely in the critical regime discussed by De Young & Heckman (1994): their mass seems to be too low to be completely protected from gas loss (as in giant ellipticals), but also too high to experience a total blowaway (as in dwarf spheroidals). In the intermediate mass range of bright cluster dEs the ellipticity could conceivably be the dominant parameter for gas loss, and hence metallicity.

Of course, reality must be more complicated. For one thing dwarf galaxies are believed to have large amounts of dark matter, so the gas escaping the stellar body should remain bound to the galaxy and be re-accreted on a rather short time scale (Mac Low & Ferrara 1999, Ferrara & Tolstoy 2000). In this context, it is interesting to note that we have found a possible difference between cluster dwarfs and (local) field dwarfs. While the evidence for dark matter in field dwarfs abounds, the situation with cluster galaxies in general is much less clear. X-ray and lensing studies of clusters of galaxies suggest that the dark matter in clusters is not bound to individual galaxies, hence cluster dwarfs might be much less dark than field dwarfs. An additional difference is that cluster dwarfs are subject to ram-pressure stripping by the ICM, which might help to remove the gas flown out (e.g. Murakami & Babul (1999).

D.7 Conclusion

We have presented evidence for a metallicity-flattening relation for dwarf elliptical galaxies based on colour and metallicity data available from the literature. At a given total magnitude, rounder dEs are more metal-rich. In the narrow magnitude range of bright cluster dwarfs ($-14 \gtrsim M_B \gtrsim -18$), metallicity is more strongly correlated with ellipticity than luminosity (mass), i.e. ellipticity seems to be the primary parameter for the enrichment history of these galaxies. Possibly this holds only for *cluster* dwarfs; the effect is not significant for local dwarfs. A possible explanation is provided by the scenario of De Young & Heckman (1994), where the outflow of gas, and hence the regulation of metallicity, depends on the intrinsic shape of a galaxy in the intermediate mass range around $10^9 M_\odot$.

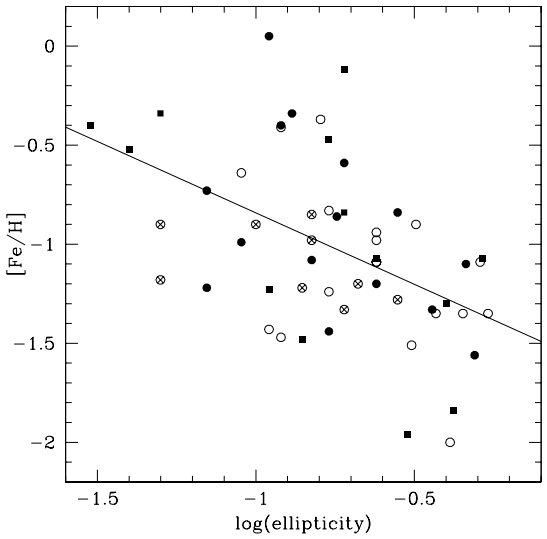

Abbildung D.5: [Fe/H] versus log ellipticity for cluster dEs. The line is a linear fit to the data (equation given in text). Symbols as in Fig. D.2.

It would be highly desirable to strengthen the evidence with further observations, especially spectroscopically well determined metallicities for many cluster dwarfs. If confirmed, the effect is likely to be of importance for our understanding of the chemodynamical evolution of galaxies.

References

Abadi, M.G., Moore, B., Bower, R.G. 1999, MNRAS, 308, 947

Alongi, M. Bertelli, G., Bressan, A. Chiosi, C., Fagotto, F., Greggio, L., Nasi, E. 1993, A&AS, 97, 851

Baade, W. 1944, ApJ, 100, 137

Baade, W. 1963, in C. Payne-Gaposchkin, ed., Evolution of Stars and Galaxies, Cambridge: Harvard, p. 223

Barazza, F.D., Binggeli, B., Prugniel, P. 2001, A&A, 373, 12

Barazza, F.D., Binggeli, B., Jerjen, H. 2001, in “Dwarf Galaxies and their Environment”, eds. K.S. de Boer, R.-J. Dettmar, U. Klein, Shaker Verlag, p. 243

Barazza, F.D., Binggeli, B., Jerjen, H. 2002, A&A, 391, 823

Barazza, F.D., Binggeli 2002, A&A, 394, L15

Bender, R., Möllenhoff, C. 1987, A&A, 177, 71

Bender, R., Surma, P., Döbereiner, S., Möllenhoff, C., Madejsky, R. 1989, A&A, 217, 35

Bender, R., Paquet, A., Nieto, J.-L. 1991, A&A, 246, 349

Bender, R., Burstein, D., Faber, S.M. 1993, ApJ, 411, 153

Binggeli, B., Sandage, A., Tarenghi, M. 1984, AJ, 89, 64

Binggeli, B., Sandage, A., Tammann, G.A. 1985, AJ, 90, 1681 (VCC)

Binggeli, B., Tammann, G.A., Sandage, A. 1987, AJ, 94, 251

Binggeli, B., Tarenghi, M., Sandage, A. 1990, A&A, 228, 42

Binggeli, B., Cameron, L.M. 1991, A&A, 252, 27 (= BC91)

Binggeli, B., Cameron, L.M. 1993, A&AS, 98, 297 (= BC93)

Binggeli, B., Popescu, C.C., Tammann, G.A. 1993, A&AS, 98, 275

Binggeli, B. 1993, in G. Hensler, Ch. Theis, J. Gallagher, eds., Panchromatic View of Galaxies, Kiel, Germany

Binggeli, B., Popescu, C.C. 1995, A&A, 298, 63

Binggeli, B., Jerjen, H. 1998, A&A, 333, 17

Binggeli, B., Barazza, F.D., Jerjen, H. 2000, A&A, 359, 447

Binney, J. 1978, MNRAS, 183, 779

Binney, J., Merrifield, M. 1998, "Galactic Astronomy", Princeton University Press

Bothun, G.D., Mould, J.R., Caldwell, N., Mac Gillivray, H.T. 1986, AJ, 92, 1007

Bower, R.G., Lucey, J.R., Ellis, R.S. 1992, MNRAS, 254, 601

Bremnes, T. Binggeli, B., Prugniel, P. 1998, A&AS, 129, 313

Bremnes, T. Binggeli, B., Prugniel, P. 1999, A&AS, 137, 337

Bremnes, T. Binggeli, B., Prugniel, P. 2000, A&AS, 141, 211

Brodie, J.P., Huchra, J.P. 1991, ApJ, 379, 157

Buta, R., Crocker, D.A. 1993, AJ, 106, 939

Byun, Y.-I., Grillmair, C.J., Faber, S.M., Ajhar, E.A., Dressler, A., Kormendy, J., Lauer, T.R., Richstone, D., Tremaine, S. 1996, AJ, 111, 1889

Caldwell, N. 1983, AJ, 88, 804

Caldwell, N., Bothun, G.D. 1987, AJ, 94, 1116

Caldwell, N., Armandroff, T.E., Seitzer, P., Da Costa, G.S. 1992, AJ, 103, 840

Caon, N., Capaccioli, M., D'Onofrio, M. 1993, MNRAS, 265, 1013

Carter, D. 1987, ApJ, 312, 514

Colbert, J.W., Mulchaey, J.S., Zabludoff, A.I. 2001, AJ, 121, 808

Conselice, C.J., Gallagher III, J.S., Wyse, R.F.G. 2001, ApJ 559, 791

Davies, J.I., Phillipps, S. 1988, MNRAS, 233, 553

Debattista, V.P., Sellwood, J.A. 1998, ApJ, 493, L5

Debattista, V.P., Sellwood, J.A. 2000, ApJ, 543, 704

Dekel, A., Silk, J. 1986, ApJ, 303, 39

De Rijcke, S., Dejonghe H., Zeilinger, W.W., Hau, G.K.T. 2001, ApJ, 559, 21

De Vaucouleurs, G. 1959, Handbuch der Physik 53, ed. S. Flügge (Springer, Berlin), 275

De Young, D.S., Heckman, T.M. 1994, ApJ, 431, 598

de Zeeuw, P. T., Bureau, M., Emsellem, E., Bacon, R., Carollo, M.C., Copin, Y., Davies, R. L., Kuntschner, H., Miller, B. W., Monnet, G., Peletier, R. F., Verolme, E. K. 2002, MNRAS, 329, 513

Dressler, A. 1980, ApJ, 236, 351

Duc, P.-A., Mirabel, I.F. 1994, A&A, 289, 83

Duc, P.-A., Brinks, E., Wink, J.E., Mirabel, I.F. 1994, A&A, 326, 537

Durrell, P.R. 1997, AJ, 113, 531

Efstathiou, G., Fall, S.M. 1984, MNRAS, 206, 453

Elmegreen, B.G., Elmegreen, D.M., Seiden, P. 1989, ApJ, 343, 602

Faber, S.M. 1973, ApJ, 179, 731

Fasano, G., Bonoli, C. 1990, A&A, 234, 89

Ferguson, H.C., Sandage, A. 1988, AJ, 96, 1520

Ferguson, H.C., Sandage, A. 1989, ApJ, 346, 53L

Ferguson, H.C. 1989, AJ, 98, 367 (FCC)

Ferguson, H.C., Binggeli, B. 1994, A&AR, 6, 67

Ferguson, H.C. 1994, in Meylan, G., Prugniel, P., eds, ESO/OHP Workshop on Dwarf Galaxies, ESO, Garching, p. 475

Ferrara, A., Tolstoy, E. 2000, MNRAS, 313, 291

Franx, M., Illingworth, G., de Zeeuw, T. 1991, ApJ, 383, 112

Galletta, G. 1980, A&A, 81, 179

Gavazzi, G., Zibetti, S., Boselli, A., Franzetti, P., Scodeggio, M., Martocchi, S. 2001, A&A, 372, 29

Geha, M., Guhathakurta, P., van der Marel, R. 2001, in “The Shapes of Galaxies and their Halos”, Yale Cosmology Workshop, ed. P. Natarjan

Geha, M., Guhathakurta, P., van der Marel, R.P. 2002, AJ, 124, 3073

Gerhard, O.E., Binney, J. 1985, MNRAS, 216, 467

Gerola, H., Seiden, P.E., Schulman, L.S. 1980, ApJ, 242, 517

Grosbol, P. 1987, in “Selected Topics on Data Analysis in Astronomy”, ed. L. Scarsi, V. DiGesu & P. Crane, World Scientific, p. 57

Harris, W.E. 1996, AJ, 112, 1487

Harris, W.E., Durrell, P.R., Pierce, M.J., Secker, J. 1998, Nature, 395, 45

Held, E.V., Mould, J.R. 1994, AJ, 107, 1307

Held, E.V., Saviane, I., Momany, Y. 1999, A&A, 345, 747

Hoffman, G.L., Williams, H.L., Salpeter, E.E., Sandage, A., Binggeli, B. 1989, ApJS, 71, 701

Holmberg, E. 1950, Medd. Lunds Astron. Obs. 2, 128

Hubble, E. 1925, ApJ, 62, 409

Idiart, T.P., Michard, R., de Freitas Pacheco, J.A. 2002, A&A, 383, 30

Jedrzejewski, R.I. 1987, MNRAS, 226, 747

Jerjen, H., Binggeli, B. 1997, in The Nature of Elliptical Galaxies, 2nd Stromlo Symposium, ed. M. Arnaboldi et al., ASP Conf. Ser. Vol. 116, p. 239

Jerjen, H., Binggeli, B., Freeman, K.C. 2000, AJ. 119, 593

Jerjen, H., Binggeli, B., Kalnajs, A. 2000, A&A, 358, 845

Jerjen, H., Kalnajs, A., Binggeli, B. 2001, in Galaxy Disks and Disk Galaxies, ASP Conf. Ser., Vol. 230, eds. J.G. Funes S.J. & E.M. Corsini, Astronomical Society of the Pacific, p.239

King, I.R. 1966, AJ, 71, 64

Kobayashi, C., Arimoto, N. 1999, ApJ, 527, 573

Kormendy, J. 1982, in "Morphology and Dynamics of Galaxies", 12th Advanced Saas-Fee course, eds. J. Binney, J. Kormendy, S.D.M. White, Swiss Society for Astrophysics and Astronomy, p. 149

Kormendy, J. 1985, ApJ, 295, 73

Kormendy, J., Djorgovski, S. 1989, ARA&A, 27, 235

Kormendy, J., McClure, R.D. 1993, AJ, 105, 1793

Kormendy, J., Richstone, D. 1995, ARA&A, 33, 581

Landolt, A.U. 1992, AJ, 104, 340

Larson, R.B. 1974, MNRAS, 169, 229

Lauer, T.R., Faber, S.M., Groth, E.J., Shaya, E.J., Campbell, B., Code, A., Currie, D.G., Baum, W.A., Ewald, S.P., Hester, J.J., Holtzman, J.A., Kristian, J., Light, R.M., Ligynds, C.R., O'Neil, E.J., Jr., Westphal, J.A. 1993, AJ, 106, 1436

Lauer, T.R., Ajhar, E.A., Byun, Y.-I., Dressler, A., Faber, S.M., Grillmair, C., Kormendy, J., Richstone, D., Tremaine, S. 1995, AJ, 110, 2622

Lauer, T.R., Tremaine, S., Ajhar, E.A., Bender, R., Dressler, A., Faber, S.M., Gebhardt, K., Grillmair, C.J., Kormendy, J., Richstone, D. 1996, ApJ, 471, L79

Lotz, J.M., Telford, R., Ferguson, H.C., Miller, B.W., Stiavelli, M., Mack, J. 2001, ApJ, 552, 572

Mac Low, M.-M., Ferrara, A. 1999, ApJ, 513, 142

Malin, D.F., Zealey, W.J. 1979, S&T, 57, 354

Mateo, M. 1998, ARA&A, 36, 435

Matthews, L.D., Gallagher, J.S., III, Krist, J.E., Watson, A.M., Burrows, C.J., Griffiths, R.E., Hester, J.J., Trauger, J.T., Ballester, G.E., Clarke, J.T., Crisp, D., Evans, R.W., Hoessel, J.G., Holtzman, J.A., Mould, J.R., Scowen, P.A., Stapelfeldt, K.R., Westphal, J.A. 1999, AJ, 118, 208

Melotte, P.J. 1926, MNRAS, 86, 636

Mendez, M., Orsatti, A.M., Forte, J.C. 1989, ApJ, 338, 136

Miller, B.W., Lotz, J.M., Ferguson, H.C., Stiavelli, M., Whitmore, B.C. 1998, ApJ, 508, L133

Miller, R.H., Smith, B.F. 1992, ApJ, 393, 508

Moore, B., Lake, G., Katz, N. 1998, ApJ, 495, 139

Mould, J.R. 1984, PASP, 96, 773

Murakami, I., Babul, A. 1999, MNRAS, 309, 161

Nieto, J.-L., Bender, R., Poulain, P., Surma, P. 1992, A&A, 257, 97

Norman, C., May, A., van Albada, T.S. 1985, ApJ, 296, 20

Norman, C. 1986, in Star-Forming Dwarf Galaxies and related objects, Kunth, D., Thuan, T.X., Van, J.T.T (eds.), Gif sur Yvette: Edition Frontieres p. 477

Oh, K.S., Lin, D.N.C. 2000, ApJ, 543, 620

Parodi, B.R., Barazza, F.D., Binggeli, B. 2002, A&A, 388, 29

Patsis, P.A., Athanassoula, E. 2000, A&A, 358, 45

Peletier, R.F., Davies, R.L., Illingworth, G.D., Davis, L.E., Cawson, M. 1990, AJ, 100, 1091

Phillips, A.C., Illingworth, G.D., MacKenty, J.W., Franx, M. 1996, AJ, 111, 1566

Pierini, D. 2002, MNRAS, 330, 997

Rakos, K., Schombert, J., Maitzen, H.M., Prugovecki, S., Odell, A. 2001, AJ, 121, 1974

Reaves, G. 1956, AJ, 61, 69

Reaves, G. 1983, ApJS, 53, 375

Rix, H.-W., White, S.D.M. 1990, ApJ, 362, 52

Rix, H.-W., Zaritsky, D. 1995, ApJ, 447, 82

Ryden, B.S. 1992, ApJ, 386, 42

Ryden, B.S., Terndrup, D.M. 1994, ApJ, 425, 43

Ryden, B.S., Terndrup, D.M., Pogge, R.W., Lauer, T.R. 1999, ApJ, 517, 650

Saglia, R.P., Maraston, C., Greggio, L., Bender, R., Ziegler, B. 2000, A&A, 360, 911

Sandage, A., Visvanathan, N. 1978, ApJ, 223, 707

Sandage, A., Binggeli, B. 1984, AJ, 89, 919

Sandage, A., Binggeli, B., Tammann, G.A. 1985, AJ, 90, 1759

Sarajedini, A., Claver, C.F., Ostheimer, J.C., Jr. 1997, AJ, 114, 2505

Saviane, I., Held, E.V., Bertelli, G. 2000, A&A, 355, 56

Schlegel, D.J., Finkbeiner, D.P., Davis, M. 1998, ApJ, 500, 525

Schweizer, F., Ford, W.K. Jr. 1985, in "New Aspects of Galaxy Photometry", ed. J.L. Nieto, Springer Verlag, p. 145

Sérsic, J.-L. 1968, Atlas de galaxies australes, Observatorio Astronomico, Cordoba

Shane, C.D., Wirtanen, C.A. 1967, Publ. Lick Obs. 22, part I

Shapley, H. 1938, Harv. Bull., 908, 1

Shapley, H. 1939, Proc. Nat. Acad. Sci US 25, 565

Simien, F., Prugniel, Ph. 2002, A&A, 384, 371

Stiavelli, M., Londrillo, P., Messina, A. 1991, MNRAS, 251, 57

Stiavelli, M., Miller, B.W., Ferguson, H.C., Mack, J., Whitmore, B.C., Lotz, J.M. 2001, AJ, 121, 1385

Taga, M., Iye, M. 1998, MNRAS, 299, 111

Terlevich, R., Davies, R.L., Faber, S.M., Burstein, D. 1984, MNRAS, 196, 381

Thomas, D., Bender, R., Hopp, U., Maraston, C., Greggio, L. 2003, in The Evolution of Galaxies. III. Kiel Euroconference, G. Hensler et al. (eds.), Kluwer

Thuan, T.X., Martin, G.E. 1981, ApJ, 247, 823

Tremaine, S. 1995, AJ, 110, 628

Vader, J.P. 1986, ApJ, 305, 669

Vader, J.P. 1987, ApJ, 317, 128

Vader, J.P., Vigroux, L., Lachièze-Rey, M., Souviron, J. 1988, A&A, 203, 217

van den Bergh, S. 1972, ApJ, 171, L31

Vera-Villamizar, N., Dottori, H., de Carvalho, R., Puerari, I. 1998, in "Focal Points in Latin American Astronomy", eds. Aguilar, A., Carraminana, A., Revista Mexicana de Astronomia y Astrofisica Serie de Conferencias.

Visvanathan, N., Sandage, A. 1977, ApJ, 216, 214

Whiting, A.B., Hau, G.K.T., Irwin, M. 1999, AJ, 118, 2767

Wolf, M. 1909, Astron. Nachr. 183, 187

Worthey, G. 1994, ApJS, 95, 107

Young, C.K., Currie, M.J. 1994, MNRAS, 268, L11

Danksagung

Viele Menschen haben zum Gelingen dieser Doktorarbeit beigetragen. In erster Linien geht mein Dank an Bruno Binggeli, der mir immer helfend und unterstützend zur Seite stand und der meine kuriosen Interpretationen zu unzähligen Plots mit grosser Geduld und stoischer Ruhe über sich ergehen liess.

Ein besonderer Dank geht auch an Helmut Jerjen, dem ich den grössten Teil der verwendeten Daten verdanke und der mir viele Tipps und Tricks verriet, die die Bearbeitung der Beobachtungsdaten erheblich erleichterten.

Unvergesslich bleibt für mich die erste Beobachtungsreise nach La Silla und die folgenden Tage in und um Santiago. Mit dabei war Bernhard Parodi, dem ich für die gute Zusammenarbeit und die angenehme Atmosphäre während der Reise danken möchte. Auch die vielen interessanten Gespräche, nicht nur über Zwerge, behalte ich in bester Erinnerung.

Ausserdem danke ich Dominik Argast für die Begleitung und Unterstützung während einer zweiten Beobachtungsreise nach La Silla und meiner Zimmernachbarin Caroline Girard, deren Einzug und damit verbundenen Veräderungen sich sehr positiv auf die Ausstrahlung des Büros ausgewirkt haben, was von allen Besuchern bestätigt wurde.

Ich habe mich während meiner Zeit am Astronomischen Institut sehr wohl gefühlt und bin immer gerne aufs Bruderholz gekommen, wofür ich mich bei allen Mitgliedern des Instituts herzlich bedanken möchte.

Ein grosses Dankeschön gebührt schliesslich meiner Familie, die mich bei meinem Neuanfang immer Unterstützt hat, insbesondere danke ich meiner Frau Pasqualina, die vor über zwölf Jahren alles ausgelöst hat und der ich auch sonst viel zu verdanken habe.

Zum Schluss danke ich auch den SteuerzahlerInnen in der Schweiz, die, meistens unwissentlich, die Finanzierung übernommen haben. Ich hoffe, dass sie nie erfahren werden, was mir ein älterer, unbekannter Herr während des Fussmarsches auf das Bruderholz anvertraute: auf der Sternwarte sitzen sie nur faul herum und schlagen sich die Zeit um die Ohren.

Erklärung

Ich erkl¨are, dass ich die Dissertation

“Photometric Studies of Dwarf Elliptical Galaxies in the Virgo Cluster”

nur mit der darin angegebenen Hilfe verfasst und bei keiner anderen Fakult¨at eingereicht habe.

Fabio D. Barazza